

**Simultaneous Production of H₂ and
Sulphur by catalytic oxidative
decomposition of H₂S**

Daniela Barba



Unione Europea



*Ministero dell'Istruzione,
dell'Università e della Ricerca*



UNIVERSITÀ DEGLI
STUDI DI SALERNO

FONDO SOCIALE EUROPEO

Programma Operativo Nazionale 2000/2006

“Ricerca Scientifica, Sviluppo Tecnologico, Alta Formazione”

Regioni dell’Obiettivo 1 – Misura III.4

“Formazione superiore ed universitaria”

Department of Industrial Engineering

*Ph.D. Course in Chemical Engineering
(XVI Cycle-New Series, XXX Cycle)*

Simultaneous Production of H₂ and Sulphur by catalytic oxidative decomposition of H₂S

Supervisor

Prof. Vincenzo Palma

Ph.D. student

Daniela Barba

Scientific Committee

Eng. Michele Colozzi

Eng. Vincenzo Vaiano

Ph.D. Course Coordinator

Prof. Ernesto Reverchon

Aknowledgments

Un grande ringraziamento rivolgo a chi ha sempre creduto in me, anche quando io stessa non ci credevo, sostenendomi in ogni mia scelta e in particolare in questo percorso...grazie a miei genitori ed a mia sorella, e a Vera, Antonio per averne fatto parte e per esserci stati sempre; in modo particolare desidero rivolgere un ringraziamento di cuore a mia suocera per il suo immancabile supporto, il grande aiuto e disponibilità che per me ha significato tanto soprattutto durante il dottorato.

Un ringraziamento speciale a Francesco per avermi supportata e sopportata fino alla fine di questo percorso che grazie a te ho deciso di intraprendere anche se un po' in ritardo; grazie per avermi ascoltata tutte le volte che tornavo a casa nervosa e arrabbiata e giù di morale....infinite volte grazie!!

Un sentito ringraziamento al mio Prof. Vincenzo Palma, mio supervisor e guida in questi anni, per la costante presenza e la massima disponibilità...grazie per tutte le giornate trascorse vicino all'impianto, per l'aiuto che non è mai mancato. Grazie per la stima e la fiducia e per l'infinita pazienza...per i consigli e le lunghe chiacchierate e per aver dato ascolto sempre ad ogni tipo di problema lavorativo e personale.

Un grandissimo ringraziamento al mio caro amico Vincenzo, con il quale ho condiviso tutto il mio percorso. Grazie per le chiacchierate, le risate e i miei sfoghi che non sono stati pochi. Grazie per i consigli e per avermi trasmesso quel senso di "leggerezza" che a volte ci voleva per affrontare i problemi nella maniera più giusta o semplicemente per inquadrarli sotto un'altra prospettiva.

Un ringraziamento particolare ai colleghi di Kinetics Technology, in particolare all' Ing. Michele Colozzi, per l'opportunità più unica che rara che ho avuto la fortuna di avere, prendendo parte ad un progetto così importante, che per me ha rappresentato un'esperienza di crescita professionale davvero unica, dalla quale ho imparato davvero tanto.

Un affettuoso ringraziamento a Marino, con il quale mi sono interfacciata più intensamente, condividendo il lavoro in laboratorio per diversi mesi, ad Emma, mia ex correlatrice che ho ritrovato in questo percorso, all'Ing. Pierlorenzo Cinotti, per la sua simpatia che ho scoperto un po' di tempo

dopo durante il suo periodo in laboratorio... Ancora grazie a Lucia Barbato, Simona Cortese , Lorena Mosca, perché da tutti voi ho imparato qualcosa!!

Come non ringraziare i ragazzi del laboratorio Eugenio, Concetta, Marco, Gaetano, Olga e Mariantonietta che hanno condiviso con me quest'esperienza. Un "doveroso" e affettuosissimo ringraziamento ad Antonio per il suo supporto informatico, per le "resistenze" prestate e per la sua grandissima disponibilità. Desidero ringraziare Paola Soave e Livia che hanno lavorato con me, il cui supporto è stato davvero importante, soprattutto nei momenti più critici.

"La ricerca scientifica, benché quasi costantemente guidata dal ragionamento, è pur sempre un'avventura". (Louis de Broglie, Sui sentieri della Scienza, 1960)

Publications List

V. Palma, V. Vaiano, D. Barba, M. Colozzi, E. Palo, L. Barbato, S. Cortese (2015). "*H₂ production by thermal decomposition of H₂S in the presence of oxygen*", International Journal of Hydrogen Energy, Vol. 40, Issue 1, pp. 106-113.

V. Palma, D. Barba, V. Vaiano, The S.O.A.P.TM process: collaborative research & development project between KT-kinetics technology s.p.a. and University of Salerno, (2015).

Proceeding of "Sulphur 2015 - International Conference & Exhibition", (2015) November 9-12, Toronto, Canada.

V. Palma, D. Barba, V. Vaiano, M. Colozzi, E. Palo, L. Barbato, S. Cortese. "*Thermal Catalytic Decomposition of H₂S in presence of oxygen*". Mexican Congress on Chemical Reaction Engineering-IMCCRE, (2016), June 5-9, Queretaro, Mexico.

D. Barba, F. Cammarota, E. Salzano, V. Palma. "*Experimental and Numerical analysis of thermal behaviour of H₂S/O₂/N₂ mixtures*". Mexican Congress on Chemical Reaction Engineering-IMCCRE, (2016), June 5-9, Queretaro, Mexico.

V. Palma, D. Barba, V. Vaiano, "*Simultaneous production of sulphur and hydrogen by thermal oxidative decomposition of H₂S*", Summer School on Calorimetry and Thermal Method in Material Science, (2016) June, 19-24, Lione, Francia.

V. Palma, V. Vaiano, D. Barba, M. Colozzi, E. Palo, L. Barbato, S. Cortese. "*Thermal oxidative decomposition of H₂S for the simultaneous production of sulphur and hydrogen*". 19^o Conference on Process integration, Modeling and Optimization for Energy Saving and Pollutant reduction (PRES), (2016), August 28-31, Praga, Czech Republic.

V. Palma, V. Vaiano, D. Barba, M. Colozzi, E. Palo, L. Barbato, S. Cortese (2016). "*Thermal oxidative decomposition of H₂S for the*

simultaneous production of sulphur and hydrogen”, Chemical Engineering Transactions, Vol.52, pp. 1201-1206.

D. Barba, F. Cammarota, V. Vaiano, E. Salzano, V. Palma (2017). “*Experimental and numerical analysis of the oxidative decomposition of H₂S*”, Fuel, Vol. 198, pp.68-75.

V. Palma, V. Vaiano, D. Barba, M. Colozzi, E. Palo, L. Barbato, S. Cortese (2017). “*Oxidative decomposition of H₂S over alumina-based catalyst*”, Industrial and Engineering Chemistry Research, Vol. 56 (32), pp. 9072-9078.

Summary

Abstract	1
INTRODUCTION	3
I HYDROGEN AND H₂S PRODUCTION	5
I.1. Hydrogen Production	5
I.1.1 Fuel Processing	5
I.1.1.1 Hydrocarbon Reforming	5
I.1.1.1.1 Steam Reforming	7
I.1.1.1.2 Partial Oxidation	7
I.1.1.1.3 Autothermal Reforming	8
I.1.1.1.4 Preferential Oxidation and Water Gas Shift	8
I.1.2 Pyrolysis	9
I.1.3 Plasma Reforming	9
I.1.4 Non - reforming Hydrogen Production	10
I.1.5 Hydrogen from Water	11
I.2 Hydrogen Sulphide	13
I.2.1 Hydrodesulfurization Process	13
I.2.2 Sweetening natural gas	14
I.3 Aim of the work	16
II LITERATURE REVIEW	17
II.1 How to promote the H₂S conversion to Sulphur and H₂	17
II.1.1 Electrochemical Methods	18
II.1.2 Solar Dissociation	19
II.1.3 Photochemical Methods	19
II.1.4 Plasma Methods	20
II.1.5 Microwaves	21
II.1.6 Thermochemical Methods	21
II.2 Hydrogen and Sulphur production by H₂S thermal decomposition	22
II.3 Thermodynamic and Kinetic of the Claus Reaction	31
III CATALYSTS	37
III.1 Catalytic H₂S thermal decomposition	37
III.2 Catalytic H₂S oxidation	41
III.3 Catalytic H₂S oxidation in presence of NH₃ and CH₄	43
IV THERMODYNAMIC ANALYSIS	51
IV.1 Method to calculate the equilibrium composition	51

IV.2: Effect of the Pressure and Temperature	54
IV.3: Effect of the H₂S inlet concentration	56
IV.4: Effect of the Feeding Molar Ratio (O₂/H₂S)	58
IV.5: Effect of O₂/H₂S on ΔH reaction	61
IV.6: Thermodynamic Equilibrium for the reaction system in presence of CH₄ and NH₃	62
IV.6.1. Thermodynamic Equilibrium in presence of CH ₄	63
IV.6.2: Thermodynamic Equilibrium in presence of NH ₃	71
IV.7 Conclusion of the Thermodynamic Study	75
V MATERIALS & METHODS	77
V.1 Powder Catalyst Preparation	77
V.2 Catalyst Characterization	79
V.2.1 Thermogravimetry Analysis (TG)	79
V.2.2 X-Ray Diffraction (XRD)	80
V.2.3 Raman Spectroscopy	80
V.2.4 Specific Surface Area (SSA)	80
V.2.5 Scanning Electron Microscope	82
V.2.6 Ultrasonic Test	82
VI LABORATORY APPARATUS	83
VI.1 Human Health Effects from Exposure to Hydrogen Sulphide	83
VI.1.1 Hydrogen Sulphide: Flammability Limits	84
VI.2 Experimental Apparatus	85
VI.2.1 Feed Section	86
VI.2.2 Reaction and Quenching Section	87
VI.2.3 Heating Section	90
VI.2.4 Sulphur Abatement Section (Sulphur Traps)	91
VI.2.5 Sulphur Trap, Water Condenser and Removal Pollutants Section	93
VI.2.6 Analysis Section	94
VI.2.6.1 Calibration Procedure	98
VI.2.7 Additional equipment to work safely in the laboratory	100
VII HOMOGENEOUS PHASE RESULTS	103
VII.1 H₂S Thermal Decomposition	103
VII.2 H₂S Thermal Oxidative Decomposition	105
VIII MOLYBDENUM-BASED CATALYSTS	109
VIII.1 Catalyst characterization	109

VIII.1.1 Thermogravimetry Analysis	109
VIII.1.2 X-Ray Diffraction	111
VIII.1.3 Raman Spectroscopy	113
VIII.1.4 Specific Surface Area	114
VIII.2 Catalytic Activity Tests	115
VIII.2.1 Influence of the reaction temperature	115
VIII.2.2 Effect of H ₂ S concentration	116
VIII.2.3 Effect of the MoS ₂ content	118
VIII.2.4 Influence of CH ₄ on catalytic performance of 10 wt %MoS ₂ /Al ₂ O ₃	121
IX BIMETALLIC CATALYSTS	123
IX.1. Catalysts Characterization	123
IX.1.1 X Ray Diffraction	123
IX.1.2 Raman Spectroscopy	126
IX.2 Effect of the CH₄ on the mono-bimetallic catalysts performance	128
IX.3 NH₃ effect on 5Fe-10Mo catalyst	130
IX.4 Effect of NH₃ and CH₄ on 5Fe-10Mo catalyst	135
X STRUCTURED CATALYSTS	137
X.1. Structured Catalyst Preparation	137
X.2. Monoliths Characterization	140
X.2.1 Specific Surface Area	140
X.2.2 SEM	141
X.2.3 Ultrasonic Test	142
X.3. Catalytic Activity Test	144
X.3.1 Onset Catalytic Test: Monolith vs Powder	144
X.3.2 Stability Test	146
XI SOUR GAS SOAPTM vs Claus Process	149
XI.1 Sulphur Recovery Unit (SRU): Best Available Technique	149
XI.2 NEW Sulphur Recovery Unit	151
XI.3 Conclusion	152
XII KINETIC MODEL	153
XII.1 Homogeneous Phase	153
XII.2 Heterogeneous Phase (Catalyst 10 Mo/γ-Al₂O₃)	161
XII.3 Microscopic Kinetic Model in Homogeneous Phase	168
XIII CONCLUSIONS	177

Index of Figures

Figure II.1: H_2S Decomposition reaction as function of temperature. _____	23
Figure II.2: Thermal cracking of H_2S in modified Claus furnace. _____	24
Figure II.3: Schematic Claus Process. _____	32
Figure II.4: H_2S conversion (a) and equilibrium composition of sulphur vapor (b) from reaction of H_2S with stoichiometric air at $P= 1.0$ atm (Paskall, 1979)_____	33
Figure II.5: Comparison of model predictions and new experimental data for H_2S and SO_2 conversion. _____	35
Figure III.1: Scheme of reaction pathways in the Claus furnace (Clark et al., 2001).46	
Figure IV.1: Effect of the Pressure on H_2S conversion, H_2 yield, SO_2 selectivity to varying the temperature ($H_2S^{IN}=50\text{vol}\%$, $O_2/H_2S=0.2$). _____	55
Figure IV.2: Effect of the H_2S concentration on H_2S conversion, H_2 yield, SO_2 selectivity to varying the temperature ($P=1$ atm, $O_2/H_2S=0.2$). _____	57
Figure IV.3: Sulphur Yield (S_2 , S_6 , S_8) as a function of the temperature ($P=1$ atm, $O_2/H_2S=0.2$). _____	58
Figure IV.4: Influence of the molar feed ratio (O_2/H_2S) on H_2S conversion, H_2 yield, SO_2 selectivity as a function of the temperature ($H_2S^{IN}=50\text{vol}\%$, $P=1\text{atm}$). _____	60
Figure IV.5: Thermal Tonality by varying the molar feed ratio as a function of the temperature ($H_2S^{IN}=50\text{vol}\%$, $P=1\text{atm}$). _____	61
Figure IV.6: Effect of the CH_4 concentration on CH_4 conversion, H_2S conversion, H_2 yield to varying the temperature ($P=1$ atm, $H_2S = 60$ vol%, $O_2/H_2S=0.2$). _____	65
Figure IV.7: Effect of CH_4 concentration on H_2 yield and SO_2 selectivity by varying the temperature ($P=1$ atm, $H_2S = 60$ vol%, $O_2/H_2S = 0.2$). _____	66
Figure IV.8: Influence of the CH_4 concentration on CO_2 and CO selectivity by varying the temperature ($P=1$ atm, $H_2S = 60$ vol%, $O_2/H_2S = 0.2$). _____	67
Figure IV.9: Influence of the CH_4 concentration on COS and CS_2 selectivity by varying the temperature ($P=1$ atm, $H_2S = 60$ vol%, $O_2/H_2S = 0.2$). _____	69
Figure IV.10: Thermal Tonality by varying the molar feed ratio as a function of the temperature ($H_2S^{IN}=60\text{vol}\%$, $P=1\text{atm}$). _____	70
Figure IV.11: Influence of the NH_3 concentration on H_2S and NH_3 conversion by varying the temperature ($P=1$ atm, $H_2S = 60$ vol%, $O_2/H_2S = 0.24$). _____	72
Figure IV.12: Influence of the NH_3 concentration on H_2 yield and SO_2 selectivity by varying the temperature ($P=1$ atm, $H_2S = 60$ vol%, $O_2/H_2S = 0.24$). _____	73
Figure IV.13: Thermal Tonality by varying the molar feed ratio as a function of the temperature ($H_2S^{IN}=60$ vol%, $P=1\text{atm}$). _____	74
Figure VI.1: Scheme of the Experimental Apparatus. _____	85
Figure VI.2: H_2S pressure regulator. _____	87
Figure VI.3: Fixed Tubular Reactor. _____	88
Figure VI.4: Reactor and its components. External quartz tube (a), internal quartz tube (b), thermocouple liner (c). _____	89
Figure VI.5: Quartz reactor in the furnace (a) and sulphur trap (b) _____	90
Figure VI.6: Furnace scheme and heated furnace during the reaction _____	91

Figure VI.7: Photo and Scheme of the First trap of Sulphur abatement.	92
Figure VI.8: Section of the trap before the reaction test a); Section of the trap with Sulphur after the reaction test b).	92
Figure VI.9: Second stage of sulphur abatement (a) and water condenser with pollutants removal (b,c).	93
Figure VI.10: Activated carbon for H ₂ S residual removal by adsorption.	94
Figure VI.11: Main steps of measuring with a mass spectrometer.	95
Figure VI.12: Main components of a mass spectrometer.	96
Figure VI.13: Mass Spectrometer QIC-HPR 20 Hiden.	97
Figure VI.14: Plant and Analyzer in the suction systems.	100
Figure VI.15: Gas Alert Micro: a) Multigas, b) monogas	101
Figure VII.1: H ₂ S conversion and H ₂ yield in the range 900-1100 °C in comparison with equilibrium values (eq) (H ₂ S ^{IN} :10 vol%, residence time: 150 ms).	103
Figure VII.2: H ₂ S conversion and H ₂ yield as function of residence time in comparison with equilibrium values (eq) (H ₂ S ^{IN} :10 vol%, T = 1100 °C) (Palma et al., 2015).	104
Figure VII.3: Effect of the O ₂ /H ₂ S in terms of H ₂ S conversion, H ₂ yield, SO ₂ selectivity (H ₂ S ^{IN} :10 vol%, T = 1100 °C, residence time = 150 ms) (Palma et al., 2015).	105
Figure VII.4: Influence of the temperature on H ₂ S conversion, H ₂ yield, SO ₂ selectivity and in comparison with equilibrium (eq) values (H ₂ S ^{IN} :10 vol%, O ₂ /H ₂ S = 0.2, residence time = 150 ms) (Palma et al., 2015).	106
Figure VIII.1: TG Analysis of bulk MoS ₂ and 10Mo catalyst (Air flow rate= 100 Ncm ³ /min; 10°C/min; T=20 – 1000 °C).	109
Figure VIII.2: X-Ray patterns of bulk MoS ₂ , 5Mo, 10Mo e 20Mo.	111
Figure VIII.3: X-Ray patterns of Al ₂ O ₃ support and MoS ₂ /γ-Al ₂ O ₃ catalysts.	112
Figure VIII.4: Raman spectra of the samples 5Mo, 10Mo e 20Mo.	113
Figure VIII.5: Effect of the temperature in terms of H ₂ S conversion, H ₂ yield and SO ₂ selectivity in the absence of catalyst, 10Mo sample (H ₂ S ^{IN} =10 vol%, O ₂ /H ₂ S = 0.2, τ=33ms).	116
Figure VIII.6: Influence of the H ₂ S inlet concentration on H ₂ S conversion, H ₂ yield, SO ₂ selectivity for 10Mo catalyst. (T=1000°C, O ₂ /H ₂ S = 0.2, τ=33ms).	118
Figure VIII.7: H ₂ S conversion as function of contact time at 1000°C (z ^{IN} H ₂ S =40%, O ₂ /H ₂ S =0.2)	119
Figure VIII.8: H ₂ yield to varying the contact time for different Mo/γ-Al ₂ O ₃ catalysts. (T=1000°C, H ₂ S ^{IN} =40 vol%, O ₂ /H ₂ S = 0.2).	120
Figure VIII.9: H ₂ S and CH ₄ Conversion, H ₂ Yield, in comparison with the equilibrium data (T=1000°C, H ₂ S ^{IN} = 40 vol%, CH ₄ ^{IN} = 1 vol%, O ₂ /H ₂ S =0.2).	121
Figure VIII.10: SO ₂ , COS, and CS ₂ selectivity in comparison with the equilibrium data (T=1000°C, H ₂ S ^{IN} = 40 vol%, CH ₄ ^{IN} = 1 vol%, O ₂ /H ₂ S =0.2).	122
Figure IX.1: X-Ray patterns of the 5 Fe 10 Mo, 5 Fe and FeS ₂ samples.	123
Figure IX.2: X-Ray patterns of the 5 Fe 10 Mo, 5 Fe, 10 Mo and γ-Al ₂ O ₃ samples.	124
Figure IX.3: X-Ray patterns of 5Co-10Mo, CoS ₂ and γ-Al ₂ O ₃ catalysts.	125
Figure IX.4: Raman Spectra of 5 Fe, 10 Mo and 5 Fe 10 Mo catalysts.	126
Figure IX.5: Raman Spectra of 5 Co, 10 Mo and 5 Co 10 Mo catalysts.	127

Figure IX.6: H ₂ S and CH ₄ Conversion, H ₂ Yield in comparison with the equilibrium data ($\tau = 30$ ms, $T = 1000^\circ\text{C}$, $H_2S^{IN} = 40$ vol%, $CH_4^{IN} = 1$ vol%, $O_2/H_2S = 0.2$).	128
Figure IX.7: SO ₂ , COS, CS ₂ Selectivity in comparison with the equilibrium data ($\tau = 30$ ms, $T = 1000^\circ\text{C}$, $H_2S^{IN} = 40$ vol%, $CH_4^{IN} = 1$ vol%, $O_2/H_2S = 0.2$).	129
Figure IX.8: Concentration profiles of H ₂ S, H ₂ , H ₂ O, SO ₂ by varying the temperature ($H_2S^{IN} = 64.8$ vol%, $O_2/H_2S = 0.2$, $\tau = 1$ sec).	131
Figure IX.9: H ₂ S and NH ₃ conversion, H ₂ yield, by varying the contact time in comparison with the equilibrium data ($H_2S^{IN} = 64.8$ vol%, $NH_3^{IN} = 5.5$ vol%, $O_2/H_2S + NH_3 = 0.24$, $T = 1020^\circ\text{C}$).	132
Figure IX.10: SO ₂ selectivity by varying the contact time in comparison with the equilibrium data ($H_2S^{IN} = 64.8$ vol%, $NH_3^{IN} = 5.5$ vol%, $O_2/H_2S + NH_3 = 0.24$, $T = 1020^\circ\text{C}$).	133
Figure IX.11: H ₂ S and NH ₃ conversion, H ₂ yield, as function of the reaction temperature in comparison with the equilibrium data ($H_2S^{IN} = 64.8$ vol%, $NH_3^{IN} = 5.5$ vol%, $O_2/H_2S + NH_3 = 0.24$, $\tau = 1$ sec).	134
Figure IX.12: SO ₂ selectivity as function of the reaction temperature in comparison with the equilibrium data ($H_2S^{IN} = 64.8$ vol%, $NH_3^{IN} = 5.5$ vol%, $O_2/H_2S + NH_3 = 0.24$, $\tau = 1$ sec).	134
Figure IX.13: Concentration profiles of H ₂ S, H ₂ , NH ₃ , CO ₂ at $T = 1060^\circ\text{C}$, $\tau = 1$ sec ($H_2S^{IN} = 64.8$ vol%, $NH_3^{IN} = 5.5$ vol%, $CH_4^{IN} = 1$ vol%, $O_2/H_2S + NH_3 = 0.24$).	135
Figure IX.14: Concentration profiles of SO ₂ , COS, CS ₂ at $T = 1060^\circ\text{C}$, $\tau = 1$ sec ($H_2S^{IN} = 64.8$ vol%, $NH_3^{IN} = 5.5$ vol%, $CH_4^{IN} = 1$ vol%, $O_2/H_2S + NH_3 = 0.24$).	136
Figure X.1: Monolith dipped in the washcoat.	138
Figure X.2: Structured Catalyst after calcination at 900°C for 1h.	139
Figure X.3: SEM images of the cordierite (a) and the washcoat deposition on the carrier (b).	141
Figure X.4: Adhesion Test Stability for three different washcoat load.	142
Figure X.5: Onset Catalytic Test on 5Fe-10Mo Monolith ($H_2S^{IN} = 64.8$ vol%, $NH_3^{IN} = 5.5$ vol%, $O_2/H_2S + NH_3 = 0.24$, $\tau = 2.12$ s).	145
Figure X.6: Onset Catalytic Test on 5Fe 10Mo Powder ($H_2S^{IN} = 64.8$ vol%, $NH_3^{IN} = 5.5$ vol%, $O_2/H_2S + NH_3 = 0.24$, $\tau = 0.5$ s)	146
Figure X.7: Stability Test ($T = 1060^\circ\text{C}$, $O_2/H_2S + NH_3 = 0.24$, $\tau = 1$ s). Profile concentration of H ₂ S, H ₂ , H ₂ O, NH ₃ , SO ₂ .	147
Figure X.8: NH ₃ Conversion as function of time on stream ($T = 1060^\circ\text{C}$, $O_2/H_2S + NH_3 = 0.24$, $\tau = 1$ s).	147
Figure XI.1: Block Diagram of SRU with RAR Process.	150
Figure XI.2: Process Flow Scheme "New Concept of SRU".	151
Figure XII.1: Comparison between model calculation and experimental data at 800°C (a), 1000°C (b), 1100°C (c) as function of the residence time. ($y_{H_2S^{IN}} = 0.1$, $O_2/H_2S = 0.2$).	157
Figure XII.2: Arrhenius plot used for the evaluation of apparent activation energy.	158
Figure XII.3: Comparison between model calculation and experimental data at 900°C as a function of the residence time. ($y_{H_2S^{IN}} = 0.1$, $O_2/H_2S = 0.2$).	159

Figure XII.4: Comparison between model calculation and experimental data at 1000°C (a) and 1100°C (b) as function of the residence time. ($y_{H_2S}^{IN} = 0.1$, $O_2/H_2S=0.25$).	160
Figure XII.5: Comparison between model calculation and experimental data at 800°C 1000°C 1100°C, and a function of the contact time. ($y_{H_2S}^{IN} = 0.1$, $O_2/H_2S=0.2$).	164
Figure XII.6: Arrhenius plot of the catalytic reactions of H_2S Decomposition (R1), Claus (R3) and Partial Oxidation of H_2S (R5). ($y_{H_2S}^{IN} = 0.1$, $O_2/H_2S = 0.2$).	165
Figure XII.7: Model Prediction at 900°C and 1100°C with $y_{H_2S}^{IN} = 0.2$ ($O_2/H_2S=0.2$).	167
Figure XII.8: Schematic mechanism proposed by Zhou et al. for fuel lean H_2S oxidation with main consumption pathways (Zhou et al., 2013).	168
Figure XII.9: Comparison of model data predictions (straight line), with equilibrium (dotted line) and experimental values (markers) in terms of H_2S conversion, H_2 yield and SO_2 selectivity as a function of temperature ($O_2/H_2S = 0.2$, $RT = 150$ ms).	170
Figure XII.10: Comparison of simulation predictions with equilibrium and experimental values in terms of H_2S conversion, H_2 yield, and SO_2 selectivity as a function of O_2/H_2S ($T = 1100$ °C, $RT = 150$ ms).	171
Figure XII.11: Comparison of the model calculation (straight line) with experimental results (markers) and equilibrium values (dotted line) in terms of H_2S conversion, SO_2 selectivity and H_2 yield by changing the O_2/H_2S at 900 C and $RT = 300$ ms.	172
Figure XII.12: Comparison of experimental molar fractions (H_2S , SO_2 , H_2) (markers) with the simulation predictions (straight line) by varying the residence time ($T = 900$ °C, $O_2/H_2S = 0.35$).	174

Index of Tables

Table II.1: Activation Energy (E_a) for the homogeneous H_2S decomposition. _____	27
Table II.2: Detailed Mechanism of H_2S pyrolysis. _____	28
Table II.3: Reduced Mechanism of the H_2S pyrolysis. _____	30
Table III.1: Characteristics of the metal oxides before and after reaction (12 h) of the high-temperature H_2S decomposition (Reshetenko et al. 2002). _____	39
Table III.2: COS formation in the presence and in absence of catalysts (Gens et al., 1994). _____	47
Table V.1: Schedule of the powder catalysts with the load of active phase. _____	78
Table VIII.1: Weight loss of the catalysts and active phase content (Air flow rate= $100 \text{ Ncm}^3/\text{min}$; $10^\circ\text{C}/\text{min}$; $T=20 - 1000^\circ\text{C}$) _____	110
Table VIII.2: Average crystallite size. _____	112
Table VIII.3: Specific surface area of the $\gamma\text{-Al}_2\text{O}_3$ and the fresh catalysts. _____	114
Table VIII.4: SO_2 concentration by varying the contact time. ($T=1000^\circ\text{C}$, $H_2S^{\text{IN}}=40$ vol%, $\text{O}_2/\text{H}_2\text{S} = 0.2$). _____	120
Table IX.1: Average crystallite size. _____	125
Table X.1: Average thickness of washcoat layer. _____	139
Table X.2: Surface Specific Area of the cordierite and the different percentage of washcoat deposited on the mechanical support. _____	140
Table XII.1: Activation Energy obtained from the linear interpolation of the Arrhenius plot [kcal/mol]. _____	158
Table XII.2: Comparison of Activation Energy between Catalytic Model ($10\text{MoS}_2/\text{Al}_2\text{O}_3$, Al_2O_3) and Literature. _____	166
Table XII.3: Comparison of molar fraction experimental and calculated at 1100°C and $RT = 300 \text{ ms}$ ($\text{O}_2/\text{H}_2\text{S} = 0.2$). _____	175

Abstract

The recovery of hydrogen from H₂S has recently attracted attention because of the economic and environmental advantages: hydrogen is an energy source, a raw material for chemical industry and in the near future it could become a significant fuel.

A great amount of H₂S is obtained as a by-product during the H₂ reduction processes and the hydrodesulphurization of petroleum and, due to the stringent environmental regulations, H₂S has to be removed before its release in the environment. Hydrogen Sulphide is usually removed by the well-known Claus process, where H₂S is oxidized to water and elemental Sulphur by two-step reactions. This process is not profitable from an economic point of view because the price of the Sulphur (the primary product) is depressed and the hydrogen is lost as water. Furthermore, due to the thermodynamic limitations, H₂S conversion in the catalytic stage is limited to ~95-97%, as a consequence further treatments of the residual tail gas are necessary.

So, an attractive alternative could be to produce simultaneously Sulphur and hydrogen by thermal decomposition of H₂S ($\text{H}_2\text{S} = \text{H}_2 + 1/2 \text{S}_2$). Unfortunately, this reaction is very endothermic and it is thermodynamically favored only for extremely high temperatures, thus requiring large amounts of energy and subsequent separation stages with high fixed and operating costs.

A possible solution could be to couple the decomposition reaction with an exothermic reaction, making the system auto-thermal.

For this purpose, the reaction of H₂S oxidative decomposition at high temperature was studied; the main objective of this work was to find a catalyst active and selective to Sulphur and H₂, depressing the possible SO₂ formation related to the presence of the oxygen in the reaction system.

First of all, this reaction was studied in homogeneous phase, by varying the main operating conditions such as temperature, O₂/H₂S, residence time. The results have shown an approach of H₂S conversion and H₂ yield to equilibrium values only at high temperature (1273–1373 K) but with a SO₂ selectivity higher than one expected from equilibrium calculations.

Different sulphide-based catalysts supported on Al₂O₃, both monometallic and bimetallic, were prepared, characterized and tested under different operating conditions.

MoS₂-based catalysts have shown good results at 1273 K, even at very low contact times (20-40 ms) and at high H₂S inlet concentration (40

vol%) in terms of H₂S conversion, H₂ yield and SO₂ selectivity, exhibiting values very close to those expected from the thermodynamic equilibrium.

Based on the experimental collected data, a kinetic macroscopic model able to describe the main reactions was also developed and compared with the homogeneous phase reaction system. The results have evidenced that MoS₂/Al₂O₃ catalyst (at 10 wt % MoS₂), was able to promote the Claus reaction, besides the H₂S decomposition reaction and the partial oxidation to Sulphur, determining a decrease of the SO₂ formation.

The system was also studied in the presence of CH₄ in the feed stream. The results showed that the MoS₂-based catalysts has favored the formation of undesired by-products as COS and CS₂. Different mono and bimetallic catalysts were also tested and compared. The best results in terms of H₂S conversion, H₂ yield, and SO₂, COS and CS₂ selectivity were obtained in the case of the Mo-Fe bimetallic samples.

As a consequence, the bimetallic 10 wt% MoS₂ - 5 wt% FeS₂/Al₂O₃ sample was tested also in presence of ammonia, ensuring a complete NH₃ conversion at 1333 K with a contact time of 1 s.

Finally, the active phases were supported on cordierite honeycombs monolith, which were tested for 25 hours at T= 1333 K in presence of a feed stream with a defined composition, representative of a typical refinery stream.

The catalytic activity of the structured catalyst was also tested for 30 h of TOS at very high temperatures and very stressing conditions in terms of H₂S, NH₃, CH₄ and Oxygen concentrations. The results showed that also in these conditions, an almost total NH₃ conversion is possible without any significative apparent deactivation phenomena, making this catalyst a suitable system for H₂S oxidative decomposition in presence of other compounds, such as methane and ammonia.

INTRODUCTION

Important environmental concerns related to the hostile effects of fossil fuels combustion (greenhouse gas emission, acid rain), coupled with the progressively increasing demand of traditional fuel resources such as oil and natural gas resulting from population increase and declining reserves have set a must to search for an alternative form of energy.

Recently, hydrogen energy has been the subject of intense interest referring to its perfect combustion characteristic against the situation of ever-increasing global energy consumption. In recent years, remarkable efforts have been made to study the H₂ production from polluting substances such as H₂S.

Hydrogen sulfide is a colorless, toxic, corrosive and flammable gas that is considered harmful pollutant and poses hazardous effects on both human health and environment. Therefore, discharging hydrogen sulfide into the atmosphere is strictly regulated. Exploitation of hydrogen sulfide as fuel using conventional combustion technologies thanks to its high heating value is forbidden and criminalized by the strict environmental policies due to its deleterious effect like the formation of SO_x which are precursors of acidic precipitation. Unfortunately, hydrogen sulfide naturally exists in crude oil and natural gas wells and also formed in petroleum refining industries from the degradation of sulfur-bearing fuels, so that it must be separated out and treated prior to the fuel utilization.

Recovery of hydrogen from hydrogen sulfide is a good solution in order to produce clean hydrogen fuel while simultaneously destructing the harmful hydrogen sulfide and breaking it down to its two valuable constituents of hydrogen and sulfur.

I HYDROGEN AND H₂S PRODUCTION

1.1. Hydrogen Production

Currently, hydrogen is primarily used in the chemical industry, but in the near future, it will become a significant fuel. There are many processes for the hydrogen production.

A brief summary of significant current and developing hydrogen production technologies will be discussed, by examining the H₂ production using fuel processing technologies and from alternative resources such as biomass and water.

1.1.1 Fuel Processing

1.1.1.1 Hydrocarbon Reforming

Fuel processing technologies convert a hydrogen-containing material such as gasoline, ammonia, or methanol into a hydrogen-rich stream. Fuel processing of methane is the most common hydrogen production method in commercial use today.

There are three primary techniques used to produce hydrogen from hydrocarbon fuels: steam reforming (SR), partial oxidation (POX), and autothermal reforming (ATR).

The reforming process produces a gas stream composed primarily of hydrogen, carbon monoxide and carbon dioxide. Endothermic steam reforming of hydrocarbons requires an external heat source.

Steam reforming does not require oxygen, has a lower operating temperature than POX and ATR, and produces the reformat with a high

H₂/CO ratio (3:1). The heat is provided by the “controlled” combustion. It does not require a catalyst for operation, it has minimal methane slip and it is more sulfur tolerant than the other processes. The process occurs at high temperatures with some soot formation and the H₂/CO ratio (1:1 to 2:1).

Autothermal reforming uses the partial oxidation to provide the heat and steam reforming to increase the hydrogen production resulting in a thermally neutral process; it is typically performed at a lower pressure than POX reforming. Since POX is exothermic and ATR incorporates POX, these processes do not need an external heat source for the reactor.

However, they require either an expensive and complex oxygen separation unit in order to feed pure oxygen to the reactor or the product gas is diluted with nitrogen.

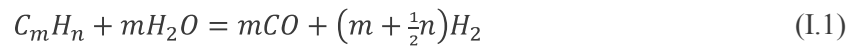
Steam reforming is typically the preferred process for hydrogen production in industry activities (Farrauto *et al.*, 2003).

Since all three processes produce large amounts of carbon monoxide, one or more water-gas-shift (WGS) reactors, typically a high-temperature reactor and low-temperature reactor, are used.

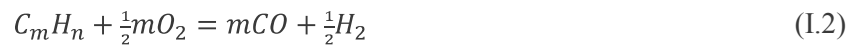
The high temperature (> 623 K) reactor has fast kinetics but is limited by thermodynamics to the amount of carbon monoxide that can be shifted. Therefore, a lower temperature reactor (483-603 K) is used to convert the carbon monoxide to a lower level. High-temperature WGS reactors commonly use an iron catalyst and lower temperature reactors often use a copper catalyst (Farrauto *et al.*, 2003).

The reforming, WGS, and oxidation reactions can be generalized as follows for hydrocarbon (Eq.I.1-4) (Geissler *et al.*, 2001 and Sorensen *et al.*, 2005):

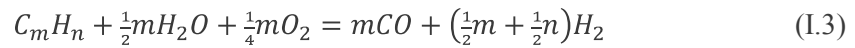
Steam Reforming



Partial Oxidation



Autothermal Reforming



Water Gas Shift (WGS)



Carbon (coke) formation



Fuel processing reactors are designed to maximize hydrogen production (Eqs. I.1–4) and minimize carbon formation (Eqs. I.5-7) using appropriate operating conditions (temperature, pressure, residence time, etc.) and catalysts (Hoogers 2003 and Pietrogrande *et al.*, 1993).

I.1.1.1. Steam Reforming

The catalysts can be divided into two types: non-precious metal (typically nickel) and precious metals from Group VIII elements (typically platinum or rhodium based).

In these systems, the noble Group VIII metals, particularly Rh (Wang *et al.*, 2004), are preferred since they exhibit much higher specific activities than nickel catalysts (Rostrup, 2003 and Wei *et al.*, 2004). However, the high cost of Rh is driving some researchers to develop alternative catalysts such as Co-based catalysts (Song *et al.*, 2007).

Coke formation is much less over the noble Group VIII metals.

Promoters, such as magnesia or potassium or other alkaline components, are added to the catalyst support to minimize the coke formation (Ross, 1974). Steam reforming is commonly used in industry for the production of hydrogen from methane where high thermal efficiencies of up to approximately 85%, based on the higher heating values, have been achieved (McHugh, 2005).

I.1.1.2 Partial Oxidation

Partial oxidation (POX) of hydrocarbons and catalytic partial oxidation (CPOX) of hydrocarbons have been proposed for use in hydrogen production for automobile fuel cells and some commercial applications (Timm *et al.*, 2001 and Pino *et al.*, 2002). The non-catalytic partial oxidation of hydrocarbons in the presence of oxygen typically occurs with

flame temperatures of 1300–1500 °C to ensure complete conversion and to reduce carbon or, in this case, soot formation (Rostrup, 2003). Catalysts can be added to the partial oxidation system to lower the operating temperatures.

For natural gas conversion, the catalysts are typically based on Ni or Rh; however, nickel has a strong tendency to coke and Rh cost has increased significantly.

Typically the thermal efficiencies of POX reactors with methane fuel are 60–75%, based on the higher heating values (McHugh, 2005).

I.1.1.3 Autothermal Reforming

Autothermal reforming adds steam to catalytic partial oxidation.

Therefore the temperature profile in the reactor is characterized by a sharp rise in the thermal zone, and then the temperature steadily decreases in the catalytic zone due to the endothermic reactions.

For ATR to operate properly both the oxygen to fuel ratio and the steam to carbon ratio must be properly controlled at all times in order to control the reaction temperature and product gas composition while preventing coke formation (Krumpelt *et al.*, 1999-2002, Bellows, 1999).

I.1.1.4 Preferential Oxidation and Water Gas Shift

The reforming process produces a product gas mixture with significant amounts of carbon monoxide, often 5% or more (Hoogers 2003, McHugh 2005, Song 2002). To increase the amount of hydrogen, the product gas is passed through a water gas - shift reactor to decrease the carbon monoxide content while increasing the hydrogen content. Typically, a high temperature is desired in order to achieve fast kinetics but results in high equilibrium carbon monoxide selectivity and decreased hydrogen production. Therefore, the high-temperature WGS reactor is often followed by a low-temperature reactor to decrease CO content to 1% or less.

The most common catalyst for WGS is Cu based (Hoogers 2003, McHugh 2005, Song 2002) although some interesting work is currently being done with molybdenum carbide (Patt *et al.*, 2000) platinum-based catalysts (Chandler *et al.*, 2000, Hilaire *et al.*, 2011), and Fe–Pd alloy catalysts (Zhao *et al.*, 2004).

To further reduce the carbon monoxide, a preferential oxidation reactor or a carbon monoxide selective methanation reactor can be used (Hoogers 2003, McHugh 2005, Song 2002).

Methanation reactors are simpler in that no air is required; the catalysts are typically noble metals such as platinum, ruthenium, or rhodium supported on Al_2O_3 (Hoogers 2003, McHugh 2005, Song 2002).

1.1.2 Pyrolysis

Pyrolysis is another hydrogen-producing technology where the hydrocarbon is decomposed (without water or oxygen present) into hydrogen and carbon (Muradov 2003).

Since no water or air is present, no carbon oxides (e.g., CO or CO_2) are formed, eliminating the need for secondary reactors (WGS, PrOx, etc). Consequently, this process offers significant emissions reduction.

Among the advantages of this process are fuel flexibility, relative simplicity, and compactness, clean carbon by-product and reduction in CO_2 and CO emissions (Muradov 2003, Demirbas 2004-2005).

The pyrolysis reaction can be written in the following form (Eq.I.8) (Muradov 2003):



1.1.3 Plasma Reforming

In plasma reforming the overall reforming reactions are the same as conventional reforming; however, energy and free radicals used for the reforming reaction are provided by a plasma typically generated with electricity or heat (Yan *et al.*, 2006).

The main reported disadvantages include the electrical requirements and high electrode erosion at elevated pressures (Bromberg *et al.*, 1999).

There are essentially two main categories of plasma reforming: thermal and non-thermal (Paulmier *et al.*, 2005).

In thermal plasma reforming a high electric discharge (> 1 kW) is used. A great deal of power is consumed in raising both the electrons and the neutral species to a very high temperature (5000–10,000 K). Even more, power is required to cool the electrodes to stop the metals from vaporizing at these high temperatures (Bromberg *et al.*, 1999, Paulmier *et al.*, 2005).

In non-thermal plasmas, only the electron temperatures are increased to high temperatures (> 5000 K). Since only the electrons are directly

excited, only a few hundred watts of power is required (Paulmier *et al.*, 2005).

1.1.4 Non - reforming Hydrogen Production

Hydrogen is produced by many methods other than reforming.

A brief description of some of the biomass-based approaches, along with production of hydrogen from water, is included here.

Biomass is available from a wide range of sources such as animal wastes, municipal solid wastes, crop residues, short rotation woody crops, agricultural wastes, sawdust, aquatic plants, short rotation herbaceous species (i.e. switch grass), waste paper, corn, and many more (Yamada 2006, Steiberg 2004).

For hydrogen generation, the current biomass technologies include: gasification, pyrolysis, conversion to liquid fuels by supercritical extraction, liquefaction, hydrolysis, etc.

Gasification technology, commonly used with biomass and coal, is very mature and commercially used in many processes.

The gasification process typically suffers from low thermal efficiency since moisture contained in the biomass must also be vaporized (Yamada 2006). It can be done with or without a catalyst (Chen *et al.*, 2004, Demirbas *et al.*, 2003, Hao *et al.*, 2002) and in a fixed or fluidized bed reactor; typically the fluidized bed reactor allows to obtain better performance (Asadullah *et al.*, 2002). Addition of steam and/or oxygen to the gasification process results in steam reforming and produces a syngas stream (H₂ to CO ratio of 2:1).

Gasification, even at high temperatures of 1073–1273 K, produces a significant amount of tar in the product gas.

Typically, gasification reactors are built on a large scale and require massive amounts of material to be continuously fed to them. They can achieve efficiencies 35–50% based on the lower heating value (Sorensen *et al.*, 2005). Currently, the high logistics costs typically limit the gasification plants to be located.

Due to increased attention to sustainable development and waste minimization, research in bio-hydrogen has substantially increased over the last several years (Wills, 2006).

The main bioprocess technologies used for bio-hydrogen production include: photolytic hydrogen production from water by green algae or cyanobacteria (also known as direct photolysis), dark-fermentative hydrogen production during the acidogenic phase of anaerobic digestion of organic material, photo-fermentative processes, two stage

dark/fermentative, and hydrogen production by water-gas shift (Levin *et al.*, 2004, Nath *et al.*, 2004, Kapdan *et al.*, 2006).

The advantage of this technology is that the primary feed is water, which is inexpensive and available almost everywhere (Kapdan *et al.*, 2006). Currently, this process requires a significant surface area to collect sufficient light. Unfortunately, these microorganisms in addition to producing hydrogen, produce oxygen, which, when sensed by the organism, causes the cessation of the hydrogen production (Kovacs *et al.*, 2006 and Kapdan *et al.*, 2006).

The addition of sulfate to the solution has been found to depress oxygen production and sensitivity; however, the hydrogen production mechanisms are also suppressed (Sorensen *et al.*, 2005 and Turner *et al.*, 2008).

Since oxygen and hydrogen are co-produced in a mixed gas, significant safety and separation issues occur.

1.1.5 Hydrogen from Water

There has been a great deal of research in splitting water to make hydrogen and oxygen; in fact its commercial uses date back to the 1890s (Norbeck *et al.*, 1996). Water splitting can be divided into three categories: electrolysis, thermolysis, and photoelectrolysis.

Water splitting in its simplest form uses an electrical current passing through two electrodes to break water into hydrogen and oxygen.

It is essentially the conversion of electrical energy to chemical energy in the form of hydrogen, with oxygen as a useful by-product. The most common electrolysis technology is alkaline based, but more proton exchange membrane (PEM) electrolysis and solid oxide electrolysis cells (SOEC) units are developing (Norbeck *et al.*, 1996 and Grigoriev *et al.*, 2006). SOEC electrolyzers are the most electrically efficient, but are the least developed of the technologies. SOEC technology has challenges with corrosion, seals, thermal cycling, and chrome migration. PEM electrolyzers are more efficient than alkaline, but cost more than alkaline systems. They have the lowest efficiency so they have the highest electrical energy costs.

In thermochemical water splitting, also called thermolysis, heat alone is used to decompose water to hydrogen and oxygen (Norbeck *et al.*, 1996 and Steinfield 2005). It is believed that overall efficiencies close to 50% are achievable using these processes (Funk, 2001). It is well known that water will decompose at 2773 K, but materials stable at this temperature and also sustainable heat sources are not easily available (Norbeck *et al.*, 1996). Therefore chemical reagents have been proposed to lower temperatures.

All the processes have significantly reduced the operating temperature from 2773 K, but typically require higher pressures.

Photoelectrolysis uses sunlight to directly decompose water into hydrogen and oxygen, and uses semiconductor materials similar to those used in photovoltaics.

The hydrogen production efficiency is generally limited by imperfections in the crystalline structure, bulk and surface properties of the photoelectrodes, the material's resistance to corrosion from the aqueous electrolytes. In addition to semiconductor devices for photoelectrolysis, it is possible to use suspended metal complexes in solution as the photochemical catalysts (Norbeck *et al.*, 1996 and Gratzel, 2000). Typically, nano-particles of ZnO, Nb₂O₅ and TiO₂ have been used (Norbeck *et al.*, 1996 and Gratzel, 2000).

Currently, the most developed and most used technology is the reforming of hydrocarbon fuels. In order to decrease the dependence on fossil fuels, significant development in other hydrogen generation technologies from renewable resources such as biomass and water is being done.

The most mature technologies are reforming and gasification. Electrolysis coupled with renewable energy is near term low emission technology. Longer term technologies include biohydrogen, thermochemical water splitting, and photoelectrolysis. While significant progress has been made in development of these alternative hydrogen production systems, more technical progress and cost reduction needs to occur for them to compete with traditional large scale reforming technologies at this time.

1.2 Hydrogen Sulphide

The Hydrogen Sulphide is one of the main waste products of the petrochemical industry, it is produced by the catalytic hydrodesulphurization processes (HDS) of the hydrocarbon feedstocks and it is a byproduct from sweetening of sour natural gas and from upgrading of heavy oils, bitumen and coals.

Hydrogen sulfide (H_2S) is a weak diprotic acid, very poisonous, corrosive, flammable, and explosive.

It is a colorless gas with the characteristic foul odor of rotten eggs and it is slightly heavier than air; a mixture of H_2S and air can be explosive, burning with a blue flame to form sulfur dioxide (SO_2) and water.

Hydrogen sulfide often results from the bacterial breakdown of organic matter in the absence of oxygen gas, such as in swamps and sewers.

Dissolved in water, hydrogen sulfide is known as hydrosulfuric acid or sulfhydic acid.

It reacts with metal ions to form metal, which may be considered the salts of hydrogen sulfide and can react with alcohols to form thiols, an important class organosulfur compounds.

Because of this, H_2S is considered a waste stream and has limited industrial application and represents an environmental pollutant to be treated. When the acid gas stream is greater than about 40%, H_2S is usually treated in the Claus process, where H_2S is oxidized to water and sulphur. The final product of all the process is the concentrated H_2SO_4 , of considerable quantitative interest, but it is a product with low added value, and it does not ensure a sufficient margin to repay the cost of H_2 used in the phase of HDS.

This process is not economic when the price of Sulphur (the primary product) is depressed, but nevertheless it is practiced to dispose of the H_2S in an environmentally acceptable manner. However, hydrogen sulphide potentially has a much higher economic value if not just sulphur, but also hydrogen could be recovered (Brancaccio, 2010).

1.2.1 Hydrodesulfurization Process

Hydrodesulfurization (HDS) is a catalytic chemical process widely used to remove sulfur compounds from refined petroleum products such as gasoline or petrol, jet fuel, diesel fuel, and fuel oils. One purpose for removing the sulfur is to reduce the sulfur dioxide emissions resulting from using those fuels in automotive vehicles, aircraft, railroad

locomotives, ships, or oil burning power plants, residential and industrial furnaces, and other forms of fuel combustion.

This process occurs in presence of large excess of H₂, that results in the cleavage of the C-X chemical bond, where C is a carbon atom and X is a sulfur, nitrogen or oxygen atom with formation of C-H and H₂S.

The hydrodesulfurization reaction takes place in a fixed-bed reactor at elevated temperatures ranging from 573 to 673 K and elevated pressures ranging from 30 to 130 atmospheres of absolute pressure, typically in the presence of a catalyst consisting of a base impregnated with cobalt and molybdenum (Beychok, 2013).

Many metals catalyze the HDS reaction, but the most active are those at the middle of the transition metal series. Ruthenium disulfide (RuS₂) appears to be the single most active catalyst, but binary combinations of cobalt and molybdenum are also highly active.

Most HDS units in petroleum refineries use catalysts based on cobalt-modified molybdenum disulfide (MoS₂) together with smaller amounts of other metals. Aside from the MoS₂ catalysts, nickel and tungsten are also used, depending on the nature of the feed. Metal sulfides are supported on materials with high surface areas. A typical support for HDS catalyst is alumina. The support allows a wide dispersion on the support, giving rise to a larger fraction of the MoS₂ that is catalytically active.

For the refinery feedstock such as heavy oils, diesel oil, kerosene, that contains a wide range of organic sulfur compounds, including thiols, thiophenes, organic sulfides and disulfides, it is necessary to remove by HDS the total sulphur down to the part per million range or lower in order to prevent poisoning the noble metal catalysts in the subsequent catalytic reforming of the naphta.

1.2.2 Sweetening natural gas

Sour natural gas compositions can vary over a wide concentration of H₂S, CO₂ and concentration of hydrocarbon components. If the H₂S content exceeds the sales gas specification limit, the excess H₂S must be separated from the sour gas and the its removal process from sour gas is called “*sweetening*”.

The feasibility and desirability of sulphur recovery leads to limitations on the selection of sweetening processes. The quality of sulphur produced from a Claus unit is quite sensitive to the presence of heavy hydrocarbons in the acid gas.

The choose of a specific solvent depends on several factors: lean or rich gas, amount of Sulphur, trace of Sulphur compounds and contaminants. The solvent are generally divided into three chemical

solvents, physical solvents and hybrid (mixture of chemical and physical) solvents.

Amine processes utilize an aqueous solvent containing a chemical reactant, the alkanolamine that are weak bases and react with the acid gases in the absorber to form soluble acid-base salts. These soluble complexes are then reversed in the regenerator at elevated temperature and low pressure. Reduced pressure in the regenerator allows acid gas release and regenerates the solvent to be reused. Alkanolamines exhibit two important chemical properties. The amino group is responsible for weak reactivity of the base, allowing heat regeneration of the salt while the OH group weakens the basicity, increases solubility in water and lowers vapour pressure when compared to a single amine. Chemical solvents are well suited for low operating pressure applications since the removal capacity is high.

The reaction between acid gases and alkanolamine is exothermic and liberates a substantial amount of heat. In the following reaction, where R₁, R₂ and R₃ indicate hydrocarbon or alkanol parts of the molecule, H₂S reacts instantaneously with alkanolamine (Eq.I.9).



Amine-based processes have dominated the gas sweetening industry: in particular Diethanolamine (DEA) and Methildiethanolamine (MDEA) have probably been applied more in refinery and natural gas sweetening industries in general.

Monoethanolamine (MEA) is used for low-pressure applications and complete acid gas removal. It is a highly reactive primary amine that exhibits low cost, good thermal stability, partial removal of COS and CS₂. However, MEA presents a low solvent vapour pressure, a highly corrosive nature, high-energy demand for regeneration, and the removal of acid gas is non-selective. DEA is a secondary amine and one of the most widely employed for gas containing H₂S, CO₂. It is less reactive, has lower solvent vapour pressure and lower corrosion potential than MEA, coupled with a lower solvent cost. DEA is non-selective and requires higher circulation rates in the sweetening unit.

MDEA is among the most recent amines and is now displacing the other alkanolamines. In highly concentrated solution, this tertiary amine is selective to H₂S. It exhibits low vapour pressure, high resistance to degradation, low corrosiveness and low energy demand for regeneration. However, its reactivity is low and solvents price higher when compared to the above.

1.3 Aim of the work

The objective of this research was to examine the possibility to obtain simultaneously hydrogen and Sulphur by developing a new process in alternative to the Claus one, based on the H₂S oxidative decomposition reaction.

On the base of this idea, two European patents have been developed and presented. The proposed process is a catalytic process named "S.O.A.P.", that is the acronym for the **S**elective & **O**xidative **A**uto-thermal **P**rocess, and is the result of the collaborative research and project development between the "Proceed" Laboratory of University of Salerno and the company Kinetics Technology S.p.A.

The research is so focused on the identification of a catalyst active in the oxidative decomposition reaction of H₂S and selective towards the H₂ production, able to maximize the H₂S conversion and minimize the SO₂ formation. At this proposal, the influence of the operating conditions such as temperature, contact time and H₂S inlet concentration on the catalytic performance were investigated.

Subsequently, a feed stream with a composition representative of a typical refinery stream containing a high H₂S concentration in the presence of methane and ammonia has been taken in account, making so more complex the reaction system for the number and type of reactions involved. For this purpose, the optimization of the catalyst formulation able to achieve simultaneously a high conversion of H₂S, CH₄, NH₃, a good H₂ yield and the minimization of the undesired by-products as COS, CS₂, SO₂, NO_x was necessary.

After that, the formulation of the catalyst in the powder form was transferred on cordierite honeycomb monolith, in order to realize a scale-up from the laboratory scale to the pilot one with a scale factor of 100.

On the base of the collected experimental data, a macroscopic kinetic model of the reaction system was also developed.

II LITERATURE REVIEW

In this chapter are briefly discussed the main processes based on the H₂S decomposition (such as *electrochemical, photochemical, plasma methods, solar dissociation, microwaves*) in comparison with the thermochemical method based on the H₂S cracking at high temperatures.

About this one, many kinetic studies regarding the H₂S pyrolysis are reported, focusing the attention on the Claus reaction, from the thermodynamic and kinetic point of view, that today represents the only process employed industrially to convert in an efficient way the H₂S in Sulphur and water.

II.1 How to promote the H₂S conversion to Sulphur and H₂

Hydrogen sulphide has a high heating value, but its use as a fuel is ruled out because its product of combustion is sulphur dioxide which is not environmentally acceptable. An immediately alternative route for the utilization of hydrogen sulphide is to devise ways to break it down to its constituent elements, hydrogen and sulphur. When compared to the existing method of utilization of hydrogen sulphide for the production of sulphur in a Claus plant, the possibility of obtaining two valuable products provides significant stimulus to the development of such a process.

The interest in the utilization of hydrogen sulphide as a source of hydrogen and sulphur is intensified in recent years because of the following reasons:

- Global tendency for hydrogen energy and waste minimization;
- Unavoidable production of hydrogen sulphide from gas plants, refineries, upgrades and metallurgical processes;
- The tail gas clean-up from Claus plants can exceed the value of the sulphur recovered if the environmental regulations are made more stringent.

Thermochemical cycles have been proposed by many researchers in order to obtain hydrogen and sulphur from hydrogen sulphide. In recent years, some methods for water splitting have been applied to H₂S decomposition and there is a whole array of methods for the decomposition of hydrogen sulphide (electrolysis, photolysis, plasmolysis and their many variants).

II.1.1 Electrochemical Methods

Because of low specific conductance and a low dielectric constant of liquid H₂S, electrolysis of liquid H₂S does not seem practical.

In water, the number of ionic species present is too small to support rapid electrolysis. Thus, a supporting electrolyte has been used to raise the conductance of the solution to obtain satisfactory rates, either an acidic solution or a basic solution. One of the largest drawbacks to direct electrolysis of aqueous H₂S is that the product elemental sulphur is a very good insulator.

Indirect electrolysis methods use a chemical oxidant to oxidize H₂S.

Acidic iodine and basic iodine based processes have been presented.

The acidic process suffers from the loss of iodine and the formation of impure sticky plastic sulphur, whereas the basic process has the drawback of low sulphur yields, excessive oxidant consumption, and high electrical energy requirements (Kalina *et al.*, 1985).

The Idemitsu Kosan Company (IKC) has developed a ferric/ferrous ion solution process that removes H₂S by bubbling the feed gas through an acidic solution of ferric chloride which is reduced to ferrous chloride with the simultaneous oxidation of H₂S to sulphur (Mizuta *et al.*, 1991).

Recently, a thin, solid-state membrane H₂S electrochemical cell was developed and operated successfully at 423 K and 138 kPa to produce liquid sulphur and hydrogen in electrolysis mode (Mbah *et al.*, 2008).

For all of the direct and indirect electrolysis methods, the major common advantage is the production of high purity hydrogen, whereas the common disadvantage is the high cost of electricity which makes these methods uneconomical at the present time for the production of large quantities of hydrogen. The other possibility for the success of electrochemical methods may lie in the integration of electrochemical technology with photovoltaic technology utilizing solar energy. In the meantime, parallel to research on improving the performance of an individual cell, the practical aspects of scale-up and design of cell modules should also be emphasized.

II.1.2 Solar Dissociation

Solar experimental studies on H₂S thermolysis indicate that high degree of chemical conversion is attainable and that the reverse reaction during quench is negligible (Steinfeld *et al.*, 2005).

In this case, the chemical system takes H₂S and converts it into gaseous hydrogen and liquid Sulphur.

Since a solar process is intermittent, a storage container for liquid H₂S must be provided. The tank must be large enough to allow constant filling from the H₂S source and removal for the solar process during hours of sunlight.

The main species in the product effluent would be H₂, S₂, and unreacted H₂S which would be recycled.

A preliminary economic assessment indicated that the capital cost of a plant would be up to ten times that of a similar capacity Claus plant.

II.1.3 Photochemical Methods

Most attempts for the photodissociation of H₂S involve irradiating an alkaline solution of the gas in which semi-conductor particles are suspended.

Many experiments have used cadmium sulphide, ruthenium dioxide/cadmium sulphide, titanium dioxide, chromium, platinum, vanadium sulphides, as the semi-conductor which participates by absorbing the incident quanta of light (Borgarello *et al.*, 1982 and 1986). None of these materials improved hydrogen production significantly and the efficiency of processes using light to dissociate H₂S to hydrogen and sulphur are around 3%.

Despite the well-known drawbacks of photochemical methods for H₂S decomposition (low quantum yield, environmental toxicity and instability of CdS photocatalyst), there has been some activity in this field recently.

In particular, the process of photochemical decomposition of H₂S has been proposed by Linkous *et al.* (2004) and then patented by Huang *et al.* (2007). The method is based on direct photolysis by UV light ($\lambda = 253.7$ nm) of H₂S absorbed by an alkaline solution. It has been found that a Na₂S aqueous solution can be photolytically dissociated into hydrogen and sodium disulfide (Na₂S₂).

The quantum efficiency of hydrogen production was as high as 27%. No photocatalysts are needed in this process, avoiding deactivation of catalysts or passivation of electrodes for electrochemical processes. The disadvantage of the approach is that electrical energy must be converted into photonic energy, causing energy loss.

Guijun Ma *et al.* (2008) found that H₂S can be directly split into hydrogen and sulphur on photocatalysts composed of CdS-based semiconductors loaded with noble metals and noble metal sulphides using nonaqueous ethanolamine solvent as the reaction media.

Diethanolamine (DEA) was found to be an excellent reaction media for this reaction, possibly because it is a suitable medium for proton transfer and also electrons on the CdS photocatalysts.

The development of a nonaqueous ethanolamine solution as a solvent and reaction medium provides a new strategy for the decomposition of H₂S by both photocatalytic and electrochemical technology.

Anyway, the photocatalytic processes are developed only on laboratory scale, as the kinetics of hydrogen production is strongly related to the specific physico-chemical and structural properties of the photocatalyst, often requiring expensive and complex manufacturing technologies that actually limit their production at large scale (Reverberi *et al.*, 2016).

II.1.4 Plasma Methods

Some researchers have used plasma reactors to dissociate H₂S, but the energy efficiency of the processes has been low, presumably because many successive dissociation-recombination processes serve only to recreate the reactant H₂S and produce heat before that H₂ is finally formed as a product (Argyle *et al.*; 2004). Most of these researchers have reported energy requirements of 0.5 to 200 eV/molecule of H₂S converted, which is many times higher than the theoretical minimum of ~0.2 eV/molecule H₂S (21 kJ/mol H₂S) based on the enthalpy of formation of H₂S at 298 K.

The results show that non-thermal plasmas are effective for dissociating H₂S into hydrogen and sulphur, but further increases in energy efficiency are necessary (Zhao and Gui-Bing, 2007).

Wang *et al.*, (2004) developed semiconductor catalysts (CdS/Al₂O₃, ZnS/Al₂O₃) that have shown a total H₂S conversion at low temperature.

In order to obtain an efficient H₂ production, it is important that the catalyst has two requirements, a high enough conduction band to ensure sufficient power for H₂S reduction to produce H₂ and a narrow band gap to allow a good utilization of light (Zhang *et al.*, 2008). For this purpose, the idea was the incorporation of ZnS in the structure of CdS to form Zn_xCd_{1-x}S solid solution (Wang *et al.*, 2010). All the catalysts showed high activities for H₂S decomposition, exhibiting higher performance of CdS/Al₂O₃, ZnS/Al₂O₃ catalysts.

Plasmas have not so far been used for any large-scale chemical processing because the biggest obstacle is the use of electrical energy.

However, the plasma process is environmentally friendly and operationally simple with minimum waste generation. None of the work

reported in the literature, however, has reached a mature level of development.

II.1.5 Microwaves

One of the principal limitations to the wider employment of microwave heating in the chemical industry is a lack of fundamental understanding of microwave heat generation and transport at the microscopic level.

Microwave fields do not couple to the ceramic support at temperatures of interest in chemical reactions, but they may couple strongly to the metallic particles of the catalysts because of their high electrical conductivity.

Seyfried *et al.*, (1994) studied the effects of microwave irradiation of an alumina-based catalyst with 0.2 wt% platinum.

However, some investigators suggest that the tiny metallic particles typical of supported metal catalysts cannot achieve a temperature significantly higher than that of the support or the fluid medium because of the efficiency of energy transport in this small case.

Chemat *et al.*, (1998) investigated heterogeneous catalytic reactions using a continuous microwave reactor and compared the results to those obtained by conventional heating. It was concluded that selective heating is possible with microwave fields of high frequency and that it has a strong dependence on the catalyst particle size and of the microwave frequency. The temperature of the spatial hot spot within the catalyst bed is different from the average temperature of the catalyst bed. The catalytic conversion of H₂S into hydrogen and sulphur has recently been investigated by Zhang *et al.*, (1999) and (2006) that have compared microwave and conventional heating conditions of two catalysts, an impregnated catalyst and a mechanical mixture of MoS₂/γ-alumina (both 30% by weight MoS₂).

Surprisingly, the conversion efficiency for the reaction which takes place in the microwave cavity is higher than that expected by thermodynamics.

II.1.6 Thermochemical Methods

An apparent simple way of converting H₂S to Sulphur and hydrogen would be the breaking the H-S bonds (Clark and Wassink, 1990).

H₂S cleavage can be split up into two or more discrete steps which are easier to carry out. Thus, a highly energetic reaction can be broken up into a series of less energetic steps.

This simplest thermodynamic cycle can be represented by the following reactions:



The last reaction (Eq.II.3) represents the sum of the other two reactions.

The reactant may be a compound or element: every metal sulphide and some non-metallic sulphides have been considered as part of a cycle.

The most popular cycles are those using metal sulphides.

Chivers *et al.*, (1980) investigated hydrogen yields from lithium, sodium, and potassium metal sulphides and sodium and potassium polysulphides.

Although yields may be higher relative to thermal decomposition, polysulphides are very corrosive and difficult to handle above 923 K.

Al- Shamma *et al.*, (1990) and Chivers *et al.*, (1980) studied vanadium sulphide; vanadium forms a series of non-stoichiometric sulphides that are depicted below (Eq.II.4-II.7):



II.2 Hydrogen and Sulphur production by H₂S thermal

decomposition

In recent years, many efforts have been made for the H₂ production and Sulphur from H₂S by thermal non-catalytic or catalytic decomposition (Slimane *et al.*, 2002).

The thermal H₂S decomposition reaction (H₂S ↔ H₂ + ½ S₂) is highly endothermic (ΔH = 84 kJ/mol) and limited from a thermodynamic point of view; for this reason the reaction, for temperature lower than 1173 K, does not proceed to an industrially important extent (Norman, 1984).

As shown in Figure II.1, the conversion expected from the thermodynamic equilibrium is only about 20% at 1273 K and 38% at 1473 K. In order to reach a H₂S conversion of about 50% it is necessary to reach temperatures more than 1573 K.

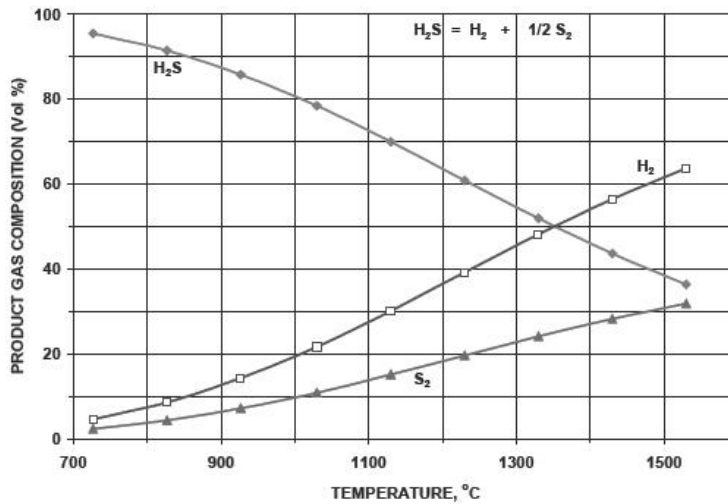


Figure II.1: H₂S Decomposition reaction as function of temperature.

The H₂S thermal decomposition has to overcome technical and economical hurdles that include (Luinstra, 1995):

- Low yields even at high temperature (equilibrium limited)
- Recycle unreacted H₂S to maximize H₂ production
- Need to separate product gases
- Rapid quenching of product gas may be necessary to block any recombination of H₂ and S₂

Anyway, other approaches based on H₂S decomposition were evaluated (such as electrochemical, photochemical, plasma methods, solar dissociation, microwave), but are not applicable on industrial scale always due to the high energy demand (Zaman *et al.*, 1995).

In a bid to solve some of the highlighted problems to make commercialization feasible and attractive, many H₂S thermal decomposition schemes were proposed.

Reed (1986) proposed and obtained a U.S. patent for a modified Claus reaction furnace in which the considerable heat generated is used for the dissociation of H₂S, that takes place in ceramic tubes loaded with a cobalt-molybdenum catalyst.

A portion of the acid gas fed to the main burner is split into the tubes where it undergoes decomposition to hydrogen and sulfur. The hydrogen-laden gas stream combines with the rest of the furnace effluents and the contained hydrogen can be used in the tail gas unit thereby saving cost and space for a reducing burner.

Cox *et al.*, (1998) carried out a simulation study together with an economic evaluation of two process schemes for the thermal decomposition of H_2S using design data. The first scheme involves the recycling of H_2S through a steam methane reforming type furnace so that all possible hydrogen could be extracted. In the second scheme, a once-through configuration was employed where H_2S was passed through a decomposition/exchanger type reactor then on to a conventional Claus sulfur recovery plant.

From the economic evaluation, the production cost of hydrogen was significantly greater for the second scheme because of the lower hydrogen recovery obtained.

Adewale *et al.*, (2016) carried out a process simulation to retrofit commercial SRU (sulphur recovery unit) to accommodate the thermal decomposition of an amount of the acid gas stream using heat from the front end of the Claus Furnace as described from the scheme proposed in Figure II.2.

In these cracking coils, which are a form of retrofit to the Claus burner, the H_2S is split into hydrogen and sulfur. The extent of decomposition depends significantly on the heat exchange between the Claus reactor furnace product gases and acid gas stream in the coils.

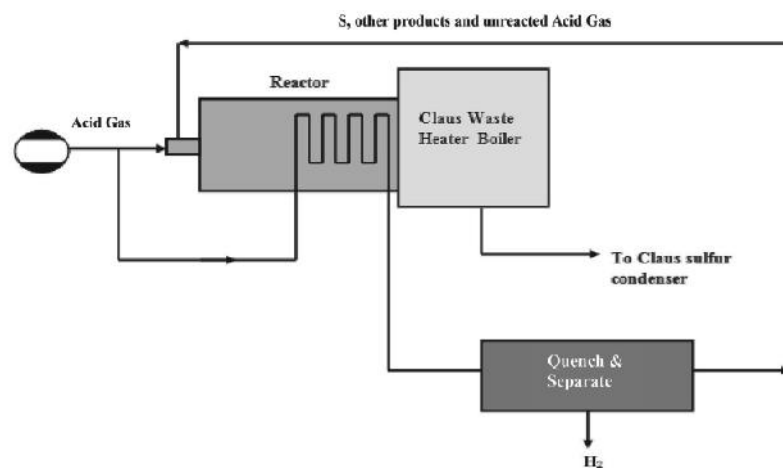


Figure II.2: Thermal cracking of H_2S in modified Claus furnace.

The influence of the split H₂S fraction was studied in terms of H₂ production, thermal reactor energy requirement, steam production.

The study has revealed that up to 24.5% of the total acid gas feed can be cracked without compromising the flame stability of the burner gas stream, the which temperature was found to increase with split amount fraction.

Anyway, in front of a decrease of Claus reaction temperature and SRU unit as a result of the retrofit, an optimized air flow rate was supplied to the Claus burner.

An innovative process that allows to overcome the limitation of the non-catalytic thermal decomposition is based on the oxidation of a small amount of H₂S with oxygen in order to provide the energy required for the H₂S thermal cracking.

Partial oxidation of H₂S reaction is performed in presence of an inert, porous, high-capacity medium and the intense heat exchange results in flame temperatures that significantly exceed the adiabatic flame temperature of the gas mixture. By coupling the partial oxidation of H₂S in the porous medium with the H₂S decomposition, temperatures as high as 1400°C (1673 K) can be achieved economically within a reaction zone without the input of external energy. In this reaction zone, the self-sustaining conditions are very favorable for the decomposition reaction to proceed to an industrially significant extent, within a slowly propagating thermal wave (Slimane *et al.*, 2002).

Slimane *et al.*, (2004), developed a thermodynamic model for the partial oxidation of H₂S in order to study the composition of the products in the superadiabatic partial oxidation regime.

Good agreement of the experimental data conversions with the thermodynamic equilibrium was observed only in the case of the fast chemical kinetics; in fact thermodynamic predictions were usually inapplicable at low temperatures because of the slow rates of chemical reactions.

Respect to the Claus process, the advantage of the superadiabatic decomposition process is the recovery of hydrogen together with Sulphur and the absence of catalyst; furthermore, it is also less stringent than the Claus from the point of view of the required feed gas conditioning and there are not problems linked to the presence of the ammonia and benzene.

The SO₂ formation is not expected to a significant extent obtaining a selectivity to Sulphur of 99%.

Furthermore, depending on the performance of the gas separation devices, the SO₂ concentration expected in the tail gas can be less than that obtained in the Claus process.

The superadiabatic decomposition process is potentially suitable for treating gases containing H₂S at levels as low as 10%.

In order to indicate the good prospects for the superadiabatic H₂S decomposition process, two systems aiming to accomplish the same goal of economically producing hydrogen from H₂S were selected. These systems have undergone significant development and are considered to have acceptable capital costs and good prospects for large-scale hydrogen production, providing that an economical way to separate the hydrogen product can be devised (Luinstra, 1995).

II.3 Kinetic Study on H₂S Pyrolysis

Many studies on the non-catalytic thermal decomposition of H₂S and the reverse reaction between H₂ and S₂ have been reported in the literature, where the kinetics of this equilibrium system over a wide temperature range has extensively examined.

Despite this type of scrutiny within the literature, the reported studies, so far, have failed to provide a unified picture of the overall kinetics within this system, often yielding conflicting results even as to the form of the rate expressions (Dowling and Clark, 1999).

In particular, Darwent and Roberts (1953) claimed a second order dependency on H₂S for the rate of the decomposition reaction, whereas both Raymont (1974) and, more recently, Adesina *et al.*, (1995) have suggested first-order kinetics. In their study of non-catalytic H₂S decomposition, Kaloidas and Papayannakos (1989) also provided a reversible kinetic treatment of the system. These authors, however, implicitly relied on the available kinetic models within the literature. For their model they chose to use first-order kinetics for the H₂S decomposition reaction and a form, $-d[H_2]/dt = k[H_2][S_2]^{1/2}$, for the rate expression of the reverse H₂/S₂ reaction first proposed by Aynsley *et al.*, (1935) at lower temperatures, containing terms first order in H₂ but half-order in S₂.

More recently, the reverse reaction involving H₂ and S₂ was extensively studied by Dowling *et al.*, (1999) over the temperature range from 873 to 1573 K. They reported an experimental rate expression for this reaction different from that used by Kaloidas and Papayannakos.

The form of the rate expression given by these authors was as follows, $-d[H_2]/dt = k[H_2][S_2]$, containing terms first order in both H₂ and S₂.

Similarly, Tesner *et al.*, (1990), have investigated the thermal decomposition reaction at a temperature between 873 and 1473 K and have obtained a second-order homogeneous reaction and an activation energy of 226 kJ/mol.

Many authors have found different values of activation energy E_a in a wide range of temperature shown in Table II.1:

Table II.1: Activation Energy (E_a) for the homogeneous H_2S decomposition.

	Temperature, K	E_a , KJ/mol
Darwent and Roberts (1953)	873	209
Kaloidas and Papayannakos (1989)	873-1133	197
Fukuda <i>et al.</i> (1990)	823-1073	176
Tesner <i>et al.</i> (1990)	873-1473	226
Dowling <i>et al.</i> , (1990)	873-1573	201
Adesina <i>et al.</i> , (1995)	1033-1073	243
Dowling and Clark (1999)	873-1573	218

Although the reported activation energies for the gas-phase decomposition are not in good agreement, they are all much lower than the energy required for S-H bond cleavage (Benson, 1976).

A more rigorous reversible kinetic model was utilized by Dowling *et al.*, (1999), where the experimental data of the thermal H_2S decomposition and $H_2 + S_2$ reaction have been successfully fitted in the range of temperature of 873-1573 K. This model also accurately has predicted the equilibrium behavior system $H_2S/H_2/S_i$ ($i=2-8$) as function of temperature and pressure, species concentrations.

Theoretical models based on a free radical mechanism have been studied at temperatures of 1303-1343 K in a wide range of H_2S concentration (20 -100 vol%) (Adesina *et al.*, 1995). The authors have found a first order respect to the H_2S and a linear rate H_2 production in H_2S partial pressure at all four temperatures examined. Furthermore, the initial step involving the breaking H-S bond appears to be the rate-controlling step rather than the termination involving the combination of two hydrogen radicals.

Dowling and Hyne (1990) studied the kinetics of the reaction between hydrogen and Sulphur under high-temperature Claus furnace conditions (873-1573 K) at different residence times (0.03-1.5 s). They have obtained that the recombination reaction occurs by a reversible homogeneous phase reaction that is the first order in both H_2 and Sulphur concentration.

Faraji *et al.*, (1998) investigated the H_2S cracking at 1273-1473 K in homogeneous phase in a quartz reactor. The authors have obtained H_2S conversion values increasing with the temperature and decreasing with its partial pressure. At 1473 K and with a residence time of 48 s the H_2S conversion reached was 35.6% corresponding to 97.5 of the thermodynamic value. The highest experimental conversion value (66%)

was observed at 1473 K in a more diluted stream containing 5 vol% of H₂S. To the increase of the flowrate and decreasing the initial partial pressure of H₂S, an improvement of the conversion value is obtained.

The higher percentage conversion with increasing the flowrate is due to the inhibiting effect of the high flow rate on the reverse reaction between H₂ and S₂.

At a temperature of 1273 K or higher, the decomposition of hydrogen sulfide proceeds to equilibrium in three seconds or shorter residence time when heat transfer to the substrate gas is sufficiently fast.

Equally significantly, it has been established that the reverse reaction between hydrogen and sulfur to reform hydrogen sulfide upon cooling of the reaction mixture exiting the reactor can be arrested by high flow rates.

A detailed kinetic mechanism was proposed by *Binoist et al.*, (2003) that have studied the pyrolysis of H₂S at a temperature range of 1073-1273 K in a continuous perfectly mixed quartz reactor.

The complete mechanism includes 22 reactions, that 15 are reversible (Table II.2).

Table II.2: Detailed Mechanism of H₂S pyrolysis.

	A (cm ³ ·mol ⁻¹ ·s ⁻¹)	n	E (cal·mol ⁻¹)	no.
H ₂ S + M = H + SH + M	1.76 × 10 ¹⁵	0.0	66 200	R1
H ₂ S + M = H ₂ + S + M	2.39 × 10 ¹⁵	0.0	60 250	R2
H + SH = H ₂ + S	1.29 × 10 ¹³	0.0	7210	R3
reverse	2.70 × 10 ¹⁴	0.0	21 030	R-3
H + H ₂ S = H ₂ + SH	2.90 × 10 ¹⁴	0.0	13 000	R4
reverse	1.18 × 10 ¹⁴	0.0	27 100	R-4
H ₂ S + S + M = H ₂ S ₂ + M	3.60 × 10 ¹²	0.0	0.0	R5
reverse	3.00 × 10 ²⁰	-1.0	52 800	R-5
SH + H ₂ S ₂ = H ₂ S + HS ₂	5.20 × 10 ¹⁴	0.0	6100	R6
reverse	6.80 × 10 ¹⁴	0.0	29 700	R-6
SH + HS ₂ = H ₂ S + S ₂	2.00 × 10 ¹³	0.0	4700	R7
reverse	4.80 × 10 ¹³	0.0	38 400	R-7
SH + S + M = HS ₂ + M	6.00 × 10 ¹¹	0.0	0.0	R8
reverse	6.00 × 10 ¹²	0.0	70 900	R-8
H + S ₂ + M = HS ₂ + M	1.00 × 10 ¹⁸	0.0	1510	R9
reverse	1.00 × 10 ¹⁷	0.0	31 070	R-9
SH + S = H + S ₂	8.97 × 10 ¹⁵	0.0	15 000	R10
reverse	6.98 × 10 ¹⁶	0.0	31 300	R-10
SH + SH + M = H ₂ S ₂ + M	3.20 × 10 ¹³	0.0	0.0	R11
reverse	2.70 × 10 ²²	-1.0	58 600	R-11
SH + S ₂ = S + HS ₂	1.40 × 10 ¹²	0.0	33 700	R12
H ₂ S ₂ + M = H + HS ₂ + M	9.10 × 10 ¹⁹	-1.0	70 200	R13
H ₂ S + S = H + HS ₂	1.80 × 10 ¹³	0.0	25 800	R14
SH + SH = H ₂ S + S	0.75 × 10 ⁸	1.14	100	R15
reverse	2.29 × 10 ⁸	1.30	17 100	R-15
S + S + M = S ₂ + M	1.00 × 10 ¹⁵	0.0	0.0	R16
HS ₂ + HS ₂ = H ₂ S ₂ + S ₂	6.00 × 10 ¹²	0.0	9100	R17
H ₂ S ₂ + H = H ₂ S + SH	6.00 × 10 ¹²	0.0	5200	R18
H + HS ₂ = H ₂ S + S	6.00 × 10 ¹³	0.0	8400	R19
H + HS ₂ = H ₂ + S ₂	4.30 × 10 ¹³	0.0	1400	R20
reverse	4.72 × 10 ¹³	0.0	57 610	R-20
SH + M = S + H + M	6.00 × 10 ¹²	0.0	73 600	R21
reverse	3.60 × 10 ¹⁵	0.0	9300	R-21
S + H ₂ S ₂ = SH + HS ₂	6.00 × 10 ¹²	0.0	8200	R22

Binoist *et al.*, (2003) in order to develop a mechanism of H₂S pyrolysis in a systematic way, determined first of all the prime mechanism considering only the formation of primary products.

In the second step, a secondary mechanism, during which the molecules formed by the primary mechanism react to form other molecules and new radicals, was taken into consideration.

The initiation of the radical reaction is the dissociation of an HS-H bond, indexed as reaction R1 (reaction numbers correspond to the final mechanism presented in Table II.2 (Eq.II.8). The H and SH radicals can then react with the initial reagent (reaction R4) (Eq.II.9).

Then, the radicals react with one another by the processes of recombination (reaction R11) (Eq.II.10), taking into account that the recombination of free atoms (here H and S) is generally negligible.

The primary mechanism of reactant consumption is written below:

Primary mechanism



To generate the secondary mechanism, it is assumed that the molecules formed by the primary mechanism react with other species following the same rules as the ones used to write the primary mechanism (Eq.II.11-14).

Secondary mechanism

Reactions of H₂S₂



(reverse of reaction R11)



Reactions of H₂



A good agreement of the experimental data with model results was achieved in terms of the H₂S conversion, H₂ and S₂ yield at five values of temperature and at different residence time values (Binoist *et al.*, 2003).

Furthermore, the authors have carried out analysis at 1000°C for two values of residence time in order to identify the main reaction paths with the aim to develop a reduced mechanism able to represent the reaction system.

It was possible to reduce the reaction mechanism to 7 species and 9 reactions for the dissociation of H₂S (Table II.3).

Table II.3: *Reduced Mechanism of the H₂S pyrolysis.*

Table 6. Reduced Mechanism of the H ₂ S Pyrolysis				
	A (cm ³ ·mol ⁻¹ ·s ⁻¹)	n	E (cal·mol ⁻¹)	no.
H ₂ S + M = H + SH + M	1.76 × 10 ¹⁵	0.0	66 200	R1
H ₂ S + M = H ₂ + S + M	2.39 × 10 ¹⁵	0.0	60 250	R2
H + SH = H ₂ + S	1.29 × 10 ¹³	0.0	7210	R3
reverse	2.70 × 10 ¹⁴	0.0	21 030	R-3
H + H ₂ S = H ₂ + SH	2.90 × 10 ¹⁴	0.0	13 000	R4
reverse	1.18 × 10 ¹⁴	0.0	27 100	R-4
SH + HS ₂ = H ₂ S + S ₂	2.00 × 10 ¹³	0.0	4700	R7
reverse	4.80 × 10 ¹³	0.0	38 400	R-7
H + S ₂ + M = HS ₂ + M	1.00 × 10 ¹⁸	0.0	1510	R9
reverse	1.00 × 10 ¹⁷	0.0	31 070	R-9
SH + S = H + S ₂	8.97 × 10 ¹⁵	0.0	15 000	R10
reverse	6.98 × 10 ¹⁶	0.0	31 300	R-10
H ₂ S + S = H + HS ₂	1.80 × 10 ¹³	0.0	25 800	R14
SH + SH = H ₂ S + S	0.75 × 10 ⁸	1.14	100	R15
reverse	2.29 × 10 ⁸	1.30	17 100	R-15

At low residence time (0.1 s) the process is initiated by these two reactions (Eqs.II.8, II-15):



These two reactions represent 17% of the overall H₂S consumption (3% for reaction R1 and 14% for reaction R2). Sulfur is accumulated as shown by reactions R10 (SH + S → H + S₂) and R14 (H₂S + S → H + HS₂) followed by reaction R9 (HS₂ + M → H + S₂ + M). These processes allow a sufficient concentration of S₂ thus promoting a kinetic auto-acceleration effect of S₂ on H₂S pyrolysis.

For a higher residence time (1 s), reactions R1 and R2, which cause the consumption of H₂S (forward direction) at low residence time, are

reversed and produce H₂S. In this way, there is an inversion of the direction of reaction for these processes when the residence time increases.

From the comparison of the simulations results obtained by the detailed and reduced mechanism the same results were observed at residence time of 1 s and T=1273 K.

Anyway, the detailed mechanism is necessary to account for large variations of experimental conditions and for the influence of the co-reactants, such as S₂. In fact only a detailed radical mechanism can be used to model coupled reactions (pyrolysis, oxidation, redox reactions of H₂S) because these reactive systems are linked by common intermediate radicals and by cross reactions.

II.3 Thermodynamic and Kinetic of the Claus Reaction

Hydrogen sulphide is considered as a waste stream and therefore the industrial application is very limited.

Currently, the process used to exploit this resource is the Claus process, characterized by the partial oxidation of H₂S to sulphur and water (Eq.II.16).



The reaction (Eq.II.16) is carried out in two stages. In the first stage, the thermal section, one third of the H₂S is oxidized to SO₂ with air or oxygen enriched air at high temperature (1200°C) (Eq.II.17):



This reaction is highly exothermic and is not limited by equilibrium. The unburned H₂S in the acid gas reacts with the SO₂ (Eq.II.18) to yield the stoichiometric H₂S/SO₂ = 2:1 to form elemental sulphur vapour:



About 60-70% of the conversion of H₂S to elemental sulphur occurs in the thermal stage.

In the second stage (i.e. catalytic section), the overall conversion of H₂S to elemental sulphur is increased in a series of catalytic reactors (1 to

3) by reaction of the generated SO_2 and the unreacted H_2S over fixed beds of Claus catalysts at much lower temperatures (463-633 K) (Eq.II.19):



A scheme of the Claus Process is reported in Figure II.3.

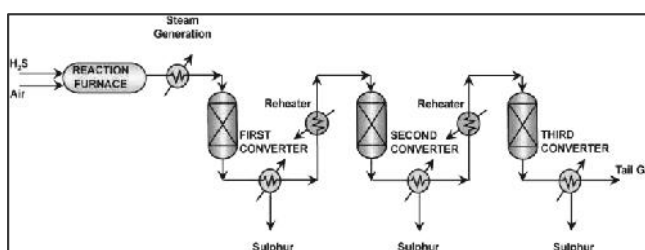


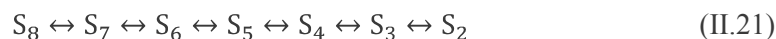
Figure II.3: Schematic Claus Process.

The efficiency of the process is strongly influenced by the thermodynamic limitations because the overall Claus reaction is a reversible reaction (Eq.II.20).



However, the reaction system can be well described by a complex equilibrium, in which there's a simultaneous formation of different products S_2 , S_6 , S_8 , SO_2 and a complex behavior of the H_2S conversion with the temperature.

The reaction (Eq.II.20) is exothermic at low temperature and endothermic at high temperature; this behavior is linked to the thermodynamic equilibrium of the dissociation/association reactions involving the different molecular Sulphur species (S_2 - S_8), that can be represented in this way (Eq.II.21):



The dissociation reactions from forms with a higher number of S atoms in forms a lower number of atoms of S (to the right) are endothermic, while the association reactions (to the left) are exothermic (Eqs.II.22-24):





In Figure II.4 are shown the behavior of the H_2S conversion with the temperature and the Sulphur composition to varying the temperature.

All the curves were calculated without sulphur removal from the system. The shape of the curves in Figure II.4 is a direct result of the temperature dependency of the sulphur vapor composition shown in Figure II.4.

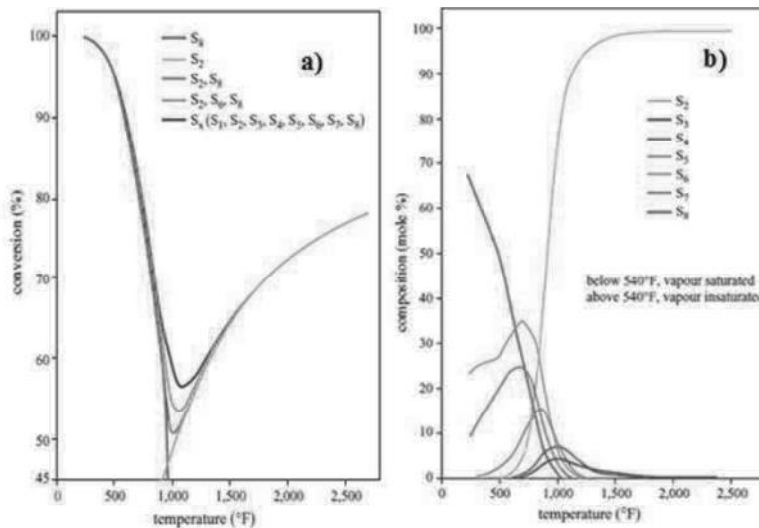


Figure II.4: H_2S conversion (a) and equilibrium composition of sulphur vapor (b) from reaction of H_2S with stoichiometric air at $P= 1.0 \text{ atm}$ (Paskall, 1979)

High molecular weight species predominate at lower temperatures, and vice versa. Thus, for a fixed number of sulphur atoms, fewer moles of sulphur vapour are formed at lower temperatures. This decreases the sulphur vapour partial pressure and tends to shift the equilibrium of reaction (Eq.II.5) to the right as well as increase the conversion. The opposite is true at higher temperatures. The same phenomenon causes the conversion to increase at low temperatures and decrease at high temperatures, as the total system pressure is increased. The theoretical

degree of conversion is high at low temperature, falls off rapidly and passes through a minimum of 833 K (1,040°F), and then increases more slowly at higher temperatures. In the thermal stage region, it is not possible to reach sulphur recoveries of over 70%.

Moreover, care must be taken to quench the reaction mixture rapidly in order to avoid a reverse reaction. To convert more gases to sulphur, thermodynamics suggests lower temperatures in the catalytic region. Before entering catalytic converters, elemental sulphur must be condensed from the gas stream to prevent sulphur condensation on the catalytic bed and improve thermodynamic equilibrium yields. For thermodynamic reasons, the catalytic unit should be operated at as low temperature as possible above the sulphur dewpoint, provided that the rate of the reaction is fast enough. In practice, sulphur recovery is maximized by using two or more catalytic converters with sulphur removal between each converter, and by decreasing temperature in successive converters.

Most studies have focused in the oxidation of H₂S at very high temperatures (Levy & Merryman, 1965; Muller *et al.*, 1979; Zachariah & Smith, 1987), while the second part of the Claus front-end reaction furnace sequence, has received little attention with only one previous study published in open literature (Tesner *et al.*, 1990).

Monnery *et al.*, (2000) studied the Claus reaction by varying the temperature and the residence time with the aim to find a kinetic data in order to develop a new reaction rate expression. Experimental tests were carried out in an isothermal plug-flow reactor at temperatures between 1123 and 1423 K and residence times between 0.05 and 1.2 s.

In Figure II.5 are reported the model predictions and experimental data for H₂S and SO₂ conversion as a function of residence time and temperature.

The H₂S conversion was low at 1123 K for whatever residence time, while at 1423 K, it was relatively high, changing from about 40 to 85% over the same residence time range. Also, the SO₂ conversion is also low at 1123 K, reaching the 5% at a residence time of 1.1 s; conversely at 1423 K, SO₂ conversion has assumed a value about 70% at residence times of 0.63 s. The experimental data have approached equilibrium values at long residence times.

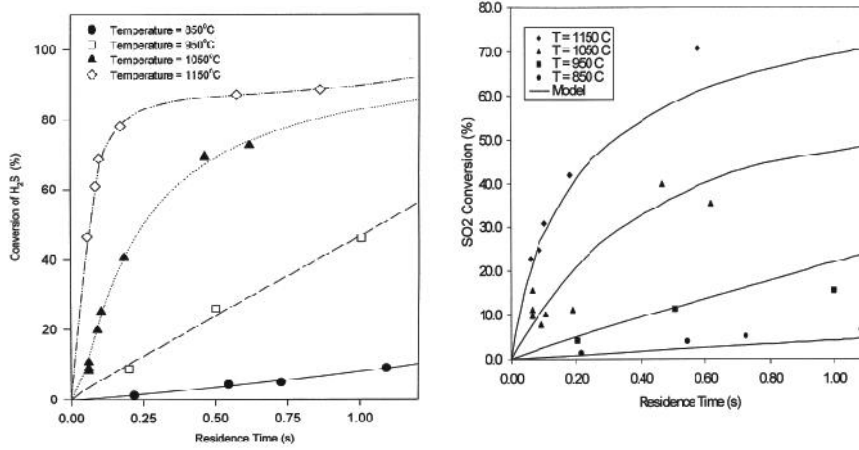


Figure II.5: Comparison of model predictions and new experimental data for H_2S and SO_2 conversion.

Literature Review

III CATALYSTS

III.1 Catalytic H₂S thermal decomposition

The requirement of high temperatures for non-catalytic decomposition of H₂S has motivated several experimental studies in the search of catalysts for its low-temperature decomposition with high H₂ yield.

The sulfides (Fukuda *et al.*, 1978 and Chivers *et al.*, 1987) and oxides (Bishara *et al.*, 1987 and Al Shamma *et al.*, 1989) of transition metals are used as catalysts for heterogeneous high-temperature decomposition of hydrogen sulphide.

The decomposition of hydrogen sulphide on molybdenum disulfide and tungsten catalyst was studied at 773-1073 K by Fukuda *et al.*, (1978). It has been found that molybdenum disulfide catalyst decomposes H₂S effectively into H₂ and elementary Sulphur over the whole range of temperature and it was possible to convert more than 95 %.

Furthermore, also the sulphides of transition metals other than molybdenum and tungsten can be presumed to be effective catalysts for the decomposition of hydrogen sulphide. Lower sulphides as FeS, NiS and CoS are likely to be easily converted in higher sulphides by contact with H₂S at elevated temperatures according to the equations (Eqs.III.1-3):

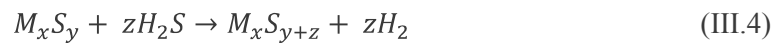


Fukuda and Kotera (1978) compared the catalytic activities of the compounds FeS, NiS and CoS, MoS₂, WS₂ at temperatures and pressures from 773 to 1073 K and from 0.08 to 0.13 atm.

Those higher sulfides are assumed to have poor or no catalytic activities towards H₂S decomposition. The catalytic activity of NiS₂ is much lower as compared with those of MoS₂ and WS₂ likely due to the difficult complete sulfurization of the NiS.

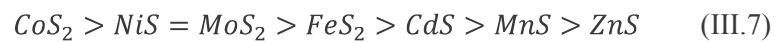
Chivers and Lau (1987) compared the catalytic activity of some metal sulfides powders in the range of temperature of 673-1073 K. For the series Cr₂S₃, MoS₂, WS₂ it was obtained that, MoS₂ is the most active catalyst at T>873 K, but Cr₂S₃ and WS₂ have shown a greater yield of hydrogen at T<873 K, than MoS₂.

Furthermore, they have suggested that the H₂S decomposition can be represented in the form of a two-stage process (Eqs.III.4-6)



The “lowest” metal sulfide M_xS_y interacts with H₂S, forming the “highest” sulfide M_xS_{y+z} and hydrogen (Eq.III.4). The lowest sulfide appears as a result of regeneration of the highest (Eq.III.5), leading to the formation of elementary Sulphur.

Zazhigalov *et al.* (1975) report the following activity order as obtained from experiments carried out in the temperature range of 453-693 K (Eq. III.7):



Yang *et al.*, (1994) have investigated the use of the platinum as a catalyst for H₂ recovery by oxidation and decomposition reactions of H₂S.

The platinum was chosen because the reaction with H₂S is favored up to 1173 K, its oxide decomposes at relatively low temperature. The authors have studied the catalytic performance of the bulk Pt and supported on SiO₂.

Anyway, the based-catalyst noble metal (Pt, Pd, Rh), are rarely employed because are not very active at high reaction temperatures. The Pt-based catalysts supported exhibit good performance towards reactions of hydrogenation, isomerization/hydrocracking of paraffin and nafta reforming. These catalysts easily are poisoned from sulphur compounds; in this way, in order to increase the resistance of the noble metals to the

poisoning by sulphur, it is necessary to modify the electronic properties, realizing bi-metallic catalysts.

Cao *et al.* (1999) verified the activity of many bi-metallic catalysts. The experimental tests were carried out in a fluidized bed reactor in the range of temperature of 883-1003 K at a pressure of 160 kPa. The based-Ru catalysts were supported on γ -Al₂O₃ with addition of another component (MoS₂-RuS₂, MnS-RuS₂, CuS-RuS₂, NiS-RuS₂, FeS₂-RuS₂, ZnS-RuS₂)

Among all the catalysts, the Ru-Mo catalyst was been the more active and selective to the H₂ production, having a low activation energy (70 kJ/mol).

Reshetenko *et al.* (2002), studied the reaction of H₂S thermal decomposition on bulk oxides γ -Al₂O₃, α -Fe₂O₃ and V₂O₅ between 773 and 1173.

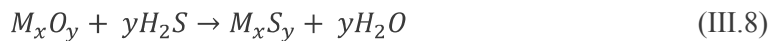
The transformation of oxides to sulfides is accompanied by the decrease in specific surface area, as showed in Table III.1.

Table III.1: Characteristics of the metal oxides before and after reaction (12 h) of the high-temperature H₂S decomposition (Reshetenko *et al.* 2002).

Catalyst	Fresh catalysts			Spent catalysts		
	color	S _{spec.} (m ² /g)	Phase composition	color	S _{spec.} (m ² /g)	Phase composition
γ -Al ₂ O ₃	white	220	γ -Al ₂ O ₃	yellow	115	40% γ -Al ₂ O ₃ , 60% δ -Al ₂ O ₃
V ₂ O ₅	yellow red	4.7	V ₂ O ₅	grey black	3.9	V ₃ S ₄ , V ₂ O ₃ , VOSO ₄
α -Fe ₂ O ₃	red black	19	α -Fe ₂ O ₃	black brown	0.14	Fe ₁₋₂ S

The authors have supposed that the process of H₂S decomposition on transition metal oxide catalysts proceeds in two steps.

Transition metal sulfides are formed on the first step in accordance with the following equation Eq.III.8 (Al-Shamma *et al.*, 1989):



This explains the absence of H₂ evolution along with observed hydrogen sulfide absorption in the low-temperature range. The increase in temperature probably speeds up the process of oxide catalyst reduction and appearance of non-stoichiometric sulfide. The formed sulfide plays a role of an active component of the catalyst.

The results have shown that the reaction of H₂S decomposition occurs at temperatures higher than 873 K and that, by increasing the contact time,

the H₂ yield decreases for all the samples because of the recombination reaction to form H₂S starts to be favored.

They observed that the H₂S decomposition on α -Fe₂O₃ and V₂O₅ catalysts lead to the reduction of these oxides with simultaneous formation of sulphides of Fe²⁺ and V⁴⁺. As a result of the interaction of H₂S with alumina at low temperatures, the adsorbed species of hydrogen sulphide are formed as HS⁻ and S₂⁻, which upon heating transform in the different modifications of elementary sulphur.

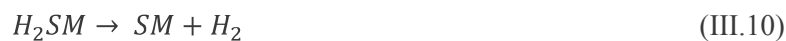
Al Shamma *et al.* (1989), studied the V₂O₅/ γ -Al₂O₃ catalyst in the range of temperature of 773-873 K and they proposed that the H₂S is consumed in two processes, involving the reaction of H₂S with the vanadium oxide that leads to the formation of V₂S₃, H₂O and elementary Sulphur and secondly V₂S₃ becomes an important active center that takes part in the reaction.

An examination of the research work conducted on thermal decomposition shows that only a limited amount of work has been carried out on the kinetics, mechanism and catalyst development.

The kinetic studies have been mostly empirical and there is a large amount of disagreement in the parameter values, with the order of reaction cited as 1 or 2 and the activation energies for the catalytic reaction varying from 50 to 112 kJ/mol. Among the catalysts, only MoS₂ has been investigated to any detail.

Kaloidas *et al.* (1991), carried out studies to determine the kinetics of H₂S decomposition on catalyst MoS₂ in a tubular reactor at a temperature range of 1013-1133 K and pressure of 1.3-3.1 atm. They have found that the rate-determining step of the decomposition reaction is the cleavage of hydrogen-sulphur bonds of the hydrogen sulphide adsorbed on the catalyst active sites and that the catalytic activity of molybdenum sulphide is time and temperature dependent. The activation energy of this step was calculated as 218 kJ/mol.

Based on the obtained results, they have proposed the following reaction scheme (Eqs.III.9-13):



The overall reaction is:



The Eq.III.9 represents the adsorption of the H_2S on the active sites (M) of the catalyst, with consequent cleavage of the bonds between Sulphur and hydrogen atoms, bond formation between the hydrogen atoms and desorption of the H_2 molecular (Eq.III.10). The Sulphur is adsorbed in monoatomic species (Eq.III.11) and reacts with the other atoms of Sulphur (Eq.III.12), leading to the formation of diatomic molecules that represent more than 97% of the Sulphur in the system. The second stage is the controlling step and it is characterized by an activation energy of 218 kJ/mol.

III.2 Catalytic H_2S oxidation

The selection of an appropriate catalyst is an essential part of modified-Claus plant optimization to achieve maximum Sulphur recovery efficiencies. A wide range of industrial catalysts is now available. There are basically five types of industrial Claus catalysts (Ballaguet and Barrere Tricca, 2006).

The most widely used Claus catalyst in sulfur recovery units is non-promoted spherical activated alumina. Properties associated with optimum non-promoted Claus catalyst include high surface area, appropriate pore size distribution, and enhanced physical properties. Catalysts with areas over $300 \text{ m}^2/\text{g}$, macroporosities over 0.15 ml/g , and macropore radii as high as allowed by pellet density should have good performance. Alumina has a surface area of $325 \text{ m}^2/\text{g}$, a macroporosity of 0.14 ml/g , and a macropore radius of 5.3 \AA . Other catalysts sometimes used in the Claus process include activated bauxite (surface area of $184 \text{ m}^2/\text{g}$), cobalt-molybdenum hydrogenation catalyst (surface area of $270 \text{ m}^2/\text{g}$).

Alumina catalysts may be deactivated generally by carbon deposition, capillary condensation of sulfur and sulfation.

Fouling by condensation of sulphur or by deposition of carbon or ammonium salts impairs catalyst activity by plugging the pores. Sulphur deposition is reversible, the catalyst is regenerated by heat soaking with no adverse effect. Carbon and ammonium salts deactivation is essentially irreversible. It is best avoided by reducing contamination of the feed gas (high molecular weight hydrocarbons, ammonia compounds and amines).

All alumina-based sulphur recovery catalysts are prone to the sulphation if exposed to sulphur and/or SO₂ and traces of oxygen. Sulphation is most likely to occur during start-up, shutdown or periods of malfunction when the feed gas/oxygen balance is disturbed. Sulphation is partly reversible with heat soaking under an H₂S/SO₂ ratio above 2:1. However, activity improvement is temporary and repeated rejuvenations result in irreversible damage to the catalyst, shortening its lifespan. It is best avoided by proper oxygen control. However, a study (Clark *et al.* 2002) has shown that the formation of sulphate on alumina is directly related to the oxidizing properties of the solid and the chemistry of H₂S/SO₂ conversion over this material.

The deactivation will lower the conversions, with the consequence of higher sulfur content in the tail gas and correspondingly increased tail gas cleanup costs. The effectiveness factor of the catalyst particle may be improved by increasing either its external area or its pore sizes.

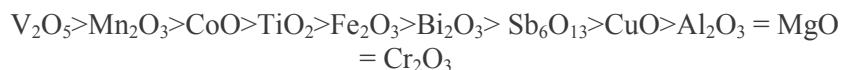
Titanium dioxide-based catalysts (TiO₂-based catalysts) have a higher activity than activated alumina towards carbon sulphide hydrolysis in the first reactor and towards the Claus reaction in all stages (Ballaguet and Barrere Tricca). TiO₂-based catalysts are much less susceptible than alumina to aging and remain virtually unaffected by sulphation. Moreover, they have a virtually unlimited lifespan under normal conditions.

Various promoted activated alumina catalysts are also available. Alumina may be promoted by alkaline earth oxides (calcium or magnesium oxides), TiO₂ or sodium monoxide (Na₂O).

The alkaline earth promoted catalysts were designed to improve the resistance of activated alumina Claus catalysts to sulphation (Ballaguet and Barrere Tricca).

Protective catalysts (iron- and nickel-promoted alumina) are used as a guard bed to protect standard alumina catalysts in Claus reactors against sulphation by reducing the oxygen content of the stream gas.

Generally, for the H₂S oxidation reaction the activity series of oxides is given in (Daydov *et al.*, 2003) :



Just like in the Claus process, standard requirements are imposed on the stability, mechanical strength and cost of the catalysts.

Application of vanadia catalysts is possible in high-temperature processes (Zagoruiko *et al.*, 2010). However, due to the low specific surface area, the activity of pure vanadium oxide per mass unit is lower than of alumina. Nevertheless, the catalytic potential of V₂O₅ can be implemented upon its support on carriers with a developed surface (γ-

alumina and TiO₂). In the case of using of titania as a support, these catalysts are notable for their appreciably high stability toward sulphation and high activity in reactions of COS and CS₂ conversion.

III.3 Catalytic H₂S oxidation in presence of NH₃ and CH₄

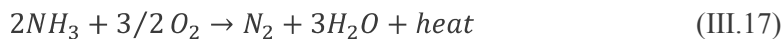
The H₂S decomposition and the oxidation reactions aren't adequate to describe completely an industrial Claus plant. In the industrial case, in fact, they occur numerous parallel reactions that involve different chemical species in a complex system C-O-S-H-N (Chin *et al.*, 2001).

These reactions occur because in the acid gas stream they are also present NH₃, CO₂, and hydrocarbons as the CH₄.

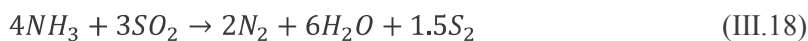
Ammonia represents an impurity and it is generally removed in the thermal stage of the Claus process due to the high temperatures (Goar *et al.* 1986). The removal is necessary to avoid the reaction with SO₂ to produce SO₃, by the following reactions (Eqs. III.14-16):



The presence of sulphur trioxide causes serious problems in the stages subsequent to the reactor, as corrosion, catalyst deactivation and salts formation (Goar *at al.* 1986). Ammonia is completely destroyed by the total oxidation reaction to nitrogen (Eq. III.17):



According to the study performed by Rameshni *et al.* (2008), the oxygen consumption is in competition between H₂S and NH₃ for which the ammonia can be oxidized in presence of SO₂, to Sulphur, nitrogen and water by the following reaction (Eq.III.17):



Industrially, this reaction could be very useful because would involve the conversion of NH_3 and SO_2 , that are undesired products in the refinery streams.

Recent researches have evidenced that such reaction can be responsible for the destruction of ammonia in the Claus furnace at 1473 K.

Usually, the ammonia is co-fed with H_2S together with air or oxygen.

At this proposal, Clark *et al.* (2004 b) have studied the possibility to totally convert the ammonia by using an opportune catalyst. They have carried out experimental tests in the range 573-973 K in presence of $\gamma\text{-Al}_2\text{O}_3$, TiO_2 , $\text{V}_2\text{O}_5/\text{Al}_2\text{O}_3$, Co-Mo oxides/ Al_2O_3 obtaining good activity respect to the oxidation reaction. The vanadium-based catalyst supported on alumina has shown the better catalytic performances, with a total NH_3 conversion at 600°C and with a contact time of 0.75 s.

Furthermore, it was not observed the NO_x formation, while they are obtained H_2S and H_2 likely due to the occurring of these reactions (Eq. III.19-20):



They have investigated how the NH_3 conversion is influenced by varying some operating conditions such as the contact time and the presence/absence of water and oxygen in the feed stream; the increase of the contact time (~ 4 s) has involved a total NH_3 conversion, while the presence of water (~ 10 vol%) has determined a decrease of the conversion differently by the positive role played from the oxygen that has enhanced the efficiency of NH_3 conversion.

The presence of the CH_4 and CO_2 in a refinery stream processed by the Claus process involve the formation of COS, CS_2 that are recognized as the problematic sulfur compounds that contribute significantly to plant sulfur emissions and are also poisons for certain catalysts.

Typically, in the Claus reactor, the CH_4 is in low concentration and should compete very actively with H_2S for the consumption of oxygen; at this proposal, different studies were performed in order to investigate the reaction pathways in medium oxidant conditions and in presence of a reaction system $\text{CH}_4\text{-H}_2\text{S}$ (Chin *et al.* 2001). In this study, however, the authors have not considered other possible reaction pathways such as the decomposition reaction and the reactions where it takes part the sulphur.

In the following studies, Clark *et al.* (1998) considered that the reactions that lead to the formation of by-products such as COS and CS_2

occur in the region anoxic of the thermal furnace where the temperature changes between 1173-1573 K with a residence time variable between 0.5-2 s (Karan *et al.* 2004).

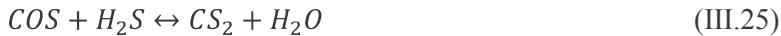
Karan *et al.*, (1999) highlighted that COS is mainly formed at low temperatures (< 1173 K) according to the molecular reaction between CO and H₂S (Eq.III.21):



At higher temperatures the pyrolysis of H₂S becomes relevant and the sulphur produced could react with CO and lead to the COS formation (Eq.III.22):

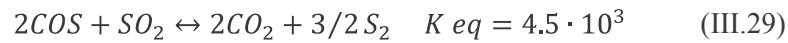
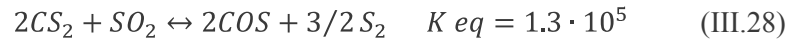


In a more recent work, Clark *et al* (2001) summarized the possible formation reactions of COS and CS₂, in addition to that reported previously (Eqs.III.23-27):



The system is fairly complex given the high number of reaction involved; in this regard, it would consider the reactions of partial oxidation and steam reforming of CH₄.

As a large number of reactions can potentially lead to or assist in the formation/destruction of COS and CO, equilibrium constants were calculated in order to determine the most likely pathways. The high values of the equilibrium constants for the reactions of CS₂, COS and CO with SO₂ suggest that these reactions might represent major pathways for conversion of these species in the Claus furnace (Clark *et al.* 2001). The values of the equilibrium constants at 1373 K are following reported (Eqs.III.28-30):



Finally, Clark *et al.* (2001) suggested a reaction scheme that shows a complex interlinkage among many reactions involving H_2S , CO_2 , CO , COS , SO_2 , and S_2 (Figure III.1).

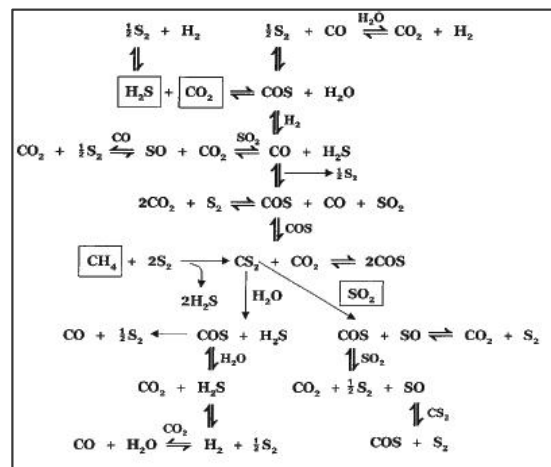


Figure III.1: Scheme of reaction pathways in the Claus furnace (Clark *et al.*, 2001).

As it is possible to see from the scheme, CO and COS can be obtained by more than one pathway.

Since it is not profitable from an economic point of view to place abatement stages for the Sulphur compounds after the Claus catalytic converters, while a valid solution could be that to employ selective catalysts able to inhibit the formation of such compounds.

Gens *et al.* (1994) studied an alumina-based catalyst to avoid the COS , CS_2 formation by favoring the water gas shift reaction next the combustion reaction, preventing to the CO to react with the H_2S to forms COS .

Different investigations were carried out in presence of Al_2O_3 , $Co-Mo$, $Fe-Cr$ - based catalysts.

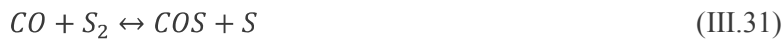
In Table III.2 are compared the results obtained in homogeneous phase and with different catalysts, that have evidenced a low concentration of sulphur compounds respect to the system without a catalyst.

Table III.2: COS formation in the presence and in absence of catalysts (Gens *et al.*, 1994).

catalyst	gas flow (L/min)	vol % of each gas in the product stream					max bed T (°C)
		H ₂	CO	COS	H ₂ S	SO ₂	
none	1.9	0.20	0.21	3.12	0.42	0.73	
none	3.5	0.21	0.22	2.36	0.02	0.07	
none	5.0	0.43	0.81	6.07	0.15	0.05	
none	6.3	0.84	1.03	6.35	0.28	0.89	
Al ₂ O ₃	2.5	0.33	0.03	0.31	0.53	0.01	805
Al ₂ O ₃	3.5	0.52	0.06	0.29	0.48	0.00	
Co-Mo	2.5	0.00	0.01	0.08	0.03	0.01	704
Co-Mo	3.5	0.00	0.01	0.13	1.00	0.00	747
Fe-Cr	2.5	0.07	0.00	0.13	0.01	0.00	797
Fe-Cr	3.5	0.08	0.01	0.17	0.01	0.00	874

Karan *et al.* (1998) have performed kinetic studies of COS/CS₂ homogeneous gas phase reactions.

In this regard, in literature, it is not a detailed and systematic study providing a clear understanding of the actual reaction mechanism that may be involved in the formation/consumption of H₂, CO, COS, and CS₂ in the reaction furnace and waste heat boiler of Claus plants. They have carried out experiments by varying the CO flow rate, the temperature of the Sulphur reservoir and the temperature of the reactor. As expected, the results have confirmed a higher COS yield in presence of longer reactors, high temperatures of sulphur reservoir and lower CO flow rates. Based on these results, they have concluded that the reaction between CO and Sulphur to form COS is very fast and then it can be quenched rapidly at higher flow rates. Since the apparent orders of reaction with respect to the CO and S₂ concentrations are unity, a plausible reaction mechanism for COS formation was proposed on the basis of the following set of reactions (Eqs.III.31-33):



The initial step involves the reaction of CO and S₂ to form COS and atomic sulfur via reaction (Eq.III.31). The sulfur atom can subsequently react with another sulfur atom or with CO (Eq.III.32-33). Association of two atoms or an atom and a diatomic molecule are known to proceed via rapid reactions. Hence, the rate-limiting step for the three reactions is expected the COS reaction formation.

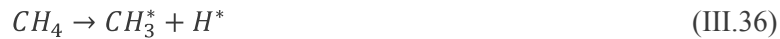
In addition, a kinetic model was developed to account for both the COS formation and decomposition reactions; a low activation energy value ($E_a = 56$ kJ/mol) for COS formation is due to probably to the fact that this reaction proceeds via the formation of the reaction intermediates which have a lower energy barrier respect to the value computed for the COS decomposition reaction ($E_a = 180$ kJ/mol).

Karan *et al.* (2004) have hypothesized that the CS₂ can be obtained by the reaction of CH₄ with sulphur or H₂S, in according to the following reactions (Eq.III.34-35):



The experimental results have evidenced that the CS₂ concentration increases with the residence time and with temperature up to 1473 K. For higher temperatures (1523 K), even increasing the residence time, no significant variations were observed respect to the CS₂ formation. They have noted a higher formation at lower residence times (100 ms) and a rate formation greatly reduced starting from 200-300 ms; this behaviour can be explained considering that the sulphur is a limiting reactant; when the sulphur is in a large amount is favored the CS₂ formation, which then decreases by increasing the residence times.

Chin *et al.* (2001) focused the attention on the possible reaction between CH₄ and SO₂, observing this distribution of the products CO > CS₂ > CO₂ > COS. The carbon monoxide was the main reaction product and was not observed the COS, CS₂ at temperatures lower than 1373 K. They have explained by the following sequence of reactions (Eqs.III.36-41):





Afterwards the C-H scission bond in a molecule of CH₄ (Eq.III.36), the methyl radical could react with SO₂ to form CO and C₂H₄ (Eq.III.37-38); a large amount of SO₂ favors the reaction that leads to the CO formation (Eq.III.37). The hydrogen, produced by the CH₄ decomposition, reduces the SO₂ with the formation of SH and sulphur (Eq.III.39) and finally, this radical within the methyl radical would lead to the CS₂ formation (Eq.III.40-41).

The COS formation was not observed by experimental tests, implicating that the reaction between CH₄ and SO₂ is not directly responsible for the COS production.

Catalysts

IV THERMODYNAMIC ANALYSIS

IV.1 Method to calculate the equilibrium composition

Thermodynamic analysis has been carried out with GasEq program, that is written as a Microsoft Windows program with an easy graphic interface based on the minimization of Gibbs free energy.

It is very useful to calculate the equilibrium product composition of an ideal gaseous mixture when there are a lot of simultaneous reactions, for which it is difficult to use the equilibrium constants only.

The thermodynamic analysis has been carried out considering the following chemical species that could be present at equilibrium: H₂S, O₂, SO₂, S₂, S₆, S₈, H₂O, H₂, and nitrogen.

Considering an initial system of n_i moles for each of the chemical species, the total Gibbs free energy of the system may be expressed as in Eq.IV.1.

$$G = \sum_{i=1}^s n_i \cdot G_i = \sum_{i=1}^s n_i \cdot [(G_i - G_i^0) + G_i^0] \quad (\text{IV.1})$$

Using Eq.IV.2

$$G_i - G_i^0 = R_g \cdot T \cdot \ln \frac{f_i}{f_i^0} \quad (\text{IV.2})$$

Eq.III.1 can be written as Eq.IV.3:

$$G = \sum_{i=1}^S n_i \cdot \left[G_i^0 + R_g \cdot T \cdot \ln \frac{f_i}{f_i^0} \right] \quad (\text{IV.3})$$

where G_i^0 is the free energy of the i_{th} species at normal temperature and pressure (NTP); G_i = free energy of i_{th} species at operating conditions; f_i^0 = fugacity of the i_{th} species at NTP and f_i = fugacity of the i_{th} species at operating conditions used.

Here, all the species are in the gaseous state. Assuming the reaction system pressure to be P , we can write Eq. IV.4.

$$\frac{f_i}{f_i^0} = y_i \cdot \gamma_i \cdot P = \frac{n_i}{n} \cdot \gamma_i \cdot P \quad (\text{IV.4})$$

where n = total number of moles in the reaction mixture included the unreacted species; γ_i = activity coefficient of the i_{th} species and y_i =mole fraction of the i_{th} species.

At low pressure and high temperatures, the system can be considered to be ideal, so that $\gamma_i=1$ and Eq. IV.3 becomes Eq. IV.5:

$$G = \sum_{i=1}^S n_i \cdot R_g \cdot T \cdot \left[\frac{G_i^0}{R_g \cdot T} + \ln \left(\frac{n_i}{n} \right) + \ln(P) \right] \quad (\text{IV.5})$$

Assuming $R_g T$ as independent, we can rewrite Eq. (IV.5) in Eq. (IV.6):

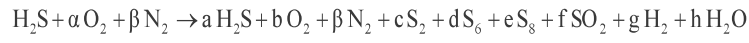
$$\frac{G}{R_g \cdot T} = \sum_{i=1}^S n_i \cdot \left[\frac{G_i^0}{R_g \cdot T} + \ln \left(\frac{n_i}{n} \right) + \ln P \right] \quad (\text{IV.6})$$

The objective function $G/R_g T$ is then minimized to determine the value of n_i .

The thermodynamic analysis has been carried out considering that the following chemical species could be present at equilibrium: H_2S , O_2 , SO_2 , S_2 , S_6 , S_8 , H_2O , H_2 , and nitrogen.

Being the reaction system described by a complex equilibrium, the general reaction used is the following Eq. IV.7:

Chapter IV



(IV.7)

The results are reported in terms of H₂S conversion, selectivity to SO₂, hydrogen yield, S₂ S₆ S₈ yield, defined from Eq.IV.8 to Eq.IV.13:

$$X_{\text{H}_2\text{S}} = \frac{n_{\text{H}_2\text{S}}^{\text{in}} - n_{\text{H}_2\text{S}}^{\text{out}}}{n_{\text{H}_2\text{S}}^{\text{in}}} \quad (\text{IV.8})$$

$$S_{\text{SO}_2} = \frac{n_{\text{SO}_2}^{\text{out}}}{n_{\text{H}_2\text{S}}^{\text{in}} - n_{\text{H}_2\text{S}}^{\text{out}}} \quad (\text{IV.9})$$

$$Y_{\text{H}_2} = \frac{n_{\text{H}_2}^{\text{out}}}{n_{\text{H}_2\text{S}}^{\text{in}}} \quad (\text{IV.10})$$

$$Y_{\text{S}_2} = \frac{2n_{\text{S}_2}^{\text{out}}}{n_{\text{H}_2\text{S}}^{\text{in}}} \quad (\text{IV.11})$$

$$Y_{\text{S}_6} = \frac{6n_{\text{S}_6}^{\text{out}}}{n_{\text{H}_2\text{S}}^{\text{in}}} \quad (\text{IV.12})$$

$$Y_{\text{S}_8} = \frac{8n_{\text{S}_8}^{\text{out}}}{n_{\text{H}_2\text{S}}^{\text{in}}} \quad (\text{IV.13})$$

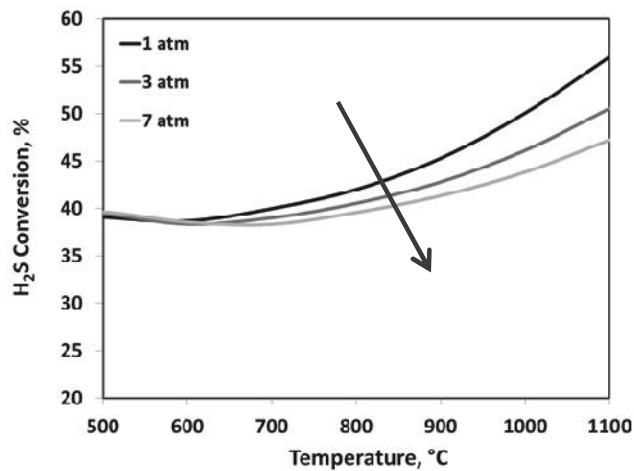
IV.2: Effect of the Pressure and Temperature

The results related to the influence of the pressure (1- 7 atm) on H₂S conversion, H₂ yield, and SO₂ selectivity are reported in the following figure (Figure IV.1).

It is noted, that the value of the H₂S conversion is approximately constant and equal to 40% up to the temperature of 600°C and the effect of the pressure is not significant, because, at low temperature are favored the reactions which, on the whole, do not involve in the variation of the number of moles.

The pressure exhibits a significant effect in terms of H₂S conversion and H₂ yield starting from the temperature of 700°C. In particular, both the H₂S conversion both the H₂ yield values are higher at the lowest operating pressure, because at high temperature, occur the endothermal reactions that are characterized by an increase of the moles number and so, they are favored by low pressures.

The H₂S conversion increases with the temperature, reaching the higher value (55%) at atmospheric pressure and at a temperature of 1100 °C.



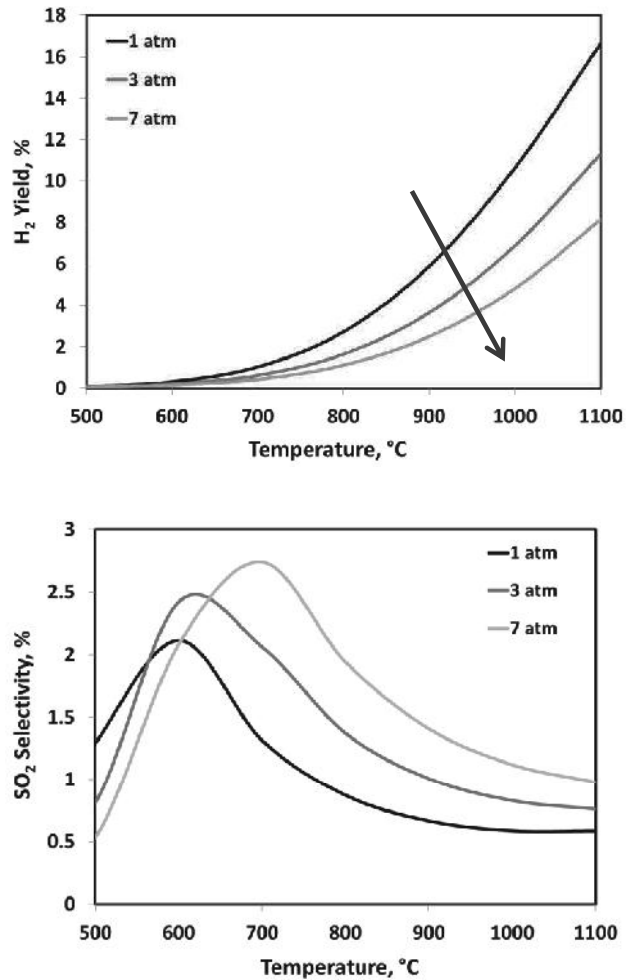


Figure IV.1: Effect of the Pressure on H_2S conversion, H_2 yield, SO_2 selectivity to varying the temperature ($H_2S^{IN}=50\text{vol}\%$, $O_2/H_2S=0.2$).

A similar behavior was obtained for the H_2 yield that increases with the temperature, because the H_2S cracking is particularly favored at high temperature.

Starting from the temperature of 700°C , the H_2 yield quickly increases up at 1100°C , the which value is about 18%.

A more complex trend is noticeable for the SO₂ selectivity that increases at lower temperature up to reach a maximum value at about 600-700 °C and then, it decreases by increasing the temperature.

This behavior is always explainable by assuming a prevalence of oxidation reactions at low temperatures (500-700 °C) while, at intermediate/high temperatures (600-1100°C), prevails the Claus reaction that leads to the consumption of SO₂.

In particular, we have obtained a low SO₂ selectivity (0.5%) value at the highest temperature (1100°C) and P=1 atm.

The influence of the pressure implicates the increase of the maximum and minimum and their displacement towards higher temperature. It is due to the Claus reaction that involves an increase of the moles number and therefore it is not favored by an increase of the pressure.

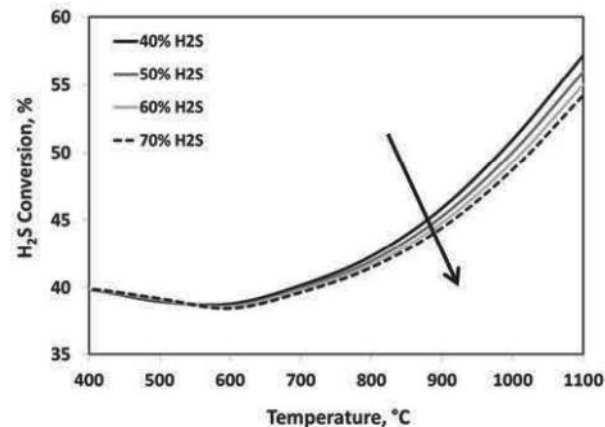
IV.3: Effect of the H₂S inlet concentration

The influence of the H₂S concentration was evaluated at fixed molar feed ratio O₂/H₂S = 0.2, at atmospheric pressure in the range of temperature of 400-1100°C.

The results are shown in Figure IV.2.

The behavior of the H₂S conversion, H₂ yield and SO₂ selectivity with the temperature was explained in the previous paragraph.

We can observe that the increase of H₂S inlet concentration between 40 vol% and 70 vol% (concentrations typically used in the industrial stream that have to be processed) determines a decrease of the H₂S conversion, the H₂ yield, and SO₂ selectivity. The increase of the SO₂ selectivity with the H₂S concentration is evident starting from the temperature of about 600°C.



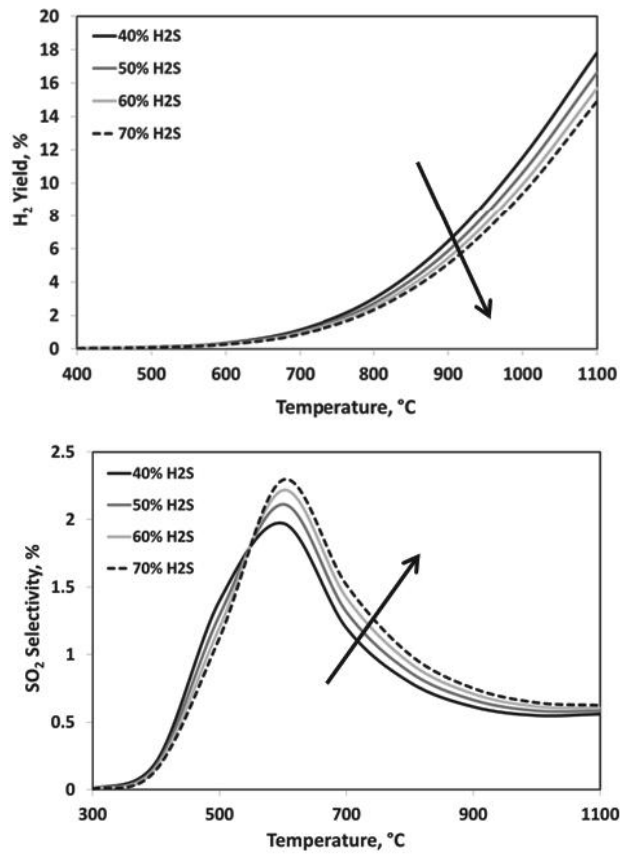


Figure IV.2: Effect of the H₂S concentration on H₂S conversion, H₂ yield, SO₂ selectivity to varying the temperature ($P=1\text{ atm}$, $O_2/H_2S=0.2$).

In Figure IV.3 the yield to the different polyatomic sulphur species (S₂, S₆, S₈) is shown as a function of the temperature at fixed H₂S inlet concentration of 40 vol%.

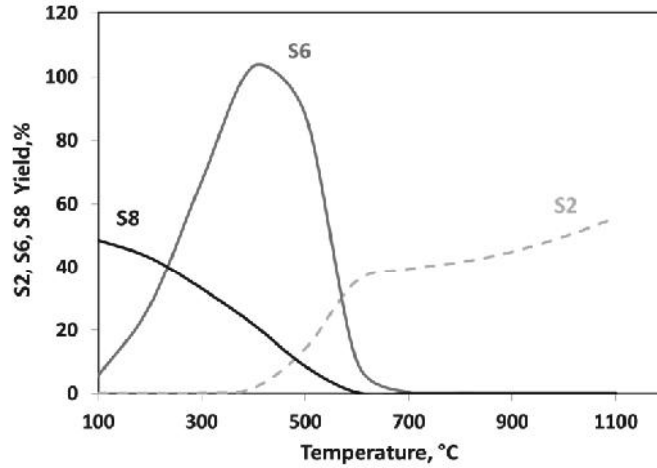


Figure IV.3: Sulphur Yield (S_2 , S_6 , S_8) as a function of the temperature ($P=1\text{ atm}$, $O_2/H_2S=0.2$).

The elemental sulphur (S_8) can be observed at very low temperature; at high temperature ($>700^\circ\text{C}$) only the diatomic S_2 exists in the reaction system, while in the range of temperature between 200-600 $^\circ\text{C}$ we can find two different sulphur species, S_2 and S_6 , respectively, in agreement with the equilibrium of the dissociation/association reactions (Eqs.IV.14-16):



The dissociation reactions are endothermic, while the association reactions are exothermic.

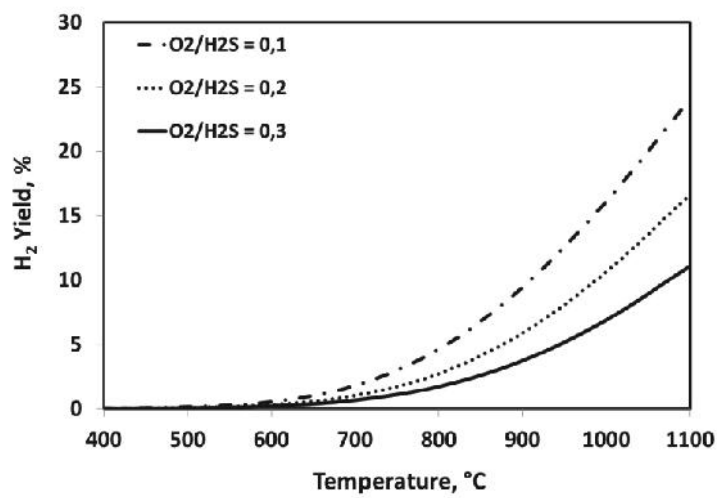
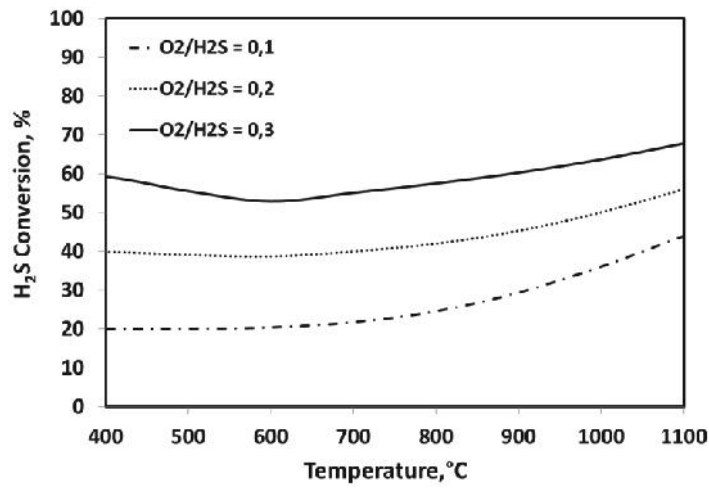
IV.4: Effect of the Feeding Molar Ratio (O_2/H_2S)

The evaluation of the molar feeding ratio O_2/H_2S was studied varying the temperature with an H_2S concentration of 50 vol%.

The results are reported in the following figure (Figure IV.4).

To the increase of the oxygen concentration in the feed stream, it is possible to observe an increase of H_2S conversion and a decrease of the H_2

yield because are more favored the oxidation reactions. In this regard, the SO_2 selectivity rises by increasing the oxygen, at the expense of the yield to sulphur.



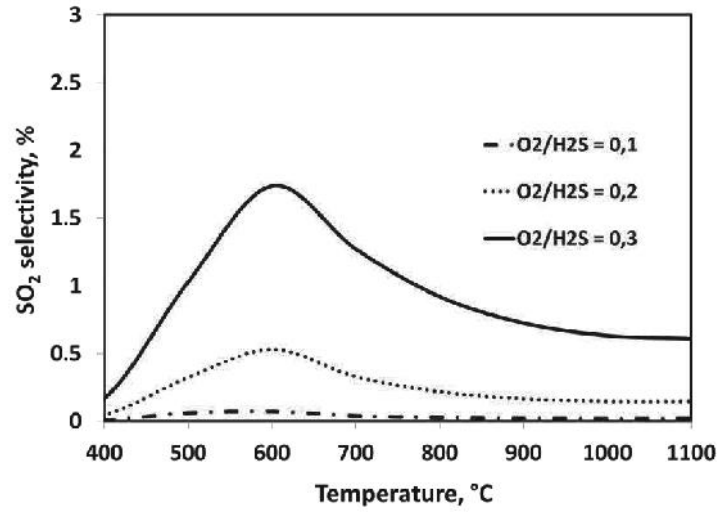


Figure IV.4: Influence of the molar feed ratio (O_2/H_2S) on H_2S conversion, H_2 yield, SO_2 selectivity as a function of the temperature ($H_2S^{IN} = 50\text{vol}\%$, $P = 1\text{atm}$).

IV.5: Effect of O_2/H_2S on ΔH reaction

The complexity of the reagent system, characterized by exothermic and endothermic reactions, implicates that the operating parameters such as molar feed ratio and temperature can have very important effects respect of the enthalpy variation.

From an industrial point of view, it can be very useful to identify operating conditions in which the system is a-thermal. In fact, in this case, the heat produced by the exothermic reactions is absorbed by the endothermic minimizing the energy intake to support the process.

In order to determine these conditions, a calculation of ΔH of the entire system has been carried out to vary the process parameters (temperature and feed ratio), referring in any condition relating to the equilibrium composition.

The Figure IV.5 shows the trend of ΔH with the temperature as a function of the molar feeding ratio.

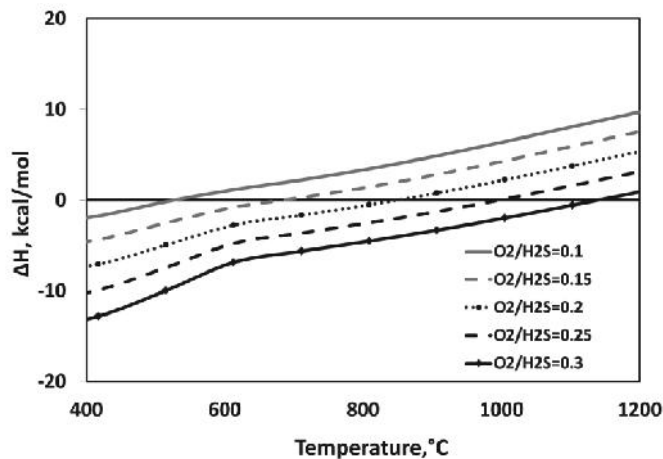


Figure IV.5: Thermal Tonality by varying the molar feed ratio as a function of the temperature ($H_2S^{IN} = 50\text{vol}\%$, $P=1\text{atm}$).

As it can be seen from Figure IV.5, for a typical industrial refinery stream containing a high H_2S concentration (50 vol%), the conditions such to give auto-thermal the reaction system, will be reached at temperatures close to 1 and for O_2 / H_2S between 0.2 and 0.25.

**IV.6: Thermodynamic Equilibrium for the reaction system in
presence of CH₄ and NH₃**

From the thermodynamic analysis carried out on the reaction of the oxidative decomposition of H₂S to sulphur, it was possible to find the operating conditions able to maximize the H₂S conversion and H₂ yield, depressing the SO₂ formation ($P = 1 \text{ atm}$, $T = 1000-1100^\circ\text{C}$, $O_2/H_2S = 0.2$).

Starting from the results obtained, a new thermodynamic study was performed in order to identify the equilibrium conditions in presence of CH₄ and NH₃ in the feed stream.

The results of the simulation were shown in terms of H₂S, CH₄, NH₃ conversion, selectivity respect to SO₂, CO, CO₂, COS, CS₂ and H₂ yield (Eqs.IV.17-26).

$$X_{H_2S} = \frac{n_{H_2S}^{in} - n_{H_2S}^{out}}{n_{H_2S}^{in}} \quad (\text{IV.17})$$

$$X_{CH_4} = \frac{n_{CH_4}^{in} - n_{CH_4}^{out}}{n_{CH_4}^{in}} \quad (\text{IV.18})$$

$$X_{NH_3} = \frac{n_{NH_3}^{in} - n_{NH_3}^{out}}{n_{NH_3}^{in}} \quad (\text{IV.19})$$

$$S_{SO_2} = \frac{n_{SO_2}^{out}}{n_{H_2S}^{in} - n_{H_2S}^{out}} \quad (\text{IV.20})$$

$$S_{CO_2} = \frac{n_{CO_2}^{out}}{n_{CH_4}^{in} - n_{CH_4}^{out}} \quad (\text{IV.21})$$

$$S_{CO} = \frac{n_{CO}^{out}}{n_{CH_4}^{in} - n_{CH_4}^{out}} \quad (\text{IV.22})$$

$$S_{CS_2} = \frac{n_{CS_2}^{out}}{n_{CH_4}^{in} - n_{CH_4}^{out}} \quad (\text{IV.23})$$

$$S_{COS} = \frac{n_{COS}^{out}}{n_{CH_4}^{in} - n_{CH_4}^{out}} \quad (\text{IV.24})$$

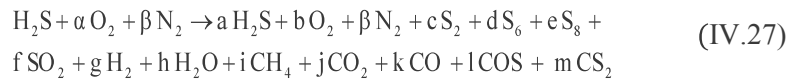
The H₂ yield was calculated respect to the feed stream containing in one case only CH₄, and the other only NH₃ where nⁱⁿ e n^{out} represent respectively, the initial moles and the produced moles.

$$Y_{H_2} = \frac{2n_{H_2}^{out}}{2n_{H_2S}^{in} + 4n_{CH_4}^{in}} \quad (IV.25)$$

$$Y_{H_2} = \frac{2n_{H_2}^{out}}{2n_{H_2S}^{in} + 3n_{NH_3}^{in}} \quad (IV.26)$$

IV.6.1. Thermodynamic Equilibrium in presence of CH₄

The thermodynamic system is described by the following global reaction (Eq.IV.27):

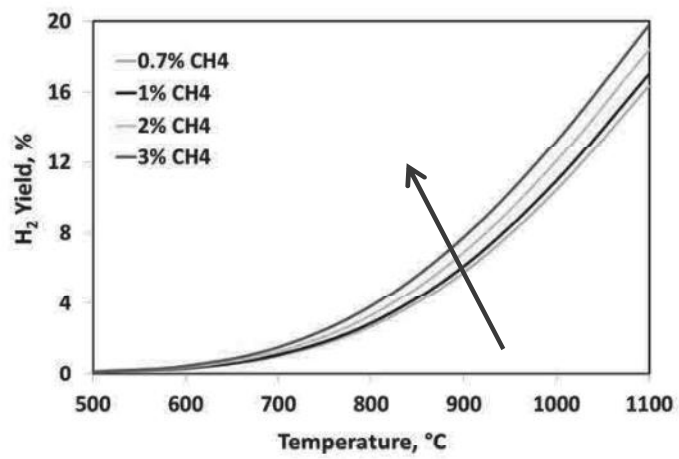
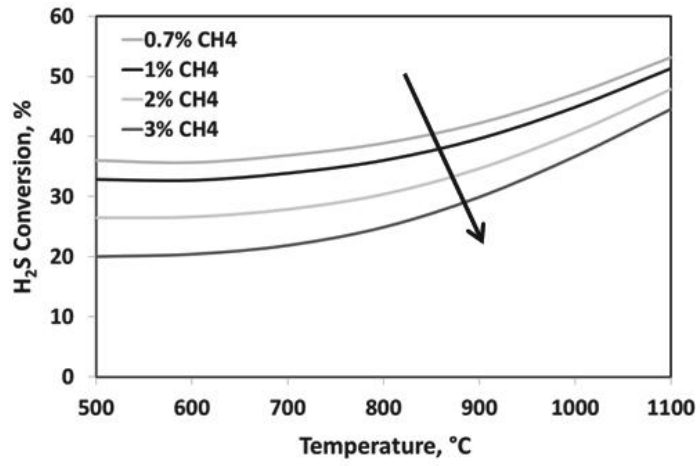
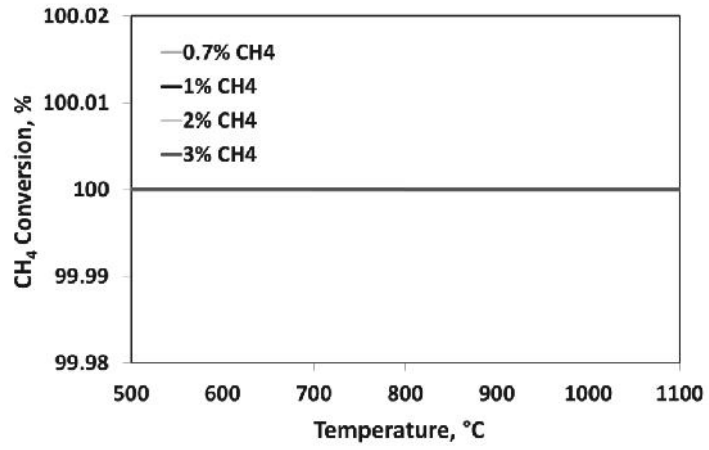


The operating conditions are:

- P=1 atm;
- T=500-1100 °C;
- H₂S inlet concentration: 60 vol%;
- CH₄ inlet concentration: 0.7-3 vol%;
- O₂/H₂S = 0.2

It was considered a high value of H₂S inlet concentration because is the one typically industrially employed.

In Figure IV.6, the influence of the CH₄ is reported in terms of H₂S and CH₄ conversion.



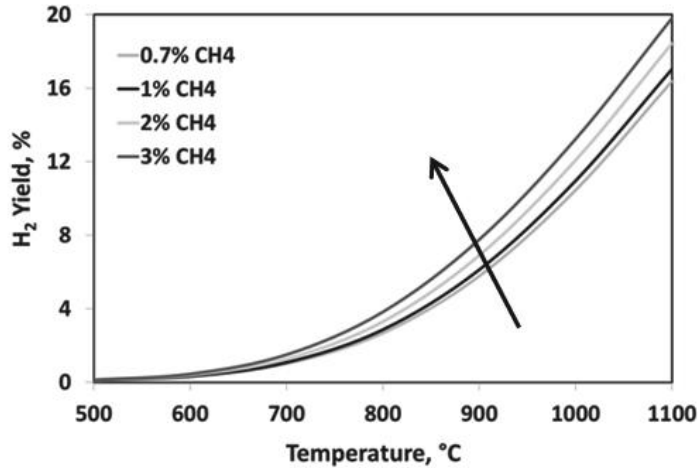


Figure IV.6: Effect of the CH₄ concentration on CH₄ conversion, H₂S conversion, H₂ yield to varying the temperature ($P=1$ atm, $H_2S = 60$ vol%, $O_2/H_2S=0.2$).

The CH₄ conversion is total in all the range of temperature investigated, while the H₂S conversion increases with the temperature but decreases to the increase of the CH₄ inlet.

In particular, the H₂S conversion is constant up to the temperature of 700°C.

In the range 600-700 °C, the increase of the CH₄ inlet involves the diminution of the H₂S conversion; this behavior can be imputed to the competition between CH₄ and H₂S for the consumption of the oxygen.

The decrease of the H₂S conversion could be due to the reaction between CH₄ and S₂ to form H₂S and CS₂ (Karan and Behie, 2004).

Starting from the temperature of 900°C, whatever it is the CH₄ concentration, the H₂S conversion quickly increases because the thermal cracking of H₂S to produce H₂ and Sulphur is favored. The H₂ yield, as it is possible to see in Figure IV.6, is very low in the range 500-600°C, while it begins to increase very quickly starting from the temperature of 700°C up to 1100°C. The trend of the H₂ yield with the temperature is due to the endothermic reaction of H₂S decomposition. Furthermore, by increasing the CH₄ concentration, the H₂ yield increases because, in addition to the H₂S cracking reaction, are also favored the reactions of steam reforming and partial oxidation of CH₄.

A different trend was obtained for the SO₂ selectivity showed in Figure IV.7.

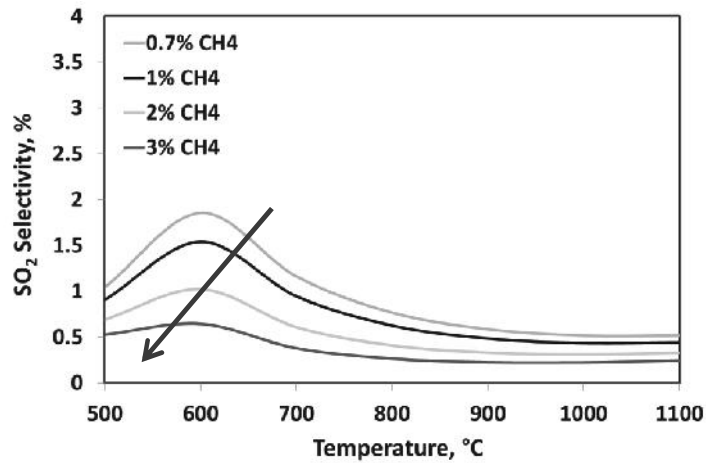


Figure IV.7: Effect of CH₄ concentration on H₂ yield and SO₂ selectivity by varying the temperature ($P=1$ atm, $H_2S = 60$ vol%, $O_2/H_2S = 0.2$).

It is noticeable the presence of a maximum value of SO₂ at 600°C, that becomes more widened to the increase of the CH₄ inlet concentration likely due to the competition of the CH₄ with H₂S for the consumption of the oxygen, or as reported in the literature (Chin *at al.* 2001), this behaviour can be ascribable to the reaction of SO₂ with the products of CH₄ oxidation (COS, CS₂). A possible reaction could be $CS_2 + SO_2 \rightarrow COS + S_2$.

After the maximum peak, the SO₂ selectivity decreases, reaching a minimum and constant value at 900-1000°C; this can be explained considering that, at low temperature (400-600°C) prevail the oxidation reactions, while at higher temperatures (600-1100°C) the Claus reaction is favored.

The trend of the CO₂ and CO selectivity with the temperature, by varying the CH₄ concentration, is reported in Figure IV.8.

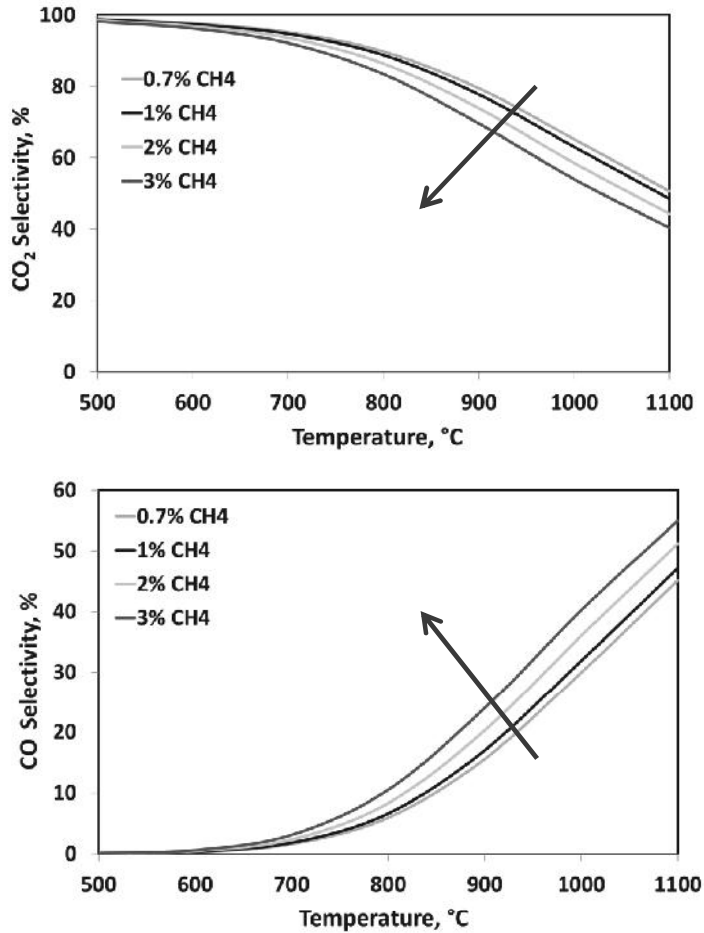


Figure IV.8: Influence of the CH_4 concentration on CO_2 and CO selectivity by varying the temperature ($P=1 \text{ atm}$, $\text{H}_2\text{S} = 60 \text{ vol}\%$, $\text{O}_2/\text{H}_2\text{S} = 0.2$).

The CO_2 selectivity decreases by increasing the temperature and with a higher CH_4 inlet concentration.

The total oxidation reaction of CH_4 to CO_2 is much favored at 500-700 °C; at higher temperatures, starting from the $T=800^\circ\text{C}$, the selectivity decreases because, in this conditions, is favored the partial oxidation that leads to the CO formation. This assertion is confirmed by the behavior of the CO selectivity by increasing the temperature.

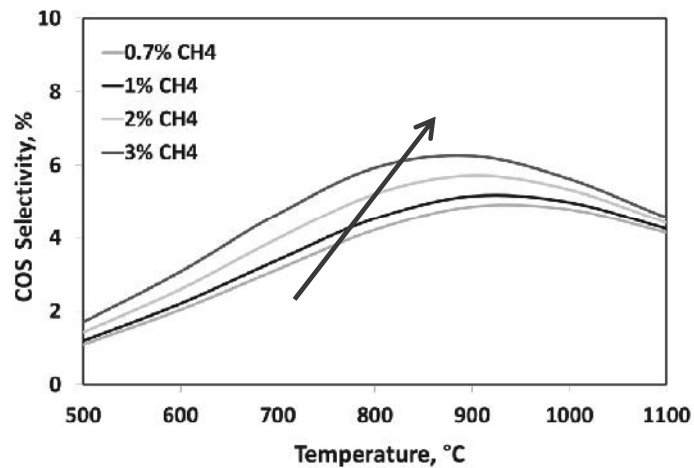
It can observe that, at a fixed temperature, and by increasing the CH_4 concentration, the CO selectivity increases with diminution of the CO_2 selectivity; furthermore, it's worth to note that, the products are not only

CO, CO₂, but also COS, CS₂, obtained from the reaction of CO, CO₂ with S₂, or H₂S and probably, even by the reaction of CH₄ with Sulphur (Eqs.IV.28-33).



Such formation is confirmed by the following graph (Figure IV.9).

For both the components (COS, CS₂), the selectivity increases with the temperature and the CH₄ inlet concentration, up to a maximum of 800-900°C and then begins to decrease.



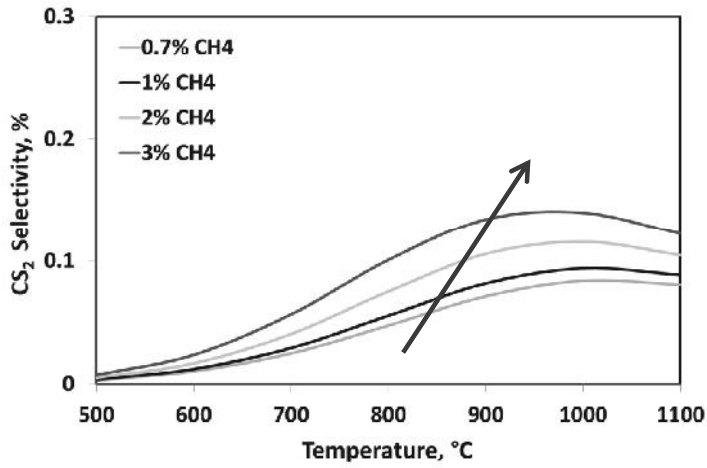
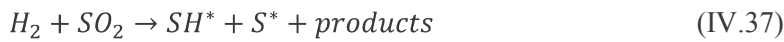


Figure IV.9: Influence of the CH₄ concentration on COS and CS₂ selectivity by varying the temperature ($P=1$ atm, $H_2S = 60$ vol%, $O_2/H_2S = 0.2$).

The formation of COS, CS₂ at temperatures <1000°C is proved by the literature (Chin *at al.*, 2001), where it is proposed a reaction mechanism that is following reported (Eqs.IV.34-39):



Also in this case, it was evaluated the thermal tonality in a wide range of temperature and by varying the molar feed ratio O₂/H₂S (Figure IV.10).

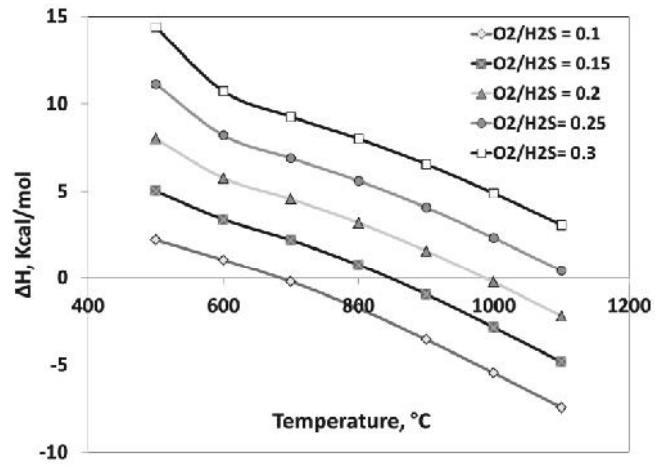
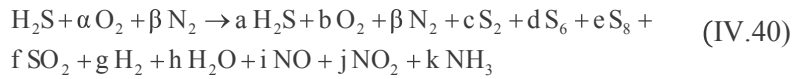


Figure IV.10: Thermal Tonality by varying the molar feed ratio as a function of the temperature ($H_2S^{IN} = 60\text{vol}\%$, $P = 1\text{atm}$).

Starting from the temperature of 1000°C, and for $O_2/H_2S = 0.1-0.2$, it is not necessary to provide heat to the reaction system, since that is able to self-sustaining.

IV.6.2: Thermodynamic Equilibrium in presence of NH₃

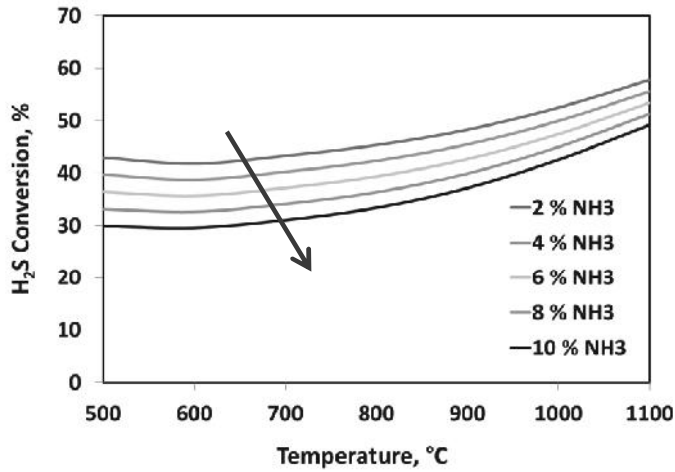
The reaction system in presence of NH₃ can be described by the following equation (Eq.IV.40):



The behavior of the H₂S conversion (Figure IV.11) as a function of the NH₃ inlet concentration is the same of the case in presence of CH₄; it increases with the temperature but decreases by feeding NH₃ in the reaction system.

The presence of ammonia involves a slight diminution of the H₂S conversion; this could be due to the occurring of the reaction between NH₃ and SO₂ to produce H₂S, N₂, and H₂O.

Relatively to the NH₃ conversion, as in the case of CH₄ studied previously, is practically total in all the range of temperature investigated (Figure IV.11).



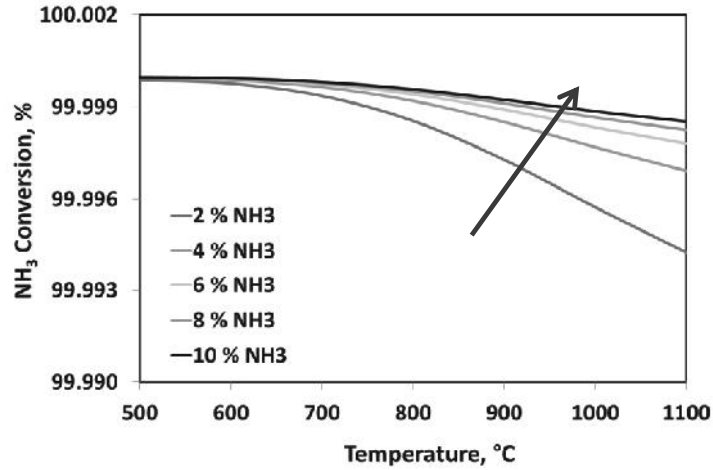
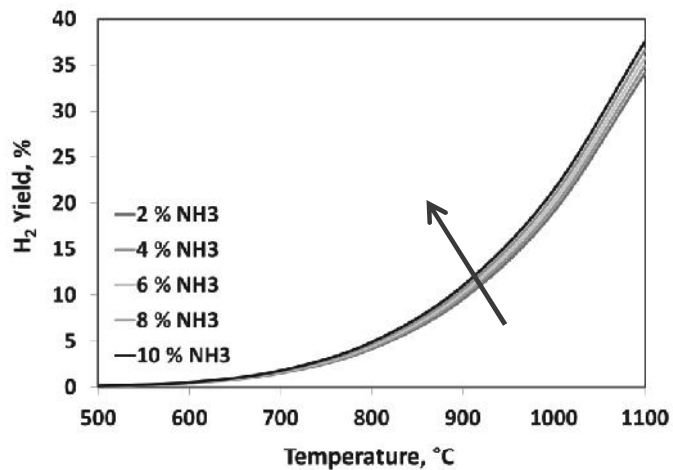


Figure IV.11: Influence of the NH₃ concentration on H₂S and NH₃ conversion by varying the temperature ($P=1\text{ atm}$, $H_2S = 60\text{ vol\%}$, $O_2/H_2S = 0.24$).

In Figure IV.12 are showed the H₂ yield and the SO₂ selectivity.

The H₂ yield increases with the temperature and NH₃; at lower temperatures, the hydrogen is produced from the NH₃ decomposition, because the cracking of H₂S does not occur in these conditions while at a higher temperature ($T > 900^\circ\text{C}$) it's formed both NH₃ and H₂S decomposition.



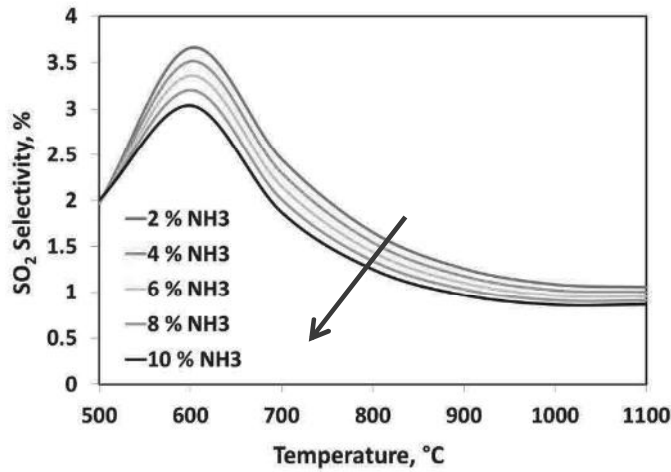


Figure IV.12: Influence of the NH₃ concentration on H₂ yield and SO₂ selectivity by varying the temperature ($P=1\text{ atm}$, $H_2S = 60\text{ vol\%}$, $O_2/H_2S = 0.24$).

The behavior of the SO₂ is characterized by the maximum value at 873 K decreasing to the increase of the temperature.

Even if the behavior is the same as the one obtained with H₂S and CH₄, the presence of NH₃ has entailed a slight increase of the SO₂ selectivity, especially at the lower concentrations.

In this study, it was considered the possible formation of NO_x (NO, N₂O, NO₂, N₂O₃, N₂O₅) and the results have not shown the presence of these components.

The thermal tonality was studied at different molar feed ratio as a function of the temperature (Figure IV.13).

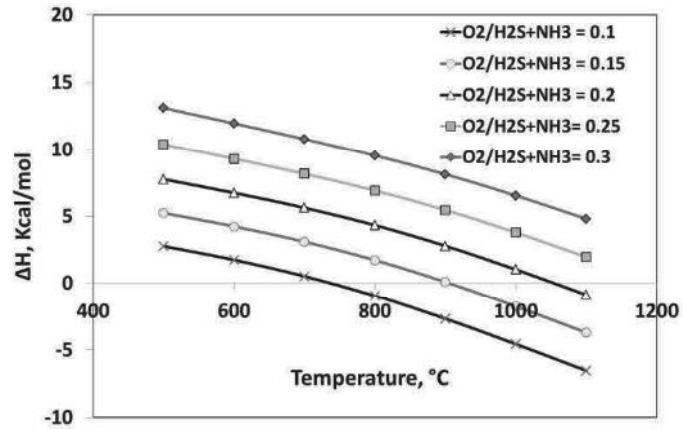


Figure IV.13: *Thermal Tonality by varying the molar feed ratio as a function of the temperature ($H_2S^{IN} = 60 \text{ vol\%}$, $P = 1 \text{ atm}$).*

Also, in this case, the reaction system is auto-thermal for the molar feed ratio between 0.15 and 0.25 starting from the temperature of 1000°C.

IV.7 Conclusion of the Thermodynamic Study

For this analysis, the attention was focused on the identification of optimal operating conditions to maximize the yield to H₂, minimize the selectivity to SO₂ and the heat absorbed when the feed stream is a mixture of H₂S, CH₄, NH₃.

In the reference case, comprising only H₂S and O₂, the calculations showed that, to ensure values of industrial interest, it is necessary to achieve temperatures greater than or equal to 1000°C in order to obtain an efficient H₂S conversion. In this aim, high temperature (1000-1100°C) favors the H₂S cracking reaction and then the H₂ production.

The pressure that enables good yields to H₂ and low SO₂ concentration is the atmospheric pressure.

As for the ratio O₂/H₂S, the value of 0.2 is the one which allows high selectivity to hydrogen and the lowest values of selectivity to SO₂.

Finally, from the evaluation of the enthalpy of the reaction system to vary of the temperature and feeding molar ratio, it was observed that, for temperatures close to 1000 °C and O₂/H₂S = 0.2-0.25, the system is athermal, and then is self-sustaining.

Based on preliminary studies, the temperatures of 1000-1200°C, molar feed ratio between 0.2 and 0.25 are the starting operating conditions for the study of the oxidative decomposition reaction by experimental tests to be conducted in a laboratory plant suitably designed.

In presence of CH₄ and NH₃, in order to guarantee a high H₂ yield and a low SO₂ selectivity, it would be better to feed high concentration of CH₄ and NH₃. The presence of these components involves, however, a lower H₂S conversion, for which, an optimal condition could be that to feed CH₄, NH₃ in low concentrations, because of the competition reactions that occur between CH₄, NH₃, and H₂S for the consumption of oxygen.

Furthermore, the thermodynamic study has evidenced that the reaction system, also in presence of CH₄ and NH₃ is self-sustaining at a temperature of 1000°C and in presence of molar feed ratio between 0.1 and 0.2.

V MATERIALS & METHODS

V.1 Powder Catalyst Preparation

MoS₂ based catalysts with a sulphide nominal loading ranging between 5 and 20 wt% were prepared by impregnation-precipitation of γ -Al₂O₃. Aqueous solution of ammonium heptamolibdate tetrahydrate (NH₄)₆Mo₇O₂₄·4H₂O, and γ -alumina (γ -Al₂O₃) provided by Sigma Aldrich, were used in the preparation procedure. The support was previously calcined at 900°C for 12h. In order to prepare each sample, a known amount of (NH₄)₆Mo₇O₂₄·4H₂O was dissolved in water, and the support was added to the solution. This solution was placed on a heating until the complete evaporation of water. The samples so obtained, were calcined in static air at 450 °C for 3 h.

After the calcination, the sulfidation procedure was carried out to transform the molybdenum oxide to molybdenum disulfide (MoS₂) that represents the active phase of the catalyst. The sulfidation was performed in a quartz reactor containing the catalyst to be sulfurized. In particular, the activation step has been realized by feeding a gaseous stream containing H₂S in N₂ with a H₂S concentration of 5 vol%, by increasing the temperature up to 1000°C with a controlled heating rate of 20 °C/min.

Finally, the catalysts have been reduced to the size 355-710 micrometer.

The same procedure was adopted for the preparation of the bimetallic catalyst.

FeS₂-MoS₂ and CoS₂-MoS₂ based catalysts supported on γ -Al₂O₃ were prepared by co-precipitation of the salts precursors, cobalt acetate tetrahydrate (CH₃COO)₂Co₄H₂O for the cobalt and iron acetate (CH₃COO)₂Fe for the iron, both provided by Sigma Aldrich.

All the catalysts prepared are listed in the following Table V.1.

Table V.1: *Schedule of the powder catalysts with the load of active phase.*

Active Phase Load, wt%		
MoS ₂	FeS ₂	CoS ₂
5	/	/
10	/	/
20	/	/
/	5	/
10	/	5
10	5	/

V.2 Catalyst Characterization

Catalyst characterization was carried out to identify the properties of the catalyst that are responsible for the catalytic activity. The different techniques used for the catalysts characterization include Thermogravimetric Analysis (TG), Powder X-Ray Diffraction (XRD), Raman Spectroscopy, Specific Surface Area measurement. The different characterization techniques are briefly described in the following sections.

V.2.1 Thermogravimetry Analysis (TG)

Thermogravimetric analysis (TGA) is a thermal analysis technique which measures the weight change in a material as a function of temperature and time, in a controlled environment. This can be very useful to investigate the thermal stability of a material, or to investigate its behaviour in different atmospheres (e.g. inert or oxidizing). It is suitable for use with all types of solid materials, including organic or inorganic materials.

Thermogravimetric analysis were carried out in a thermogravimetric analyzer *Q600, TA Instrument*, coupled with PFEIFFER ThermoStar Quadrupole Mass Spectrometer.

SDTQ600 provides a simultaneous measurement of weight change (TGA) and heat flow (DSC) on the same sample from ambient to 1000 °C. It features a proven horizontal dual beam design with automatic beam growth compensation, and the ability to analyze two TGA samples simultaneously.

DSC heat flow data is dynamically normalized using the instantaneous sample weight at any given temperature. The sample is loaded in a crucible made of alumina and heated in the horizontal oven. There are two thermocouples to control the oven temperature and the sample temperature.

The Pfeiffer Vacuum Benchtop Thermostar mass spectrometer can measure the gas evolved from thermal analyzers up to 300 AMU. Both systems, the Mass Spectrometer and the Thermal Balance, are connected to the same PC for data acquisition.

V.2.2 X-Ray Diffraction (XRD)

The diffraction with X-rays was employed for the identification and characterization of the crystalline phases present in the samples analyzed. It also allows to quantitatively detect the presence of different crystalline phases of materials.

It is composed of an X-ray generator, a detector for measuring the position and the intensity of the diffracted rays. It is designed according to the geometry of Bragg reflection.

When a beam of monochromatic X-rays with a wavelength λ is incident on a lattice plane with an angle θ , it creates a diffraction if the path of the reflected rays by the successive planes (with a distance d) is a multiple of the length wave. If the irradiated material is crystalline, as in the case of metals, the diffused waves interfere with each other giving rise to a diffraction spectrum.

The analyzes of the samples were carried out for 2θ values in the range $20-80^\circ$ while have been used, to invest the sample, $\text{CuK}\alpha$ radiation.

V.2.3 Raman Spectroscopy

Raman spectroscopy is a technique used to observe vibrational, rotational modes in order to obtain detailed information on the chemical composition, molecular structure and interactions of the sample analyzed.

It relies on inelastic scattering, or Raman scattering, of monochromatic light, usually from a laser in the visible, near infrared, or near ultraviolet range. The laser light interacts with molecular vibrations, phonons or other excitations in the system, resulting in the energy of the laser photons being shifted up or down. The shift in energy gives information about the vibrational modes in the system.

The information wave intensity / length is sent to the PC and processed by Wire 2.0 software to give the Raman spectrum.

V.2.4 Specific Surface Area (SSA)

The surface area measurement is based on B.E.T. method, acronym derived from the originators scientists (Brunauer, Emmett, Teller) according to which the nitrogen molecules are adsorbed on the material creating several successive layers and the coating of the surface can take place with different rate constants as a function of the state of the sites. During the nitrogen adsorption on the surface of the sample, the partial pressure of the gas initially decreases and then begins to increase until it

reaches the initial value. The measurement is carried out for the known pressure values, in correspondence of which it calculates the amount of adsorbed gas. It generates the adsorption isotherm that shows the adsorbed volume as pressure function.

The BET equation is the following (Eq.V.2):

$$\frac{P}{[V \cdot (P - P^0)]} = \frac{1}{c \cdot V_m} + (c - 1) \cdot \frac{P}{(c \cdot V_m \cdot P^0)} \quad (\text{V.2})$$

where:

P^0 = saturation pressure

P = partial pressure of the gas

c = constant which depends on the torque solid / gas and on the temperature

V_m = volume of the monolayer

The B.E.T. it does not provide a differentiation of the catalytic surface to the total.

The process leading to the obtaining of the surface area consists of two phases:

- *Pre-treatment phase.* The pre-treatment is an operation is necessary to free the sample surface from complexes possibly adsorbed from the atmosphere (H_2O , CO_2) without changing the chemical nature of the catalyst.

- *Measurement phase.* In this phase, a carousel robotic system moves the tube containing the sample out of the degassing furnace without exposing it to environmental contamination that would nullify the effects of pretreatment. It is then immersed in liquid nitrogen and subjected to the flow of a gaseous mixture containing He and N_2 , provided by mass flow controllers. At a fixed P / P^0 value, it starts adsorption at 77 K because the sample is immersed in a dewar containing liquid nitrogen. After the adsorption step starts the desorption step. The volume of nitrogen adsorbed will be a function of a voltage variation indicated by the conductivity detector connected to the output of the tube containing the sample. To realize a quick and net desorption of nitrogen adsorbed previously, the sample is taken back at room temperature by removing it from the liquid nitrogen dewar.

This operation will result in the generation of a desorption peak, the which area represents the volume of adsorbed nitrogen. The adsorption / desorption operation is repeated 4 times each time increasing the P / P^0 ratio. In this way they are collected all the necessary points for the representation of adsorption isotherm, which are interpreted by the B.E.T.

V.2.5 Scanning Electron Microscope

A scanning electron microscope (SEM) is a type of electron microscope that produces images of a sample by scanning the surface with a focused beam of electrons. The electrons interact with atoms in the sample, producing various signals that contain information about the sample's surface topography and composition.

The most common SEM mode is detection of secondary electrons emitted by atoms excited by the electron beam. The number of secondary electrons that can be detected depends, among other things, on specimen topography. By scanning the sample and collecting the secondary electrons that are emitted using a special detector, an image displaying the topography of the surface is created.

The homogeneity of the layer of washcoat and the possible presence of macroporosity of the support was investigated with this analysis.

All the apparatus is under vacuum (10^{-4} - 10^{-6} mbar) through a ionic pump, in order to reduce the interactions between electrons and gaseous molecules.

V.2.6 Ultrasonic Test

The mechanical stability tests to investigate the adhesion of the ceria washcoat on the cordierite monolith were performed by ultrasonic vibration. The samples were immersed in a beaker containing petroleum ether (Carlo Erba) and placed in an ultrasonic bath CP104 (EIA S.p.A, 36 kHz) filled with distilled water, at a temperature of 298 K, operating at 90% of rated power.

The weight changes were recorded during the test at regular 5 min intervals after monoliths drying at 393 K and cooling up to room temperature.

The weight losses are evaluated in according with the following formula (Eq. V.3):

$$\text{Weight Loss} = \frac{\text{Initial Weight} - \text{Final Weight}}{\text{Initial Weight}} \quad (\text{V.3})$$

where the initial weight and final weight are respectively the washcoat weight before and after the ultrasonic tests.

VI LABORATORY APPARATUS

In this chapter, considerations about the peculiarity of the materials and instruments needed to operate safely with H₂S are reported.

The corrosive and toxic nature of H₂S must be considered in order to ensure that the plant would be protected both from a point of view of operations and manageability. In the first paragraph the hazards related to this gas are explained and then the safety precautions are shown.

VI.1 Human Health Effects from Exposure to Hydrogen Sulphide

The hydrogen sulphide is a highly poisonous substance, the which toxicity is comparable to the cyanide.

At room temperature and at low concentrations, H₂S is a colorless gas having a smell of rotten eggs and we are able to recognize the acrid smell already at 8 ppb (part per billion). The hydrogen sulphide becomes odorless for concentrations higher than 100 ppm (part per million) because it immediately paralyzes the sense of smell (Knight *et al.*, 2005).

In the range 8 ppb - 100 ppm many cases of olfactory problems are reported.

It can be considered as a toxic substance at broad-spectrum (Legater *et al.* 2001).

Interested parties of the human body are the mucous membranes (eyes and nose) and the ones that require more oxygen as lungs and brain.

The effects of H₂S are similar to the ones of the cyanide, because it interferes with the oxidation processes. In fact in presence of high H₂S concentrations, the human cells do not receive enough oxygen and die (Knight *et al.* 2005).

The human body reacts to the presence of H₂S transforming it in sulphur and thiosulphates that which then reach the blood or the liver. If the amount of H₂S is very high, the body will not be able to detoxify and the toxicity will become lethal.

The ways in which the H₂S enters the human body are three (Hirsh, 1999): by inhalation through the lungs; by the oral route, especially by digestion of contaminated substances absorbed in the intestinal tract and through the skin.

Exposures between 100 and 150 ppm H₂S cause inflammation of the cornea and conjunctivitis, eye irritation, watery eyes, and coughing. The major route of H₂S entering the human body and inhaled.

It was shown how the H₂S causes irritation and itching skin.

At low concentrations occur: damage to reaction time, balance, color recognition, and motor coordination speed. They are registered high levels of irritability, states of depression, confusion, loss of appetite, headaches, poor memory, fainting, tension, anxiety and fatigue (Kilburn *et al.* 1995).

Instantaneous loss of consciousness, rapid apnea (slowed or temporarily stopped breathing), and death may result from acute exposure to levels above 1000 ppm. At these higher levels, hydrogen sulphide is an asphyxiant.

VI.1.1 Hydrogen Sulphide: Flammability Limits

Flammable gases, such as hydrogen sulphide, tend to explode when ignited. The important properties to be considered when assessing the explosive hazard of a substance are its Lower Explosive Limit (LEL) and Upper Explosive Limit (UEL). Below the LEL, the concentration of the fuel (hydrogen sulphide) in the mixture is not at a sufficient concentration to support an explosion. Conversely above the UEL the concentration of the fuel is too rich and there is insufficient oxidant present (oxygen in air) to react with the fuel and produce an explosion.

Consequently any mixture of air and hydrogen sulphide between these two values has the potential to produce an explosion if ignited.

Secondly, it is remarkable that hydrogen sulphide is heavier than air and will be at higher vapour concentrations at the bottom of tanks.

The LEL of hydrogen sulphide is 4 % v/v and the UEL is 46 % v/v. This corresponds to a concentration of hydrogen sulphide in air of 40,000 ppm (0.062 g/l) and 460,000 ppm (0.71 g/l), respectively, well above the acutely toxic concentration.

The autoignition temperature is the temperature at which an additional ignition source is not required for a fuel mixture to ignite. At this temperature and above a mixture of hydrogen sulphide within the LEL and UEL could spontaneously ignite and explode. The autoignition

temperature for hydrogen sulphide (260°C), is quite high and in most situations an additional ignition source would be required to ignite the fuel mixture.

Additional ignition sources commonly include electrical sparks from electrical equipment or static electricity, naked flames, friction, impact energy or hot surfaces (Skrtec, 2006).

Furthermore, gases must be handled in a ventilated, enclosed system equipped with gas detectors.

VI.2 Experimental Apparatus

Catalytic activity tests were performed using the laboratory apparatus shown in Figure VI.1.

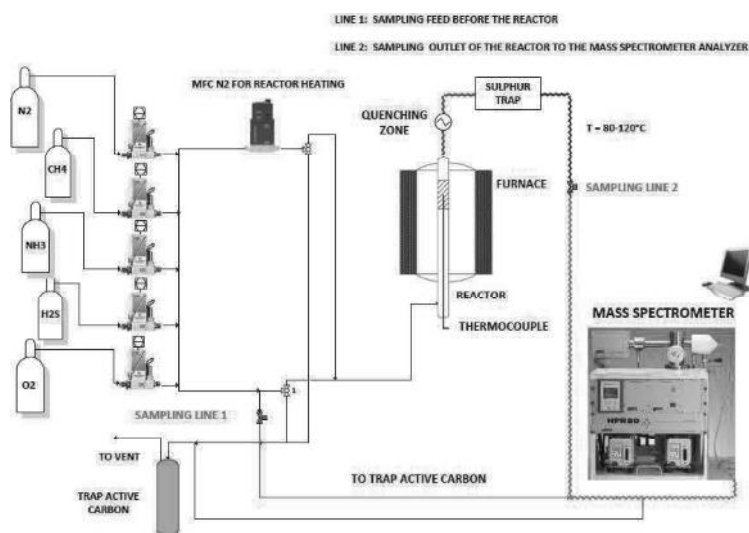


Figure VI.1: Scheme of the Experimental Apparatus.

All the gas pipes (1/4" i.d.) are in stainless steel (AISI 316), connections are made with stainless steel Swagelok union and two way valves.

The pipelines and the valves the gas flows through were made of stainless steel and Teflon that are reported as resistant to acidic corrosion.

The line at the outlet of the reactor is heated at 433 K by electrically heated tubes, or pipes with an inner polytetrafluoroethylene (PTFE

structure) to avoid the sulphur solidification produced during the reaction that would cause the occlusion, determining an overpressure condition.

The presence of the electrically heated tubes involves to maintain the water in gas phase so as to allow the analysis.

It is important to have the water in gas phase to avoid the absorption of Sulphur dioxide at the outlet of the reactor, invalidating the precision of the SO₂ analysis.

The experimental apparatus is described in detail in each section with the aid of drawings and photographs.

The main units are:

- Feed Section
- Reaction Section
- Quench Section
- Sulphur Abatement Section (Sulphur Trap)
- Water Condenser and Removal Pollutants Section
- Analysis Section

VI.2.1 Feed Section

The gas manifold system consists of cylinders containing high purity nitrogen, H₂S, O₂, methane, ammonia. All gases come from Sol S.p.A with a purity degree of 99.999 % for N₂ and O₂, and 99.5 for H₂S.

Particular attention is being given to a reducer of pressure to put on the cylinder of H₂S.

It is a single-stage cylinder pressure regulator designed to be used with compressed high purity gases to reduce cylinder pressure and maintain as constant as possible an outlet pressure.

In Figure VI.2 a picture of the pressure regulator with indications of the valves is reported.

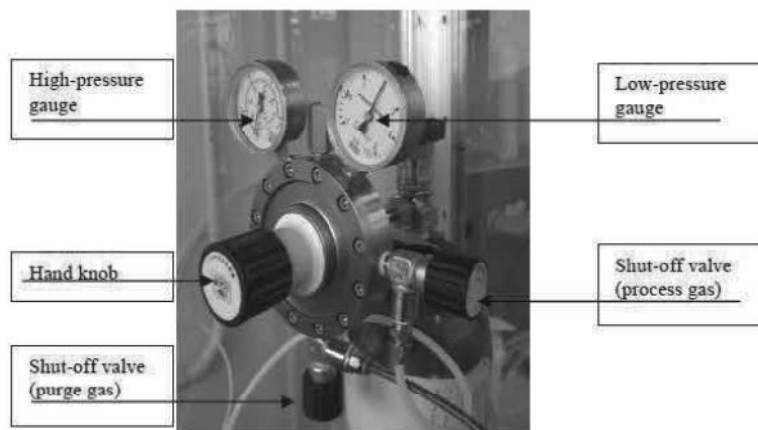


Figure VI.2: *H₂S pressure regulator.*

It has a special purging device that serves to clear itself and lines from H₂S left inside after tests are carried out.

Since we use corrosive gas, it is necessary to ensure the pressure regulators are clean and dry before start-up and after each analysis is carried out. So we need to connect an inert gas such as N₂ to the purge gas shut-off valve and execute some simple but important operation actions for safety working conditions.

To feed an accurately controlled flow of each gas, Bronkhorst measured flow controllers (MFC) are used. These controllers are able to operate with a maximum pressure drop of 2 atm.

FlowView is a DDE-client program to operate Bronkhorst digital instruments or readout-units; by this interface we modulate the desired flow rate for each gas.

VI.2.2 Reaction and Quenching Section

A system of valves allows feeding the reactants to the reaction section and the products to the analysis section. Otherwise in by-pass position the reactants go directly to the analysis section to verify the composition of the reaction feed.

Experiments were carried out in a fixed bed tubular reactor specifically designed and then realized by Microglass, s.r.l. This reactor, illustrated in Figure VI.3 and Figure VI.4, consists of a quartz tube with 300 mm length and i.d. 12 mm, equipped with porous quartz supports to retain the catalyst.

The reactor consists of three zones:

- 1 Feed
- 2 Reaction
- 3 Quenching

The feed stream is premixed at the bottom of the reactor in the concentric quartz tubes before to reach the reaction zone that is 50 mm long with a volume of 3 cm³.

At the bottom is located a thermocouple sheet (Figure VI.4c), concentric to the reactor, in order to monitor in continuous the temperature of the catalytic bed situated at the top of the reactor in the isothermal zone.

In the heating zone is located the catalytic bed and the temperature is measured by a K-type thermocouple.

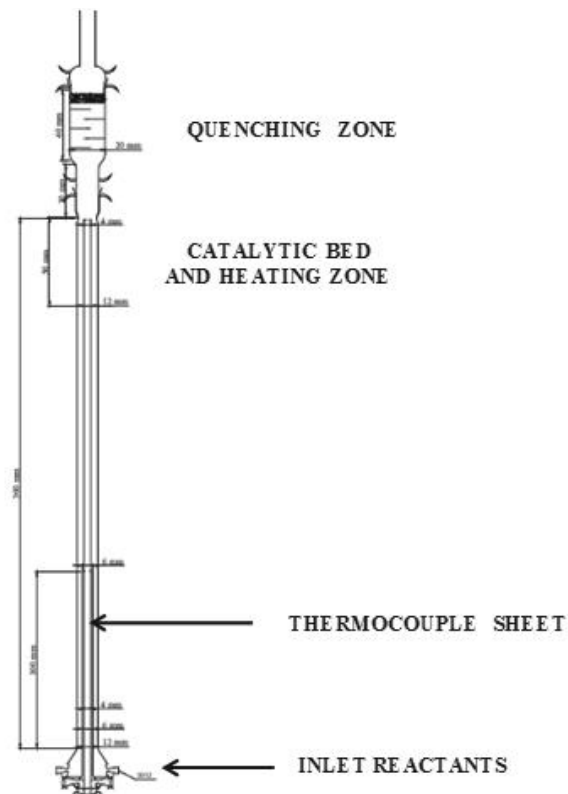


Figure VI.3: *Fixed Tubular Reactor.*

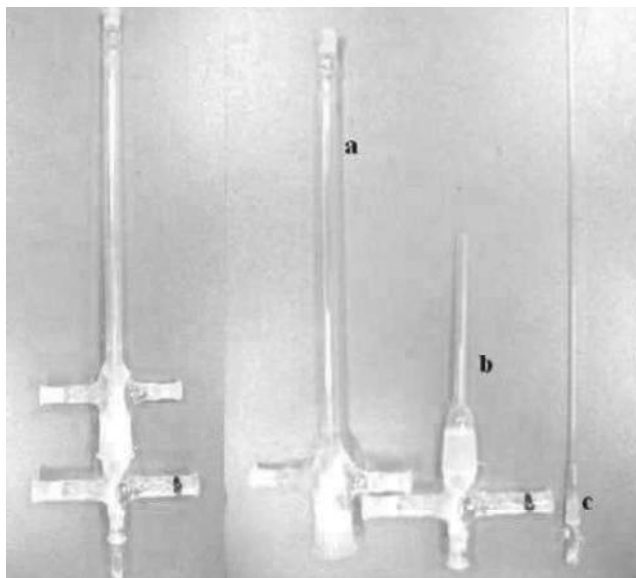


Figure VI.4: Reactor and its components. External quartz tube (a), internal quartz tube (b), thermocouple liner (c).

At the end of it there is the quench zone where the gaseous stream must be cooled as soon as possible to avoid back reaction between H_2 and sulphur vapor to produce H_2S (Figure VI.5 a-b).

The quench zone (17 cm in length) is welded to the reactor and it is an expansion vessel that allows a selective condensation of the Sulphur produced during the reaction from the gaseous stream. This expansion vessel or *sulphur-trap*, is characterized by an increase of the section to allow a rapid expansion of the gas and the presence of baffles inside enables to establish the contact of the gaseous stream with the walls, in order to realize more smoothly the cooling of the outlet stream from the reactor.

The end of the sulphur trap, as it is possible to see in Figure VI.5 b, is electrically heated by resistances, in such a way as to ensure that the sulfur remains in the liquid phase (Melting Point = 391 K); in Figure VI.5 a-b, are respectively showed, the reactor housed in the furnace during the reaction test, and the expansion vessel containing the condensed sulphur.

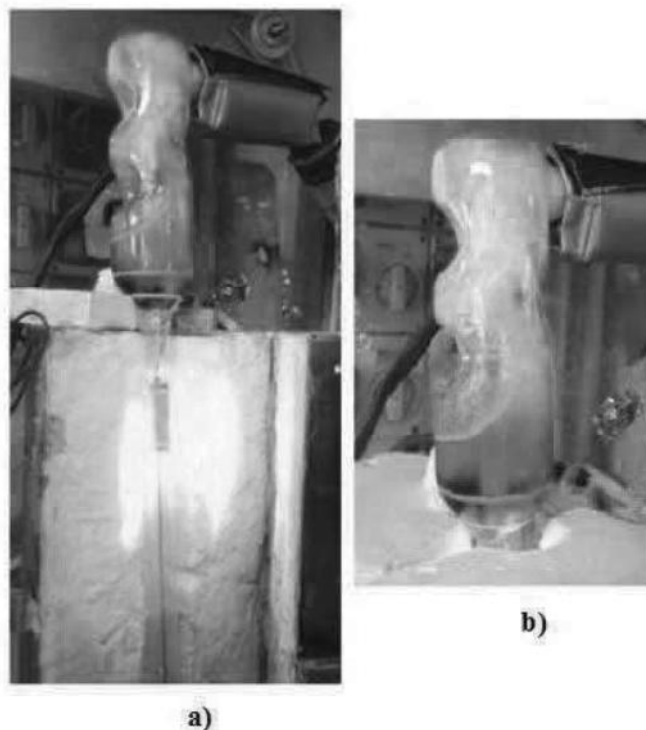


Figure VI.5: *Quartz reactor in the furnace (a) and sulphur trap (b)*

VI.2.3 Heating Section

The reactor is housed vertically in a high-temperature electric furnace with an operating range of 400-1500 °C.

The furnace has stainless steel external walls, ceramic material for insulation and silicon carbide (SiC) for resistances. The heating elements are arranged in a heated chamber surrounding the work tube, and provide even heating of the tube reactor surface for maximum temperature uniformity.

All materials are selected in order to resist at the high temperatures we could have during the reaction.

The resistance is located at the top of the reactor (Figure VI.6).

For temperature control we use PID microprocessor digital control systems connected with thermocouples placed near the resistance to measure the temperature close to the work piece.

The furnace was so designed and realized for two principal reasons:

1) The furnace would be able to move the reactor inside it easily, because the reactor has a special shape and a splitting furnace to get the quartz tube into it is needed;

2) The furnace would guarantee a high constant temperature zone at the end of the furnace and not in the middle of it as usually happens in commercial furnaces.

The heating elements are behind the cavity where we put the reactor so an uniform heating is realized especially in the reaction region where the reactor with the catalyst inside is placed. This important zone has a length of about 10 cm and it must terminate at the end of the furnace.

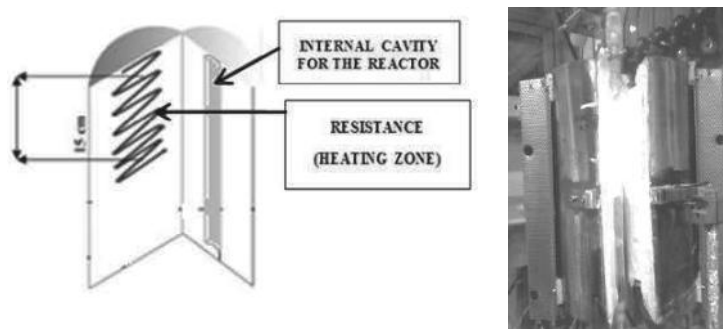


Figure VI.6: *Furnace scheme and heated furnace during the reaction*

VI.2.4 Sulphur Abatement Section (Sulphur Traps)

In order to guarantee an efficient abatement of the sulphur produced during the reaction, the output stream from the reactor is directed in two equipment located in series defined as "traps sulfur" (Figure VI.5 a-Figure VI.7 a). More precisely, in the first trap it realizes the greater sulphur abatement, in the second the residual content of sulphur. In this regards, it is strictly important to avoid that the sulphur reaches the analyzer because it could cause the occlusion of the capillary liner, with consequent damage of main parts of the spectrometer.

The sulphur traps are made of stainless steel and are electrically heated at 373-383 K to allow the solidification of the Sulphur.

As it's possible to see from the Figure VI.7 b, the presence of a septum separates the inlet section from the outlet section so as realize an expansion of the gaseous stream, in order to trap the higher sulphur amount. About that, the outlet section was realized with a larger area, to reduce the gas speed allowing so the sulphur separation.

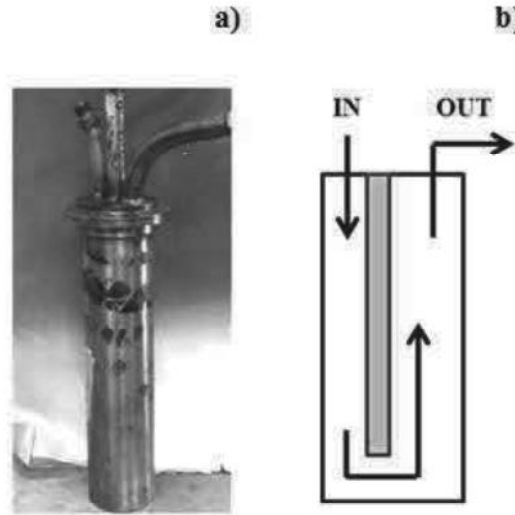


Figure VI.7: *Photo and Scheme of the First trap of sulphur abatement.*

The Sections of the trap before and after the reaction tests are illustrated in Figure VI.8 a-b. Small amount of quartz wool are loaded in the outlet section of the trap (Figure VI.8-a) so to block the smaller amounts to sulphur that could be dragged from the gaseous stream. In Figure VI.8-b it's observable the sulphur trapped and solidified after the conduction of different experimental tests.

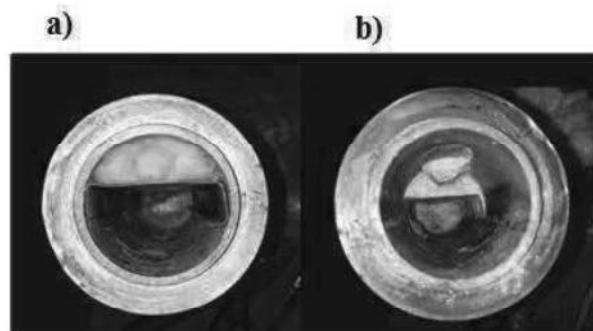


Figure VI.8: *Section of the trap before the reaction test a); Section of the trap with sulphur after the reaction test b).*

VI.2.5 Sulphur Trap, Water Condenser and Removal Pollutants

Section

In this Figure (Figure VI.9) is described the second sulphur trap, which acts as a second abatement stage for sulfur and two additional steel containers at lower temperature where it realizes a water condensation.

With the water condensation it is obtained also the partial absorption of some components such as SO_2 , NH_3 residual, and possibly also of COS , CS_2 , separating in this way by the gaseous stream.



Figure VI.9: *Second stage of sulphur abatement (a) and water condenser with pollutants removal (b,c).*

At this point, the abatement of H_2S unconverted is realized by adsorption on activated carbons loaded in a special vessel having a capacity of 20 Lt (Figure VI.10).

After the latter abatement stage, the purified stream containing only hydrogen and nitrogen, can be vented in the atmosphere.



Figure VI.10: Activated carbon for H_2S residual removal by adsorption.

VI.2.6 Analysis Section

The analyzer is a quadrupole Mass Spectrometer that allows to analyze in continuous the feed stream, in by pass to the reactor, or the product gases sulphur-free basis from the exit of the quench section.

Mass spectrometry is an analytical technique that identifies the chemical composition of a compound or sample based on the mass-to-charge ratio of charged particles.

The technique has both qualitative and quantitative uses, such as identifying unknown compounds, determining the isotopic composition of elements in a compound, the structure of a compound by observing its fragmentation, quantifying the amount of a compound in a sample.

This is a destructive analysis method (the molecule do not remain intact after the analysis), and especially not based on the interaction between radiation and matter.

The principle on which bases is the following: a molecule is ionized by expulsion of an electron; the radical cation which forms (molecular ion) in part is fragmented giving molecules and/ or neutral radicals (that the instrument doesn't detect), in part by generating cations and/ or cations radicals (fragment ions). The molecular ion and the various ions that arise for fragmentation (cations and radical cations) are discriminated against on the basis of their relationship mass / charge and revealed by a detector.

A mass spectrometer always contains the following elements, as illustrated in Figure VI.11:

- Sample inlet to introduce the compound that is analyzed
- Ionization Source to produce ions from the sample
- Analyzer to separate the various ions
- Detector to 'count' the ions emerging from the last analyzer
- Data processing system that produces the mass spectrum in a suitable form.

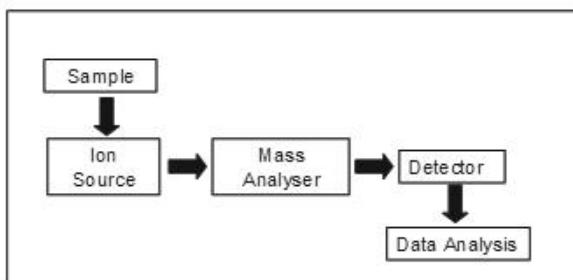


Figure VI.11: *Main steps of measuring with a mass spectrometer.*

The introduction of the sample into the ionization chamber can be made either in the solid state, using a probe, which in the liquid state or gaseous, using a system of valves that allow access to the ionization chamber without this being in contact with external atmosphere.

The sample is ionized in a separate ionization chamber, in which the electron beam is produced by an ion source that varies depending on the technique used. Typically the electrons are emitted by a hot filament of tungsten or rhenium.

The electrons that does not strike the molecules are collected by a trap for electrons, the molecules that are not ionized are removed by high-vacuum pump, while those ionized are accelerated and conveyed to the analyzer.

The ionization system plays an essential role in mass spectrometry, because it also depends on the number, nature and the abundance of molecular fragments that appear in the mass spectrum.

The Quadrupole Analyzer consists of four metal cylindrical bars, long about 20 cm., which delimit the "path" by the ions from the ionization chamber and directed to the detector.

The bars are kept to an oscillating electromagnetic potential, so that when the two vertical bars have positive potential horizontal ones have the negative, and vice versa.

The electrons are accelerated by the accelerator plate, entering the tunnel bounded by the bars and are repelled by the positive and negative poles attracted to.

However, due to the oscillation of the quadrupole, ions assume a zigzag trajectory and ending with the discharge of one of the bars, except that, for a certain period of oscillation frequency value, have a kinetic energy such that the motion it becomes sinusoidal and manage to get out of the tunnel and into the detection system (*photomultiplier*). Then operating a field oscillation frequency sweep is possible to output with increasing molecular mass ions.

As collector and detector of the ions is commonly an electronic multiplier. This involves a strong amplification of the signal which is then digitized and finally processed by the spectrometer computer for the presentation of the mass spectrum. An imagine of the analyzer is shown in Figure VI.12.

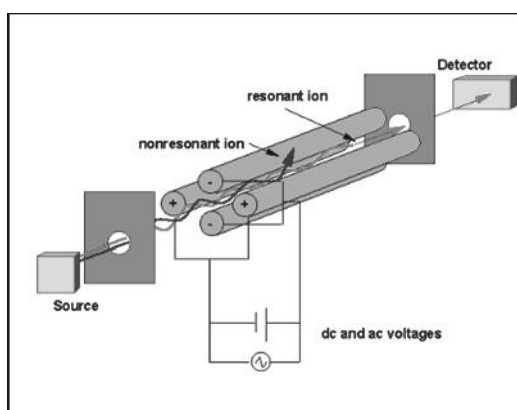


Figure VI.12: Main components of a mass spectrometer.

The mass spectrum is thus presented as a set of vertical lines (peaks) of different intensity, each corresponding to the value of mass of a fragment ion.

The spectrometer used in this work (HPR-20 QIC) was provided by Hiden (Figure VI.13).



Figure VI.13: *Mass Spectrometer QIC-HPR 20 Hiden.*

It extends the capabilities of the entry level system with an advanced differential pumping arrangement for processes that contain more than a few percent of helium or hydrogen.

The Hiden HPR-20 QIC is configured for continuous analysis of gases and vapours at pressures near atmosphere via a flexible, heated Quartz Inert Capillary (QIC) inlet. Operating to 200°C, the quartz inert capillary provides fast response times of less than 300 ms. The HPR-20 QIC system has a mass range of 200 AMU (300, 510, 1000 AMU options) and a detection capability from 100% to less than 5 ppb.

The entire gas analysis package operates under the control of Hiden's versatile MASoft software providing extensive data handling, review and export facilities that are compatible with Windows operating systems.

It is possible to:

- Choose masses from the internal library
- View data as graphical views, tabular views or both at the same time
- Output in preferred units i.e. partial pressure, % v/v, ppm, ppb
- Results as a function of time in mixed units (ppm and %).

VI.2.6.1 Calibration Procedure

The calibration procedure is required in order to measure the concentration of all the species that could be in the gas stream to analyze and for this reason it must be performed prior to carry out experimental tests.

However, it could be necessary to repeat the calibration every time that the process conditions are changed (e.g. after the replacement of the capillary, the filaments, change of pressure chamber value) or when the signal seems be affected by derivative effects.

The measurements could be affected by interference due to the presence of ions of different molecules having the same m/z ratio. Each molecule has a matrix of interference, which defines the "weight" of the disturbance of other molecules on the partial pressure of the molecule in phase of calibration. The partial pressure obtained, net of the relative interference, must be corrected by a response factor, thus returning the actual partial pressure of each molecule in the stream analyzed. At this point it is possible to calculate the correct concentration of each component.

The calibration procedure is characterized by different steps:

1) Report in a table the partial pressure of the all mass fragment for each concentration of the component to calibrate

3) Construct the *matrix of interference* and the *response factors table* relatively for the component you are calibrating

4) Calculate the concentrations of the component calibrated, by considering the relative interference of other species on the component to calibrate and correcting the measure by its response factor

For example, for each component (i) to calibrate (H_2S , O_2 , H_2 , H_2O , SO_2), the equation to be used is the following:

$$C_i = (P_i / P_{TOT}) \cdot 100$$

where

$$P_i = (P_i^0 - \sum P_m \cdot f_{m,i}) / rf_i$$

With:

C_i = concentration of the component i

P_i = partial pressure of component i

P_i^0 = non correct partial pressure of component i

Chapter VI

P_i = correct pressure partial of component i

$f_{i,m}$ = interference factor of the component m on i

rf_i = response factor of component i

VI.2.7 Additional equipment to work safely in the laboratory

As already mentioned H_2S can be smelled at very low concentrations in the air. It starts to be dangerous at 10 ppm, but it is a nasty smell for people already at 5 ppb.

To avoid any presence of this gas or to be alerted in case of any unexpected potentially dangerous leaks in the laboratory, more than one preventative measure has been taken.

First of all, the whole test plant and also the analysis instruments are positioned under a suction system as it's possible to see in Figure VI.14. In this way, it is possible to change the flows in the reactor externally and can avoid any contact with eventual traces of gas surrounding the reactor.

Moreover, gas detectors are used to check the quality of the air in the laboratory.

One multi gas (H_2S , SO_2) detector is placed inside the plant and set on a concentration value lower than the TLV for each gas. It gives out a high-pitched alarm and lights up if undesirable gases are detected and two others H_2S gas detectors are placed outside the plant in the laboratory (Figure VI.15).

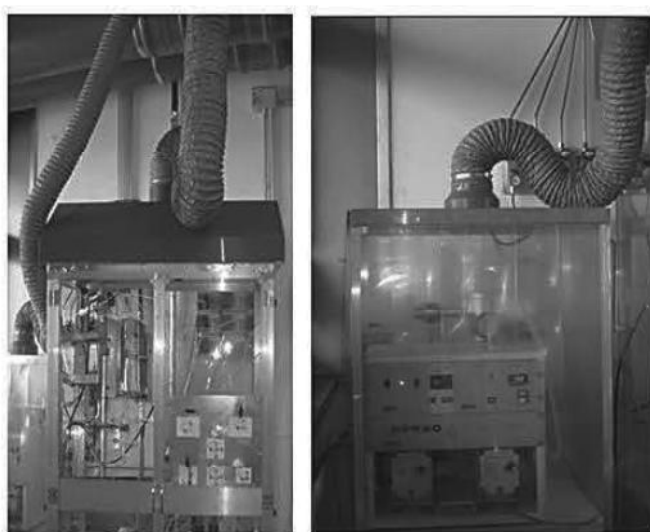


Figure VI.14: *Plant and Analyzer in the suction systems.*



Figure VI.15: *Gas Alert Micro: a) Multigas, b) monogas*

Laboratory Apparatus

VII HOMOGENEOUS PHASE RESULTS

VII.1 H₂S Thermal Decomposition

The thermal H₂S decomposition was carried out in the temperature range between 900 and 1100°C, at a fixed residence time (150 ms). The experimental results in comparison with the thermodynamic values are reported in Figure VII.1 in terms of H₂S conversion and H₂ yield as function of reaction temperature.

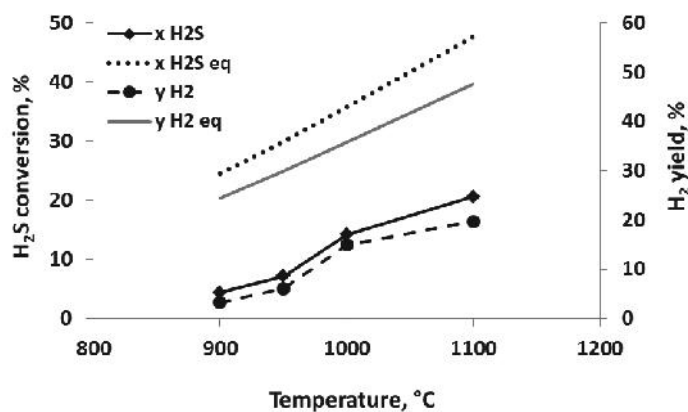


Figure VII.1: H₂S conversion and H₂ yield in the range 900-1100 °C in comparison with equilibrium values (eq) (H₂S^N: 10 vol%, residence time: 150 ms).

H₂S conversion and H₂ yield increased by increasing the reaction temperature, as also reported in the literature (Raymont, 1974). Since H₂S cracking is an endothermic reaction ($\Delta H_R = 84$ kJ/mol), H₂S decomposition is promoted by the high temperatures, obtaining the highest values of H₂S conversion and of H₂ yield (about 20%) at 1100 °C. However, the experimental values are very far from the thermodynamic ones, underlining that the kinetics of the homogeneous system is not able to lead the H₂S conversion and of H₂ yield to the thermodynamic equilibrium.

The temperature of 1100 °C was chosen to investigate the influence of the residence time of gaseous mixture in the reaction zone (Figure VII.2).

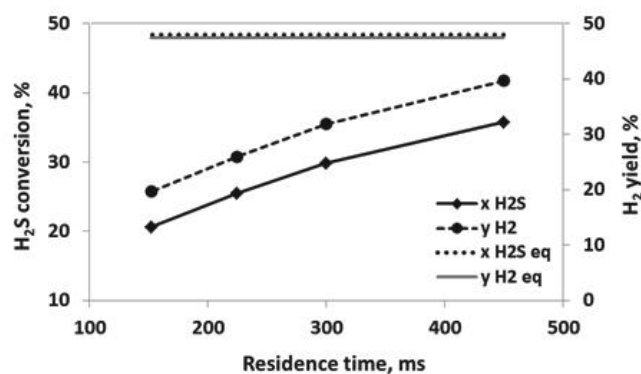


Figure VII.2: H₂S conversion and H₂ yield as function of residence time in comparison with equilibrium values (eq) (H₂S^{DN}: 10 vol%, T = 1100 °C) (Palma *et al.*, 2015).

By increasing the residence time, an increase of H₂S conversion and H₂ yield was achieved. For a residence time of 450 ms, H₂S conversion and H₂ yield were 30% and 40%, respectively. The increase of the residence time, as expected, allowed to the reaction system to better approach the thermodynamic values (Palma *et al.*, 2015).

VII.2 H₂S Thermal Oxidative Decomposition

The effect of O₂/H₂S feeding molar ratio was investigated at 1100 °C and at the residence time of 150 ms. In Figure VII.3 the results are reported in terms of H₂S conversion, H₂ yield and SO₂ selectivity.

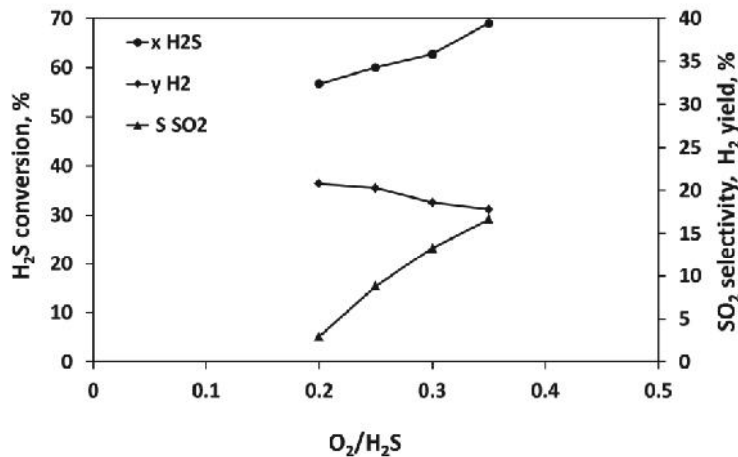


Figure VII.3: Effect of the O₂/H₂S in terms of H₂S conversion, H₂ yield, SO₂ selectivity (H₂S^{IN}:10 vol%, T = 1100 °C, residence time = 150 ms) (Palma *et al.*, 2015).

An increase of oxygen inlet concentration enhanced the H₂S conversion, but reduced slightly the H₂ yield and promoted the SO₂ formation. In particular, SO₂ selectivity increased from 2% to 15% by varying the O₂/H₂S molar ratio from 0.2 up to 0.35. As expected, the increase of O₂ concentration favors the total H₂S oxidation to sulfur dioxide, determining the increase of SO₂ selectivity. In order to minimize the SO₂ selectivity, which is the undesired product of this process, the next experimental tests have been carried out with O₂/H₂S molar ratio of 0.2, for which SO₂ selectivity value was the lowest. The influence of the temperature is reported in Figure VII.4.

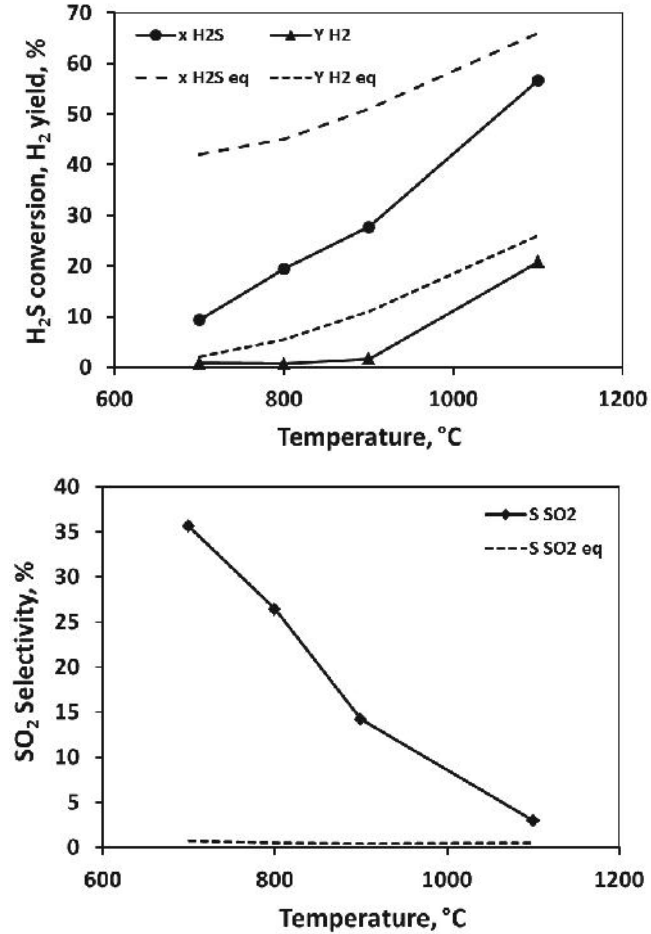


Figure VII.4: Influence of the temperature on H₂S conversion, H₂ yield, SO₂ selectivity and in comparison with equilibrium (eq) values ($H_2S^{IN}:10$ vol%, $O_2/H_2S = 0.2$, residence time = 150 ms) (Palma *et al.*, 2015).

The increase of the temperature in the range 700-1100 °C determines the increase of H₂S conversion and H₂ yield, with a reduction of SO₂ selectivity.

The decrease of the SO₂ production with the increase of temperature is likely due to the promotion of Claus reaction that involves the SO₂ consumption, previously produced with the H₂S residual. For temperatures lower than 1100 °C, the experimental SO₂ selectivity approaches to the values expected from the thermodynamic equilibrium, even if it is about of 3% (Palma *et al.*, 2015).

This last result can be explained considering the complexity of the kinetics of the reactions involved. In particular, it may happen that, in the lower temperature range, the SO₂ formation rate is higher than the competitive reactions giving as a consequence the enrichment of SO₂ in the gas phase. Finally, in order to obtain the higher H₂S conversion and H₂ yield, together with a low SO₂ selectivity, at a residence time equal to 150 ms, a reaction temperature at least of about 1100 °C must be considered.

Homogeneous Phase Results

VIII MOLYBDENUM-BASED CATALYSTS

VIII.1 Catalyst characterization

VIII.1.1 Thermogravimetry Analysis

Thermogravimetric curves of bulk MoS_2 , and 10Mo are reported in Figure VIII.1.

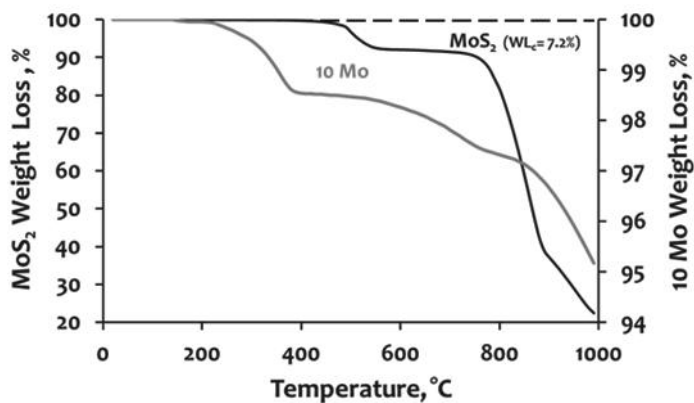


Figure VIII.1: TG Analysis of bulk MoS_2 and 10Mo catalyst (Air flow rate = $100 \text{ Ncm}^3/\text{min}$; $10^\circ\text{C}/\text{min}$; $T=20 - 1000^\circ\text{C}$).

In the range of temperature between 200 and 400 °C, it is possible to observe a weight loss attributable to the decomposition/oxidation of MoS_2 phases interacting with Al_2O_3 ; for the bulk MoS_2 this

decomposition/oxidation stage occurs at higher temperature (400 – 600 °C), likely due to the interaction of the active phase with the support (Wang *et al.*, 2004).

The weight loss in the range 800 – 1000 °C is attributable to the conversion of MoS₂ to molybdenum oxide, and the following sublimation as reported in the literature (Ciambelli *et al.*, 2008 & Shobaky *et al.*, 1999). The formation of molybdenum oxide from MoS₂ occurs through the reaction reported below (Eq. VIII.1) (Wang *et al.*, 1997):



The weight loss step associated to the MoS₂ oxidation, can be used to determine the effective MoS₂ loading (as wt%) of the catalysts according to the following relationship (Eq. VIII.2):

$$\text{MoS}_{2\text{loading}} = 100 \cdot \frac{WL_c}{7.2} \quad (\text{VIII.2})$$

where WL_c is the of weight loss associated to the release of sulfur dioxide according to Eq. VIII.1 and MoS_{2loading} is the MoS₂ estimated content (Figure VIII.1).

In Table VIII.1, the nominal and estimated MoS₂ loading are reported.

Table VIII.1: *Weight loss of the catalysts and active phase content (Air flow rate= 100 Ncm³/min; 10°C/min; T=20 – 1000 °C)*

Catalyst	Nominal MoS ₂ loading [wt%]	Estimated MoS ₂ loading [wt %]
5Mo	5	5.9
10Mo	10	15
20Mo	20	25

It was found an effective MoS₂ loading equal to 5.9, 13 and 23 wt% for 5Mo, 10Mo and 20Mo, respectively, which well agrees with the nominal content.

VIII.1.2 X-Ray Diffraction

In Figure VIII.2 XRD patterns of bulk MoS_2 , and of $\text{MoS}_2/\gamma\text{-Al}_2\text{O}_3$ catalysts are reported.

For bulk MoS_2 , it is possible to observe two main diffraction patterns at 14.5° and 39.5° , as reported in the literature (Wang *et al.*, 1997) and other peaks of lesser intensity at 32.5 , 33.5 , 36 , 44.5 , 50 , 56 , 58.5 , 60.5 , 63 and 68.5° due to the hexagonal crystalline structure of molybdenum disulfide.

After supporting MoS_2 on Al_2O_3 , all samples were X-Ray amorphous (Kokhubei *et al.*, 2003). In fact, for the catalysts, the main peaks related to MoS_2 are not detectable except to for the peak at 14.5° that is slightly broad indicating a small amount of MoS_2 crystalline. In addition, it is possible to see an increase of the peak intensity by increasing the MoS_2 content.

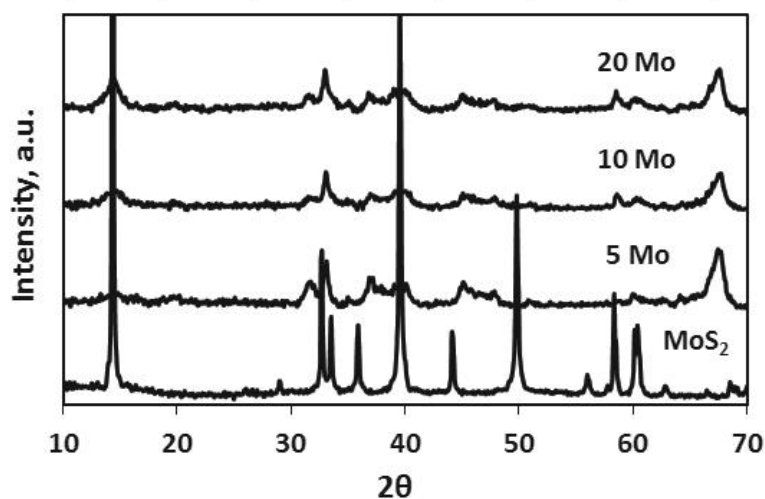


Figure VIII.2: X-Ray patterns of bulk MoS_2 , 5Mo, 10Mo e 20Mo.

Furthermore, other peaks are not ascribable to the active phase but to the support, as evidenced in Figure VIII.3, where the characteristic peaks of Al_2O_3 were observed at 31 , 33 , 38 , 39 , 46 , 60 , 67.5° associated to Al_2O_3 crystalline phases (Song *et al.*, 2006).

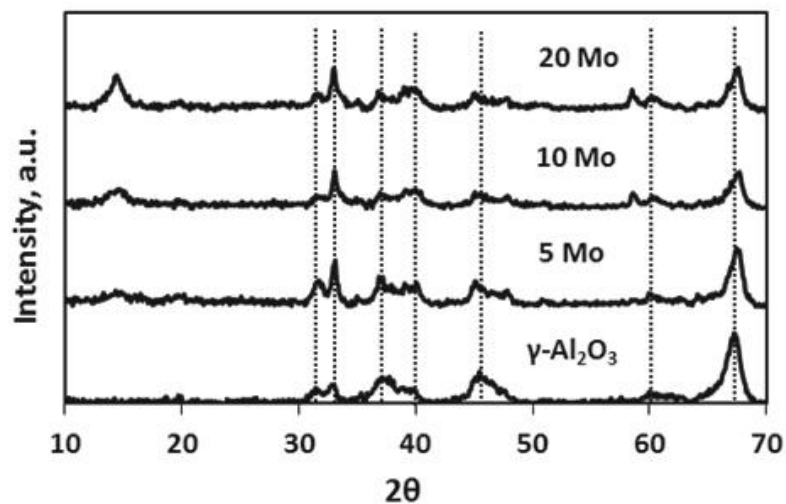


Figure VIII.3: X-Ray patterns of Al_2O_3 support and $MoS_2/\gamma-Al_2O_3$ catalysts.

In Table VIII.2 the average crystallite size of the different samples are reported.

Table VIII.2: Average crystallite size.

SAMPLE	$\langle L \rangle$, nm
MoS_2	44
5Mo	3
10Mo	4
20Mo	5

For unsupported MoS_2 , the average crystallite size is larger than MoS_2 supported on Al_2O_3 ; the average crystallite size of the catalysts is very similar and lies in the range 3-5 nm lower, likely due to the better dispersion of the sulfides on the support.

VIII.1.3 Raman Spectroscopy

The Raman spectra of MoS₂/ γ -Al₂O₃ catalyst are showed in Figure VIII.4.

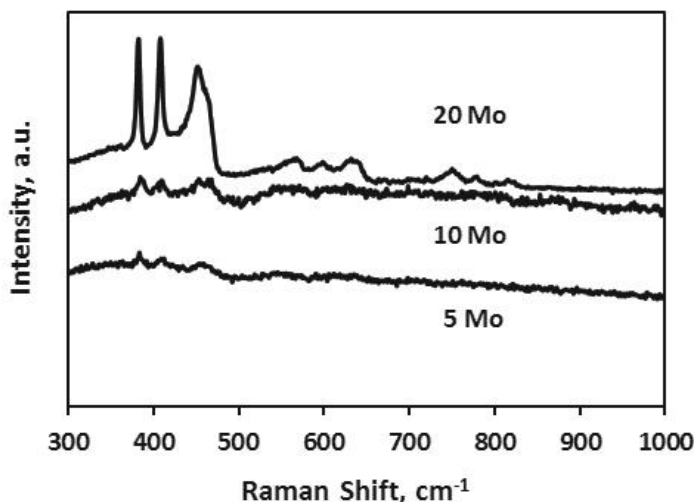


Figure VIII.4: Raman spectra of the samples 5Mo, 10Mo e 20Mo.

The sample 20Mo has shown strong Raman bands at 383, 408 and 452 cm⁻¹ characteristics of MoS₂ (Bergwerff *et al.*, 2006). These signals are slightly shifted with respect to the bands concerning bulk MoS₂ Raman spectra reported in literature at 375, 403, and 445 cm⁻¹ (Bergwerff *et al.*, 2006 & Digne *et al.*, 2007). This difference could be likely due to the interaction of the phase active with the support, confirming the results obtained from thermogravimetric analysis. In addition, for 5Mo and 10Mo catalysts, the intensity of these bands is lower because of the good dispersion of the MoS₂ on Al₂O₃.

Also, the absence of any Mo-O stretch vibration bands in the 900 – 1000 cm⁻¹ region indicates that the sulfurization was complete (Bergwerff *et al.*, 2006).

VIII.1.4 Specific Surface Area

The values of surface area of the support and of the samples with different content of active phase are reported in Table VIII.3.

Table VIII.3: Specific surface area of the γ -Al₂O₃ and the fresh catalysts.

SAMPLE	SSA [m ² /g]
γ -Al ₂ O ₃	70
5Mo	70
10 Mo	69
20 Mo	56

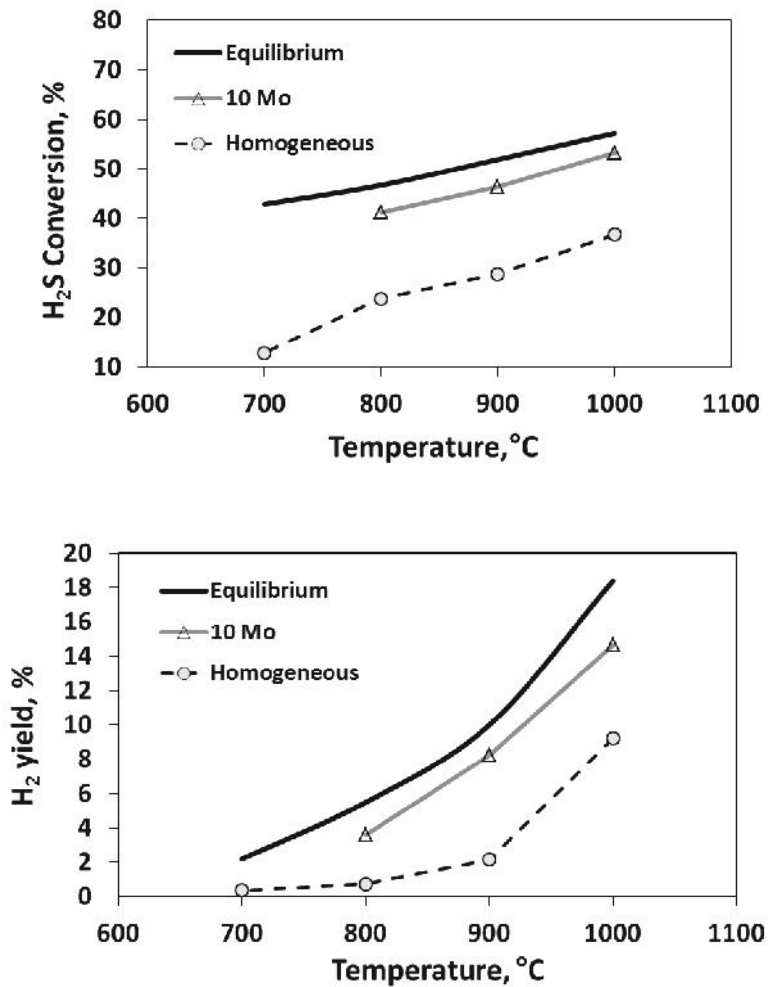
For the samples 5Mo and 10Mo, it is not possible to observe any significant variation of the surface area with respect to the support. A significant decrease of surface area was observed for the sample having the highest content of active phase, likely attributable to the worst dispersion on the support. This last results is a confirmation of experimental data obtained from Raman spectra.

VIII.2 Catalytic Activity Tests

VIII.2.1 Influence of the reaction temperature

The influence of the reaction temperature between 700 - 1000 °C was investigated on 10Mo catalyst in comparison with the homogeneous phase and the equilibrium data (Figure VIII.5).

By increasing the reaction temperature, it was observed both an increase of H₂S conversion and H₂ yield; in particular, in the presence of catalyst, their values were closer to the equilibrium ones.



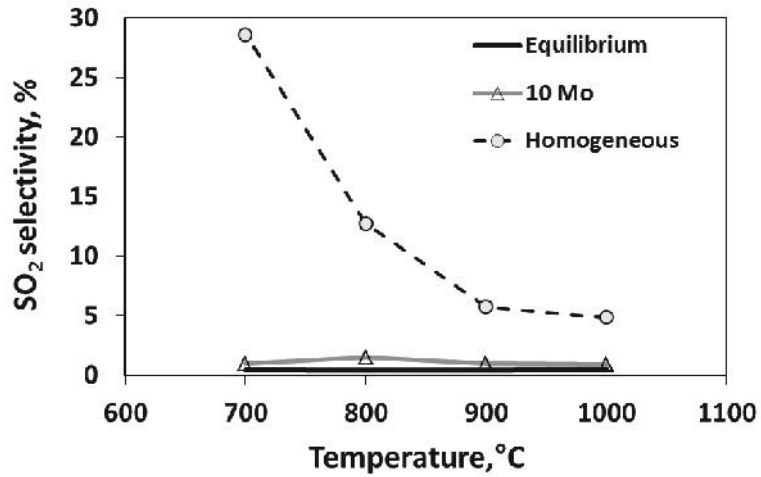
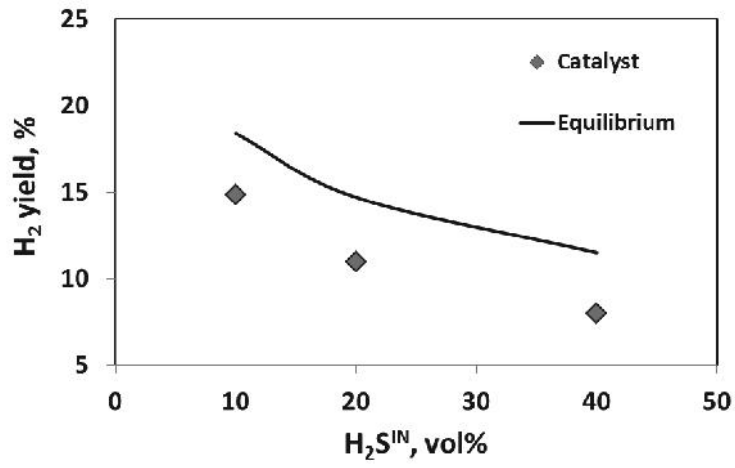
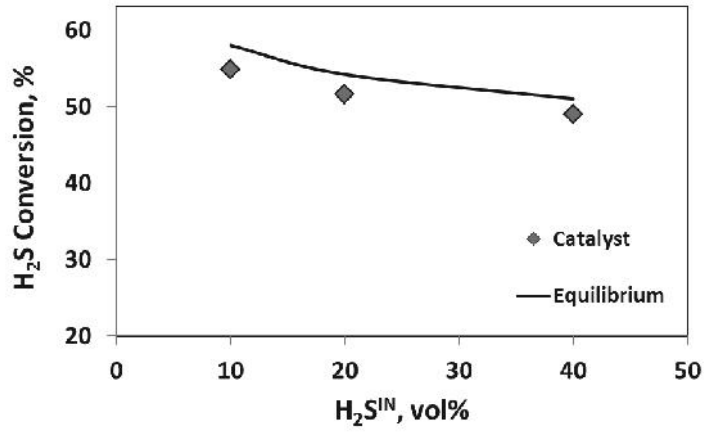


Figure VIII.5: Effect of the temperature in terms of H_2S conversion, H_2 yield and SO_2 selectivity in the absence of catalyst, 10Mo sample ($H_2S^{DN} = 10$ vol%, $O_2/H_2S = 0.2$, $\tau = 33ms$).

A negligible SO_2 formation was obtained in presence of 10Mo catalyst in the whole range of temperature. It is important to note that the SO_2 selectivity obtained in homogenous phase showed values higher than the thermodynamic equilibrium data. The presence of the catalyst has allowed to minimize the SO_2 selectivity, approaching to the equilibrium value, promoting the Claus reaction and then the SO_2 consumption.

VIII.2.2 Effect of H_2S concentration

The results related to 10Mo catalyst obtained at different H_2S inlet concentration, between 10 vol% and 40 vol% were shown in terms of H_2S conversion, H_2 yield and SO_2 selectivity at 1000°C with a O_2/H_2S feeding ratio equal to 0.2 (Figure VIII.6).



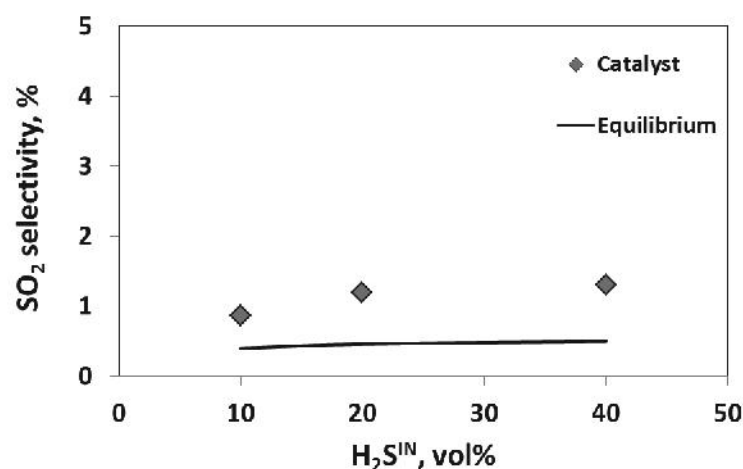


Figure VIII.6: Influence of the H₂S inlet concentration on H₂S conversion, H₂ yield, SO₂ selectivity for 10Mo catalyst. ($T=1000^{\circ}\text{C}$, $O_2/H_2S = 0.2$, $\tau=33\text{ms}$).

By increasing H₂S inlet concentration, there was a decrease of H₂S conversion and the H₂ yield. The value of SO₂ selectivity is slightly higher than the one expected by the equilibrium calculations. This result may be due to the contact time that is too low to allow to the Claus reaction to occur completely.

The best results were obtained by feeding a H₂S concentration of 10 vol%, for which the H₂S conversion was about 50%, the H₂ yield near to the equilibrium value (15%) and the lowest SO₂ selectivity (0.9%).

VIII.2.3 Effect of the MoS₂ content

The effect of the MoS₂ content on the catalytic performance was studied at 1000°C as function of the contact time. The H₂S conversion values for the three different MoS₂ contents are shown in Figure VIII.7. It was not obtained a significant effect of the MoS₂ loading on H₂S conversion that was ~50% for the three samples and very close to the thermodynamic equilibrium value (51%). A slight decrease of the H₂S conversion was instead observed by increasing the contact time.

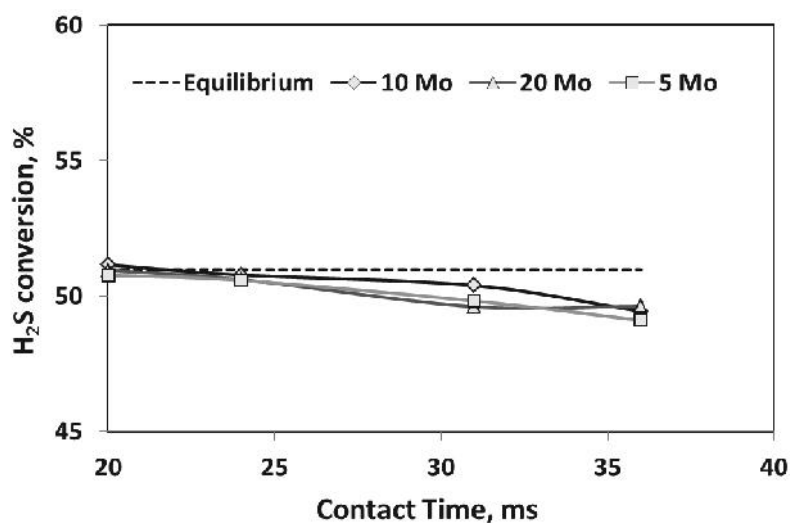


Figure VIII.7: H_2S conversion as function of contact time at $1000^\circ C$ ($H_2S^{IN} = 40\%$, $O_2/H_2S = 0.2$)

In Figure VIII.8, it is reported the trend of the H_2 yield for 5Mo, 10Mo, 20Mo catalysts by increasing the contact time and the comparison with the H_2 yield equilibrium value.

The highest H_2 yield, equal to 8%, was obtained for the sample 10Mo, whose value was not influenced by the contact time.

For the other samples, the H_2 yield values were lower, showing only a slight decrease with the increase of the contact time.

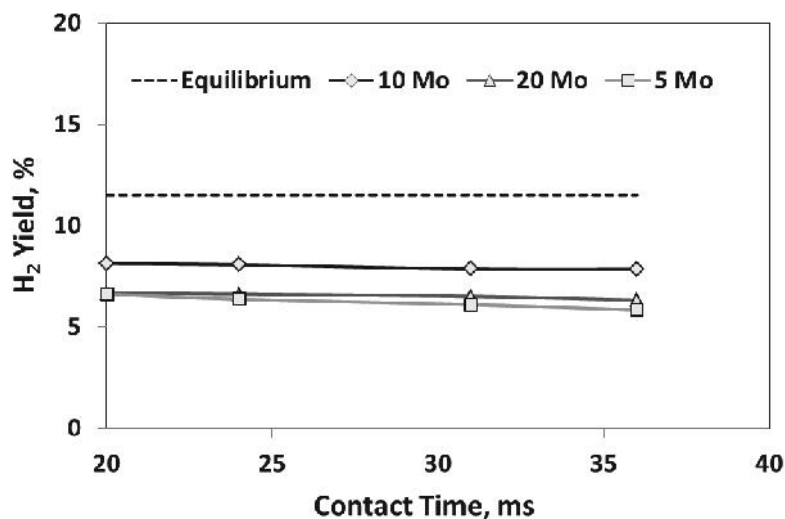


Figure VIII.8: H_2 yield to varying the contact time for different Mo/ γ - Al_2O_3 catalysts. ($T=1000^\circ C$, $H_2S^{dN}=40$ vol%, $O_2/H_2S = 0.2$).

The values of the SO_2 concentration are reported in Table VIII.4. The variation of the SO_2 concentration with the contact time is not significant due to the uncertainty of the experimental measure.

Table VIII.4: SO_2 concentration by varying the contact time. ($T=1000^\circ C$, $H_2S^{dN}=40$ vol%, $O_2/H_2S = 0.2$).

CATALYST	CONTACT TIME, ms			
	20	24	31	36
5 Mo	2560	2700	2430	2950
10 Mo	2600	2430	2880	2780
20 Mo	2800	2660	2500	3010

Based on these preliminary results, it was possible to identify the optimal content of active phase equal to 10 wt% of MoS_2 , suitable to obtain a high H_2S conversion, a good H_2 yield and very low SO_2 selectivity ($\sim 1.2\%$).

VIII.2.4 Influence of CH_4 on catalytic performance of 10 wt % $\text{MoS}_2/\text{Al}_2\text{O}_3$

The catalytic performance of 10wt% $\text{MoS}_2/\text{Al}_2\text{O}_3$ was also tested in presence of 1 vol% of CH_4 at fixed contact time of 30 ms.

The H_2S conversion and the H_2 yield are close to the equilibrium values, while the CH_4 conversion is about 90% (Figure VIII.9).

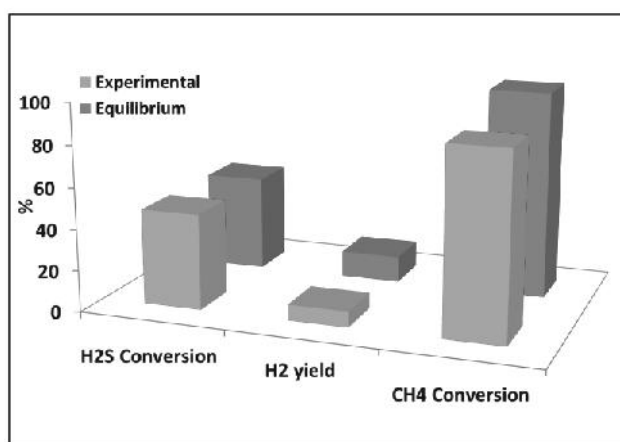


Figure VIII.9: H_2S and CH_4 Conversion, H_2 Yield, in comparison with the equilibrium data ($T=1000^\circ\text{C}$, $\text{H}_2\text{S}^{\text{IN}} = 40 \text{ vol}\%$, $\text{CH}_4^{\text{IN}} = 1 \text{ vol}\%$, $\text{O}_2/\text{H}_2\text{S} = 0.2$).

Furthermore, as evidenced in Figure VIII.10, the catalyst favors the formation of by-product as COS , CS_2 ; in particular the selectivities to COS and CS_2 are much higher than that expected by the thermodynamic equilibrium.

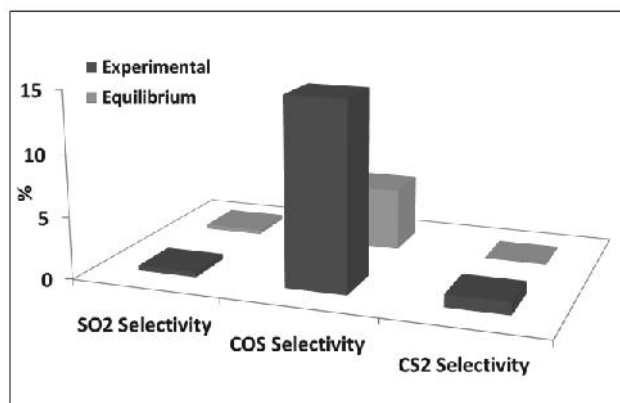


Figure VIII.10: *SO₂, COS, and CS₂ selectivity in comparison with the equilibrium data ($T=1000^{\circ}\text{C}$, $H_2S^{IN} = 40 \text{ vol}\%$, $CH_4^{IN} = 1 \text{ vol}\%$, $O_2/H_2S = 0.2$).*

Based on these results, it is necessary to identify a new catalyst that is able to maximize the CH₄ conversion and minimize, as much as possible, the formation of COS, CS₂. This study will be object of the next chapter.

IX BIMETALLIC CATALYSTS

IX.1. Catalysts Characterization

IX.1.1 X Ray Diffraction

The XRD spectra of bulk FeS_2 , 5 FeS_2 and the bimetallic catalysts are shown in Figure IX.1.

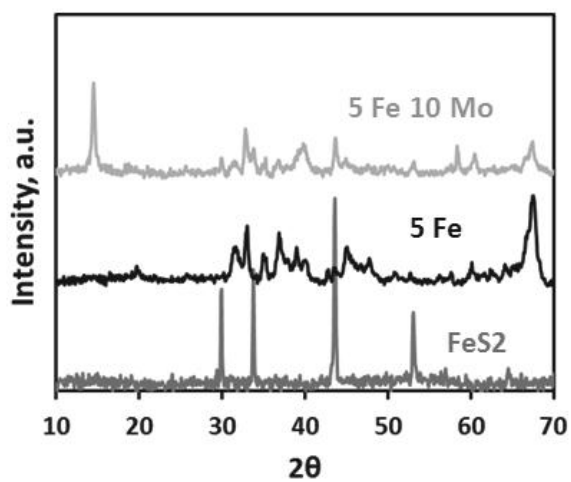


Figure IX.1: X-Ray patterns of the 5 Fe 10 Mo, 5 Fe and FeS_2 samples.

The characteristics peaks of the bulk FeS_2 are observed at $2\theta = 29, 34, 45$ and 52° in agreement with the literature (Amorim *et al.*, 2012).

Spectra of lower intensity were observed on the catalysts supported and they were attributable to the alumina as is shown in the following figure (Figure IX.2).

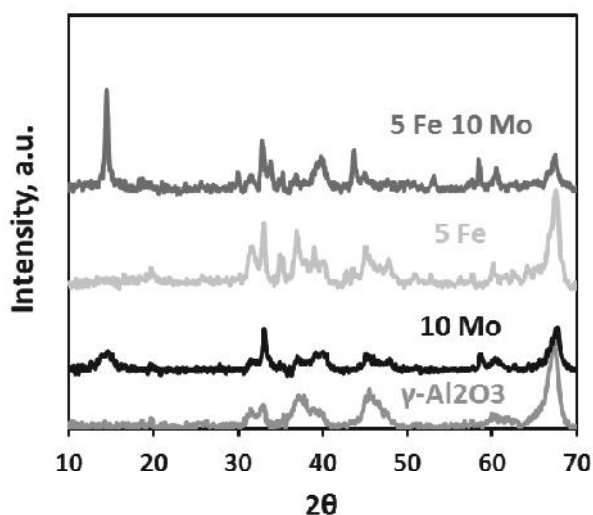


Figure IX.2: X-Ray patterns of the 5 Fe 10 Mo, 5 Fe, 10 Mo and $\gamma\text{-Al}_2\text{O}_3$ samples.

For the bimetallic catalyst 5Fe-10Mo, there is an additional peak ascribable to the MoS_2 .

In Figure IX.3, the patterns of bulk CoS_2 and the bimetallic catalysts 5Co-10Mo are illustrated in comparison with the alumina.

The characteristics peaks of CoS_2 were observed at $2\theta = 28, 32, 36, 42, 48$ e 57° . Both for the catalyst 5Fe-10Mo (Figure IX.2) and the catalyst 5Co-10Mo are observable the peaks of MoS_2 .

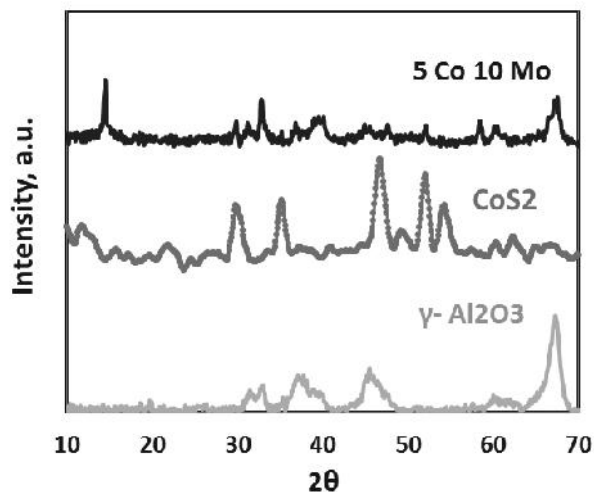


Figure IX.3: X-Ray patterns of 5Co-10Mo, CoS_2 and $\gamma\text{-Al}_2\text{O}_3$ catalysts.

In the following table (Table IX.1) the average crystallites size of the different catalysts are shown.

Table IX.1: Average crystallite size.

SAMPLE	$\langle L \rangle$, nm		
	MoS_2	FeS_2	CoS_2
FeS_2	/	34	/
CoS_2	/	/	40
5 Fe	/	10	/
5 Fe 10 Mo	19	14	/
5 Co 10 Mo	20	/	15

For the samples supported on alumina, the dimensions of the crystallites are lower than the same samples *in bulk*, likely due to the dispersion of the sulphides on the support surface. At the same MoS_2 -load, the bimetallic catalysts show a crystallite size (20 nm) higher than the respective monometallic sample (4 nm). This difference seems to suggest that the presence of the FeS_2 on the catalyst surface induced a lower dispersion of MoS_2 .

IX.1.2 Raman Spectroscopy

The Raman spectra of the monometallic (5 Fe, 10 Mo) and bimetallic (5Fe-10Mo) supported catalysts are showed in Figure IX.4.

As reported in the literature (Moraesa *et al.*, 2012), the Raman bands below 300 cm^{-1} , are ascribable to the bond Fe-S, while for Raman bands higher, are attributable to the bond S-S.

The Raman spectra of the sample 5Fe does not show any band, unlike the same bimetallic sample that shows the characteristic MoS_2 signal at 445 cm^{-1} .

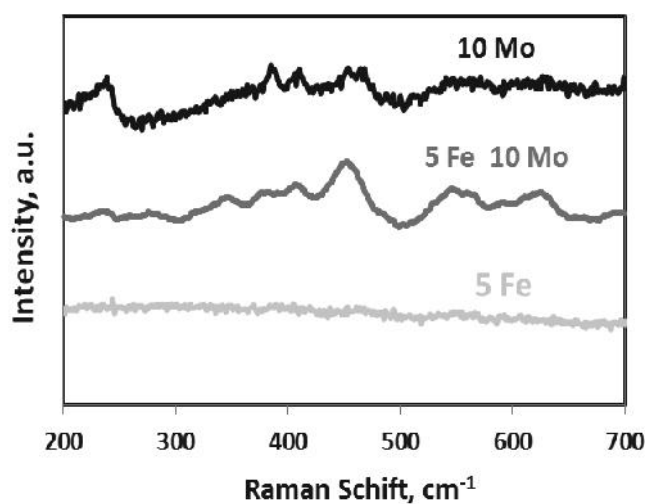


Figure IX.4: Raman Spectra of 5 Fe, 10 Mo and 5 Fe 10 Mo catalysts.

In Figure IX.5 the Raman spectra of the bimetallic catalyst (5Co-10Mo) is compared with the 10 Mo and 5 Co catalysts.

The sample 5 Co does not exhibit any spectra in the whole range $200\text{--}700\text{ cm}^{-1}$.

In fact the only observable signals for the bimetallic sample are attributable to MoS_2 ($375, 403$ e 445 cm^{-1}) and to Al_2O_3 (220 cm^{-1}).

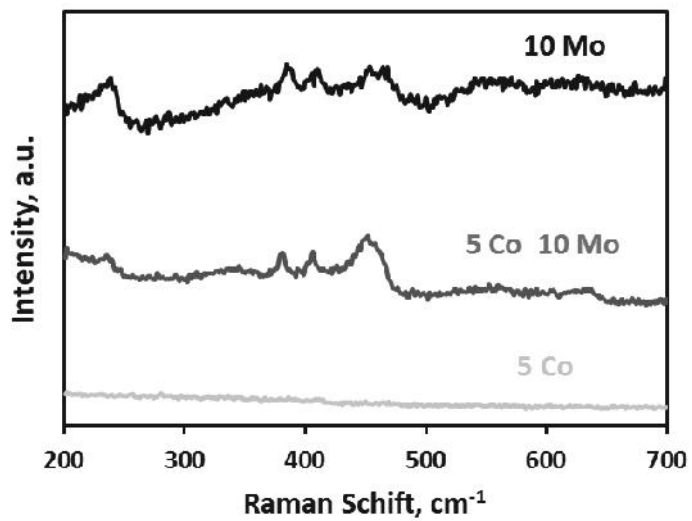


Figure IX.5: Raman Spectra of 5 Co, 10 Mo and 5 Co 10 Mo catalysts.

IX.2 Effect of the CH_4 on the mono-bimetallic catalysts

performance

The mono and bimetallic samples were tested also in the presence of 1 vol% of CH_4 and the catalytic performance were evaluated in terms of H_2S and CH_4 conversion, H_2 yield and selectivity towards Sulphur compounds (SO_2 , COS , CS_2).

The H_2S conversion is quite similar for all the samples and very close to the equilibrium value; the H_2 yield is slightly lower than the one expected from the equilibrium, in particular for the sample 5 Co -10 Mo (Figure IX.6).

A total CH_4 conversion for the Fe-based catalysts was obtained, while for the Co Mo -based catalysts (10 Mo and 5 Co -10 Mo) it was lower than 90%.

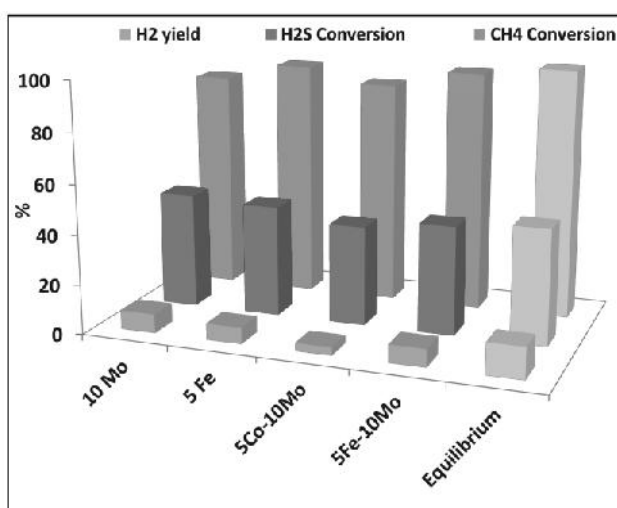


Figure IX.6: H_2S and CH_4 Conversion, H_2 Yield in comparison with the equilibrium data ($\tau = 30$ ms, $T = 1000^\circ C$, $H_2S^{IN} = 40$ vol%, $CH_4^{IN} = 1$ vol%, $O_2/H_2S = 0.2$).

From the data reported in Figure IX.7, it is possible to note that these last one have exhibited also a high selectivity towards COS , CS_2 , unlike to the Fe-based catalysts (5Fe, 5Fe-10Mo), that have shown a very low formation of COS , by indicating that in presence of methane, were obtained essentially CO and CO_2 .

Between two Fe-based catalyst, the bimetallic sample (5 Fe-10 Mo) has allowed to obtain a lower SO_2 selectivity respect to the monometallic catalyst. This result can be explained considering that the molybdenum is necessary as active phase to depress the SO_2 formation while the presence of the iron is able to inhibit the COS , CS_2 formation.

Based on the obtained results, it is appeared that, at low contact time, the bimetallic catalyst 5 Fe-10 Mo allows to improve the reactants conversion (H_2S , CH_4) and H_2 yield, depressing the SO_2 selectivity; furthermore, it allows the abatement of sulfurized by-products toxic and poisonous such as COS , CS_2 .

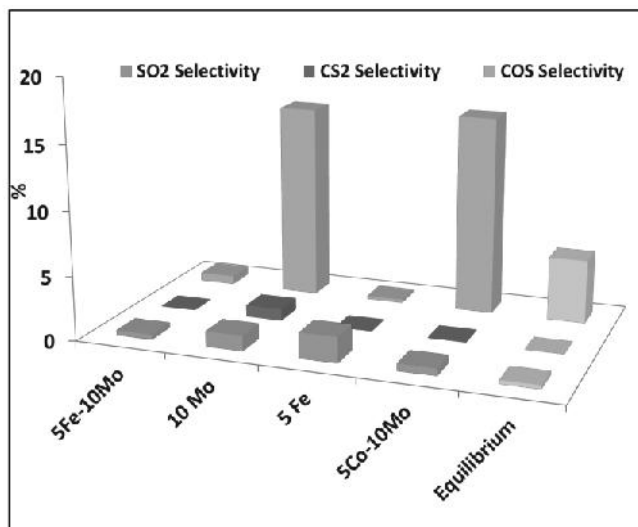
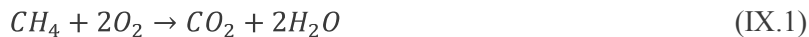


Figure IX.7: SO_2 , COS , CS_2 Selectivity in comparison with the equilibrium data ($\tau = 30$ ms, $T = 1000^\circ\text{C}$, $\text{H}_2\text{S}^{\text{IN}} = 40$ vol%, $\text{CH}_4^{\text{IN}} = 1$ vol%, $\text{O}_2/\text{H}_2\text{S} = 0.2$).

A possible reaction mechanism in presence of CH_4 was hypothesized.

The CH_4 addition gives the reaction system more complex for the presence of more reactions that can occur simultaneously (Eq.IX.1-2). Some of these that are following reported, can lead to the formation of the by-products poisonous as COS , SO_2 , CS_2 (Eqs.IX.3-5):



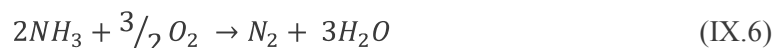


In fact the CH_4 can react with the oxygen to form CO (*partial oxidation*) and CO_2 (*total oxidation*), but it can react with the H_2S and sulphur to produce CS_2 , that could then react with the SO_2 to produce COS.

IX.3 NH_3 effect on 5Fe-10Mo catalyst

Starting by the promising results obtained by the bimetallic 5Fe-10Mo catalyst in the presence of CH_4 , same sample was tested also in presence of ammonia (5.5 vol%), with a feed stream composition very similar to that typical of a refinery, characterized by a high percentage of H_2S (64.8 vol%).

Prior to carry out the catalytic tests, it was necessary to modulate the feed molar ratio in order to obtain the oxygen concentration able to guarantee also the ammonia conversion. The new feed molar ratio (O_2/H_2S+NH_3) was defined on base of the stoichiometric oxygen required for the NH_3 oxidation reaction and considering that the ratio of O_2/H_2S had to be equal 0.2 (Eq.IX.3):



As it is possible to see by the stoichiometry of the reaction, for each mole of NH_3 occur 0.75 mole of O_2 ; so, the feed molar ratio $O_2/(H_2S+NH_3)$ is equal to 0.24 with a total oxygen concentration of 17 vol%.

The first catalytic activity test was carried out with 64.8 vol% of H_2S , $O_2/H_2S = 0.2$ in absence of ammonia by varying the temperature between 800 and 1000°C at the fixed contact time of 1 sec. The experimental data reported in terms of H_2S , H_2 , H_2O and SO_2 concentration were compared with the respective equilibrium values for each value of temperature (Figure IX.8).

By increasing the temperature, the increase of the H_2 concentration has a specular trend to the H_2S diminution, because at these temperatures the H_2S decomposition reaction is particularly favored; the SO_2 concentration decreases with the temperature reaching a constant value of ~2400 ppm.

The experimental composition is very close to the ones expected from the thermodynamic equilibrium.

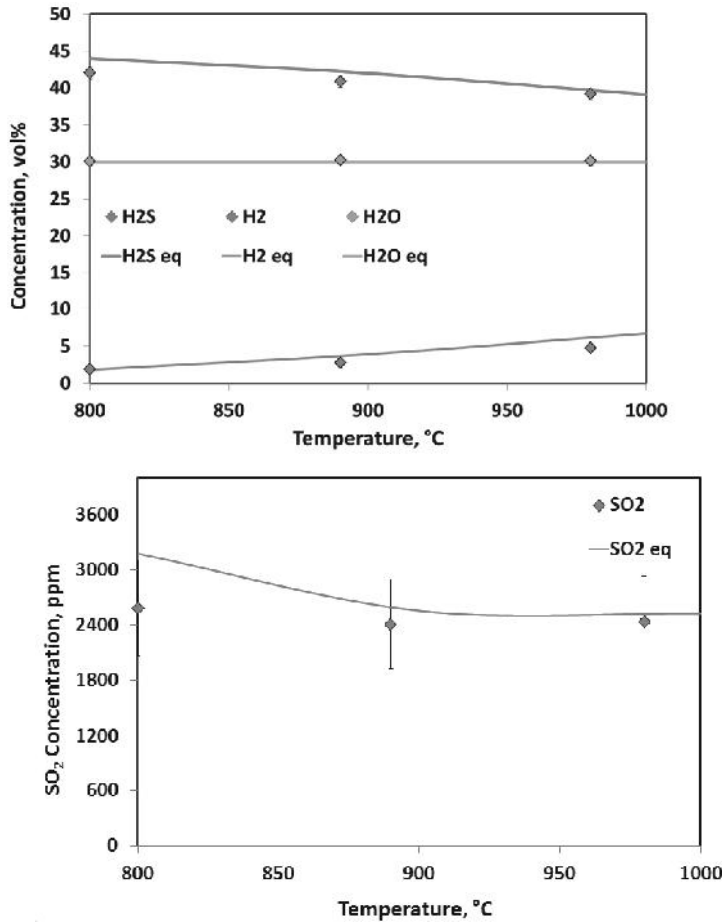


Figure IX.8: Concentration profiles of H_2S , H_2 , H_2O , SO_2 by varying the temperature ($H_2S^{IN} = 64.8 \text{ vol\%}$, $O_2/H_2S = 0.2$, $\tau = 1 \text{ sec}$).

Ammonia is usually present in refinery streams with not negligible concentrations and it can constitute a problem for the plants relatively to the salts formation, if the conversion isn't enough high.

Ammonium salts can be obtained from the reaction of NH_3 with H_2S (ammonium sulphide) (Eq.IX.7) or with SO_2 and water (ammonium sulphite) (Eq.IX.8):



The influence of the contact time was investigated in terms of NH_3 and H_2S conversion, H_2 yield and SO_2 selectivity at temperature of 1020°C (Figure IX.9, Figure IX.10). The H_2S conversion, H_2 yield and the SO_2 selectivity does not seem to be influenced by the variation of the contact time. In particular, the SO_2 selectivity is even lower than the equilibrium value (1%).

A different behaviour was observed for the NH_3 conversion; although the ammonia is not thermodynamically limited, the approach to the equilibrium conversion is observable only for contact times values of about 1 s, because, from the kinetic point of view, the ammonia conversion seem to be sensibly slower than the hydrogen sulphide.

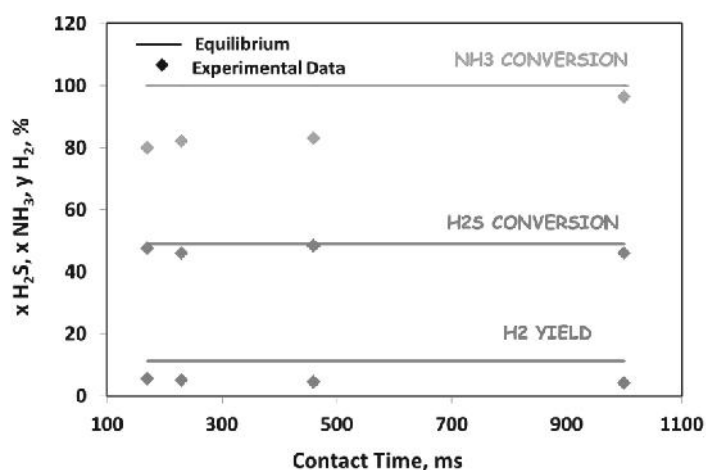


Figure IX.9: H_2S and NH_3 conversion, H_2 yield, by varying the contact time in comparison with the equilibrium data ($\text{H}_2\text{S}^{\text{IN}} = 64.8 \text{ vol}\%$, $\text{NH}_3^{\text{IN}} = 5.5 \text{ vol}\%$, $\text{O}_2/\text{H}_2\text{S}+\text{NH}_3 = 0.24$, $T = 1020^\circ\text{C}$).

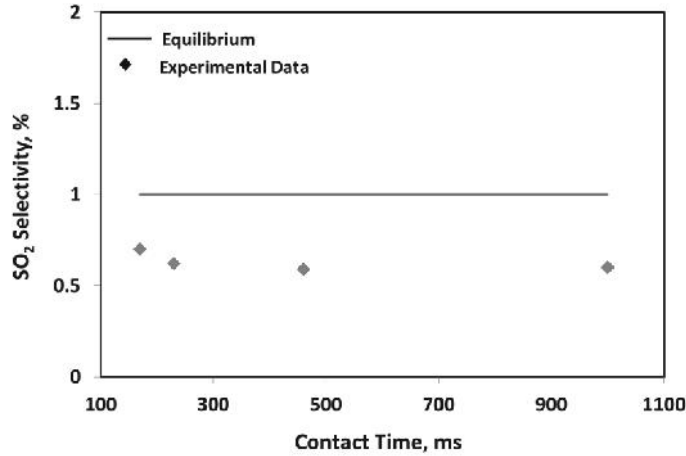


Figure IX.10: *SO₂ selectivity by varying the contact time in comparison with the equilibrium data ($H_2S^{IN} = 64.8$ vol%, $NH_3^{IN} = 5.5$ vol%, $O_2/H_2S+NH_3 = 0.24$, $T = 1020^\circ C$).*

Based on the results obtained, the influence of the temperature was investigated at contact time of 1 s.

As it is possible to note in Figure IX.11, the effect of the temperature on the NH_3 conversion is less strong respect to the contact time because the conversion is even higher than 90% in all the range of temperature investigated. In particular, it is important to observe that, at temperature of $1020^\circ C$, the NH_3 conversion is very high, corresponding to about 96%. Unfortunately, due to the problematic of the salts formation, in order to assure the very low ammonia concentration able to ensure a good plant operativity, it is necessary to work at temperatures higher than $1050^\circ C$, where the NH_3 conversion is about 99%. The H_2S conversion and the H_2 yield approach to the thermodynamic equilibrium, also if it is possible that the recombination reaction between sulphur and hydrogen to form H_2S may also occurs at the outlet of the catalytic bed, in the temperature range $1000-700^\circ C$, determining a slight decrease of the H_2 yield with a corresponding decrease of the H_2S conversion.

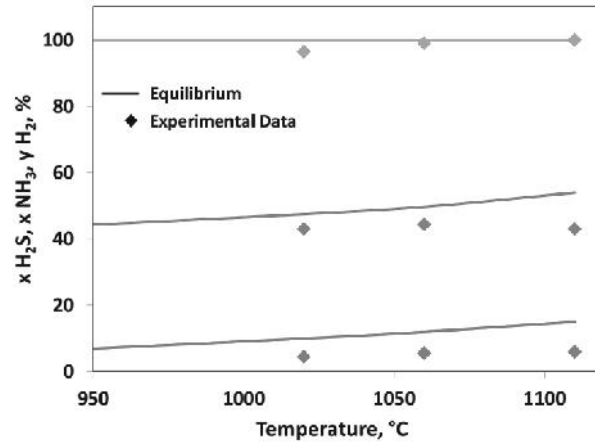


Figure IX.11: H_2S and NH_3 conversion, H_2 yield, as function of the reaction temperature in comparison with the equilibrium data ($H_2S^{IN} = 64.8 \text{ vol\%}$, $NH_3^{IN} = 5.5 \text{ vol\%}$, $O_2/H_2S+NH_3 = 0.24$, $\tau = 1 \text{ sec}$).

The trend of the SO_2 selectivity is slightly increasing with the temperature approaching to the equilibrium value at 1110°C (1%).

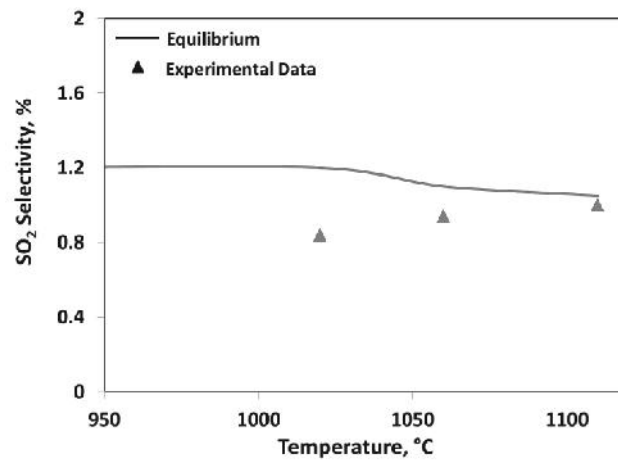


Figure IX.12: SO_2 selectivity as function of the reaction temperature in comparison with the equilibrium data ($H_2S^{IN} = 64.8 \text{ vol\%}$, $NH_3^{IN} = 5.5 \text{ vol\%}$, $O_2/H_2S+NH_3 = 0.24$, $\tau = 1 \text{ sec}$).

IX.4 Effect of NH_3 and CH_4 on 5Fe-10Mo catalyst

The simultaneous presence of CH_4 and NH_3 , that are typically in a refinery stream was investigated at temperature of 1060°C and contact time of 1 s.

The concentration profiles of the reactants and the products are reported in the following figures (Figure IX.13, Figure IX.14).

The NH_3 conversion is quasi total (99%), in fact the concentration at the outlet of the reactor is very small (500 ppm).

Relatively to the H_2S and H_2 concentration, it is very probable that with this contact time, the recombination reaction between Sulphur and H_2 occurs, determining a H_2S concentration higher (~ 43 vol%) and a H_2 concentration lower (~ 5 vol%) than the values expected from the thermodynamic equilibrium, respectively equal to 38 vol% and 11 vol%.

The CH_4 is totally converted especially to CO_2 , the which concentration is in agreement with the one expected from the equilibrium (~ 7000 ppm) and CO . Low concentrations of COS , CS_2 , and SO_2 evidence that the presence of methane and ammonia does not affect in a sensible way the reaction mechanism, and consequently on the catalytic performances.

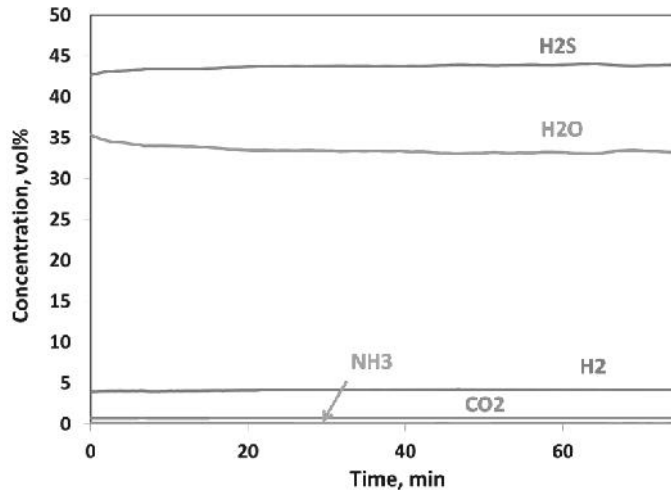


Figure IX.13: Concentration profiles of H_2S , H_2 , NH_3 , CO_2 at $T= 1060^\circ\text{C}$, $\tau= 1$ sec ($\text{H}_2\text{S}^{\text{IN}} = 64.8$ vol%, $\text{NH}_3^{\text{IN}} = 5.5$ vol%, $\text{CH}_4^{\text{IN}} = 1$ vol%, $\text{O}_2/\text{H}_2\text{S}+\text{NH}_3=0.24$).

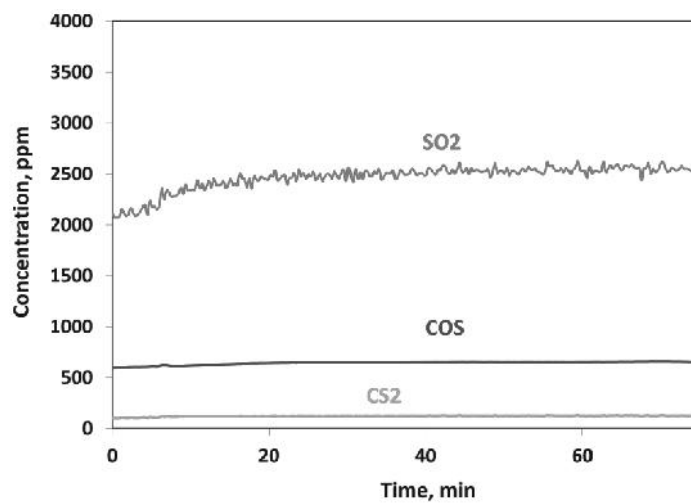


Figure IX.14: Concentration profiles of SO_2 , COS , CS_2 at $T= 1060^\circ C$, $\tau= 1$ sec ($H_2S^{IN} = 64.8$ vol%, $NH_3^{IN} = 5.5$ vol%, $CH_4^{IN} = 1$ vol%, $O_2/H_2S+NH_3 = 0.24$).

X STRUCTURED CATALYSTS

X.1. Structured Catalyst Preparation

The formulation of the Fe-Mo bimetallic catalysts was transferred on cordierite monoliths.

The honeycomb monoliths were prepared by dip coating method.

Cordierite honeycomb monoliths (226 cpsi, average wall thickness 0.23 mm) 30 mm in length, 6 mm wide and 6 mm high were used as a substrate (9 channels). The apparent density of the monolith was 0.47 g/cm³.

For the washcoat preparation it was prepared a suspension of boehmite (AlOOH), provided by Sigma Aldrich, nitric acid (60-65 vol%) and distilled water. The objective of the washcoating procedure was to obtain a washcoat load of about 30 wt% on the monoliths in order to realize an average washcoat layer on the monoliths channels walls of about 100 micrometer.

The active phase deposition was started with an aqueous solution of iron acetate (CH₃COO)₂Fe with ammonium heptamolibdate tetrahydrate (NH₄)₆Mo₇O₂₄·4H₂O.

Before the washcoat deposition, the monolith was thermally pretreated at 500°C in a muffle furnace for 2 h. The slurry formation was obtained by adding the nitric acid (HNO₃) to the suspension in agitation in order to obtain a pH value of 1-2, to ensure good rheological properties that are necessary for the achievement of a uniform and homogeneous washcoat deposition. The optimal adhesion to the substrate is an important requirement, because the operating reaction conditions could cause the separation of the washcoat from the carrier involving the deterioration of the catalyst efficiency.

The dip coating procedure was realized by dipping the ceramic support in the slurry for 1h (Figure X.1).



Figure X.1: *Monolith dipped in the washcoat.*

After the impregnation of the monolith, the excess suspension inside the channels of the cordierite substrate was aspirated by a vacuum pump. Then, the monoliths were dried at 120°C for 12 h and after calcined at 500°C for 2h. For all the coating cycles after the first one, the same procedure was adopted until the reaching the desired washcoat load.

The percentage of the desired washcoat was evaluated by considering the initial weight of the monolith and the weight after each step of impregnation/calcination. In particular, the number of the cycles of the impregnation/calcination has been such as to allow a final percentage of the washcoat equal to 15, 20, 30 wt%.

The estimation of the average thickness of the washcoat layer deposited on the cordierite was made through the evaluation of the apparent density of the powder alumina after the calcination at 500°C for 2h and the calculation of the total surface of the monolith considering a parallelepiped geometry.

The formula used for the calculation of the average thickness of the washcoat is following reported (Eq.X.1):

$$\text{Average thickness} = \frac{\rho_{APP} \cdot \text{washcoat weight}}{S} \quad (\text{X.1})$$

where:

ρ_{APP} : apparent density of alumina;

washcoat weight: mass of the washcoat deposited

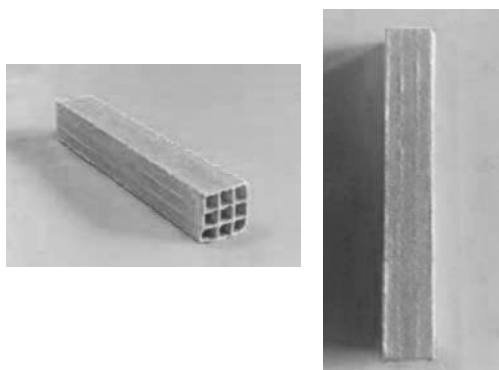
S : total surface of the monolith

In Table X.1 is reported the average thickness of the washcoat layer for three different percentage of washcoat deposited.

Table X.1: Average thickness of washcoat layer.

Samples	Average Thickness (μm)
Washcoat 15 wt%	46
Washcoat 20 wt%	64
Washcoat 30 wt%	90

After the achievement of the desired washcoat load, the monoliths were calcined at 900°C for 1h at a heating rate of $20^{\circ}\text{C}/\text{min}$ (Figure X.2).

**Figure X.2:** Structured Catalyst after calcination at 900°C for 1h.

The active phase deposition was started by an aqueous solution of ammonium heptamolibdate tetrahydrate $(\text{NH}_4)_6\text{Mo}_7\text{O}_{24}\cdot 4\text{H}_2\text{O}$ and iron acetate $(\text{CH}_3\text{COO})_2\text{Fe}$.

A known amount of the salts precursors able to assure a nominal load of MoS_2 and FeS_2 , respectively of 10 wt% and 5 wt%, were dissolved in water and this solution was placed on a heated plate at $200\text{-}250^{\circ}\text{C}$. The monoliths, after washcoat deposition and stabilization at 900°C for 1h, were dipped into the solution until to the complete water evaporation to ensure the precipitation of the salts on the external surface and in the channels of the monolith. After the impregnation, the excess of the solution from the channel is aspirated and the sample was dried at 120°C for 12 h and then calcined 450°C for 3 h.

The impregnation/drying steps in the salt precursor solution of the active phase were repeated for numerous times until the desired load of the active phase was reached. Furthermore, at the end of each impregnation/drying cycle, the samples were calcined at 450°C for 3 h.

Also, in this case, the percentage of the desired load of active phase was evaluated by considering the initial weight of the monolith without active phases and the weight after each step of impregnation/calcination with the active phases.

Similarly to the powder catalysts, the monolith was sulfided with the procedure previously described in order to obtain the active species desired.

X.2. Monoliths Characterization

In this paragraph are illustrated the results of the characterization techniques relating to each preparation steps of the structured catalysts, starting from the cordierite carrier to the washcoat impregnation; the successive phase to the washcoat deposition that involves the impregnation of the monolith with the active phase is realized at the same way of the powder sample.

The washcoat stability and the uniform distribution on the carrier were evaluated by ultrasonic tests and SEM.

X.2.1 Specific Surface Area

In Table X.2 are listed the values of the surface area of the cordierite, before and after washcoat deposition with three different loading (15-20-30 wt%).

Table X.2: *Surface Specific Area of the cordierite and the different percentage of washcoat deposited on the mechanical support.*

SAMPLE	SSA (m²/g)
Cordierite	0.8
Washcoat 15%wt	8.6
Washcoat 20%wt	9.2
Washcoat 30%wt	29.0

As it can be seen from the table, the surface area of the cordierite is very low (<1 m²/g) due to a low porosity. For this reason, it was necessary the washcoat deposition in order to increase the surface area and assure a

good dispersion of the active phases. By increasing the washcoat load from 15 wt% to 30 wt%, the surface area is enhanced from 8.6 m²/g to 29 m²/g.

X.2.2 SEM

The homogeneity of the layer of washcoat and the possible presence of macroporosity of the support was investigated with the SEM analysis.

The SEM images of the cordierite and the cordierite after the washcoat deposition are shown in Figure X.3.

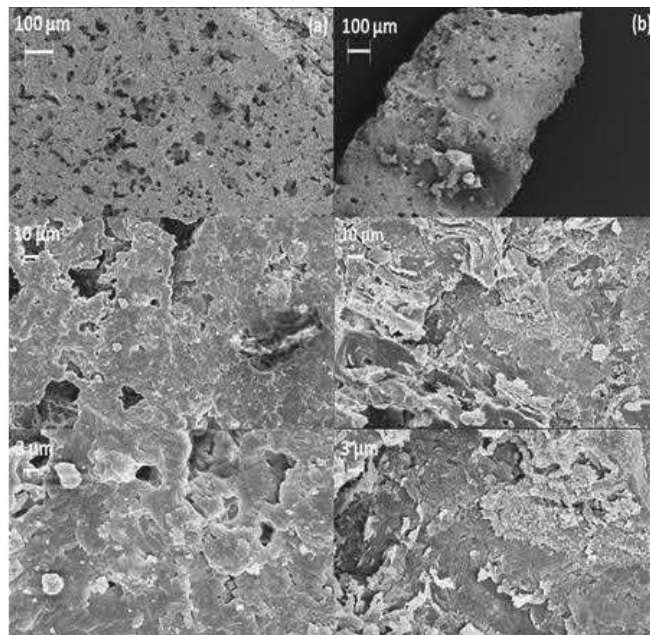


Figure X.3: SEM images of the cordierite (a) and the washcoat deposition on the carrier (b).

In the left image (a) we can observe the presence of the macropores of the cordierite that represent anchoring points for the washcoat layer that will be deposited; the presence of these macropores is also justified from the value as low of the specific surface area (<1 m²/g).

In the right image (b), it's obvious that during the coating procedure all the macropores in the cordierite walls were completely covered and filled by the washcoat.

It is also interesting to note that such porosity had additional anchoring points for the washcoat layer with the potential beneficial effect of an improved final catalyst-carrier adhesion.

For a higher enlargement (100 μm) the images show the presence of small micro cracks also on the washcoat layer. According to current literature, this kind of small crack, due to the limited dimensions, may act as additional anchoring points for the active species and generate other surfaces available for the chemical reaction (Dongfang and Zhang, 2013).

X.2.3 Ultrasonic Test

The mechanical stability of the washcoat layer deposited on the cordierite was investigated by ultrasonic tests. In Figure X.4, the results are reported, with regard to three different washcoat loads (10-20-30 wt%), where the weight loss (Eq.V.3.1-V.2.6 *Ultrasonic Test*) is a function of the exposure time to the ultrasonic.

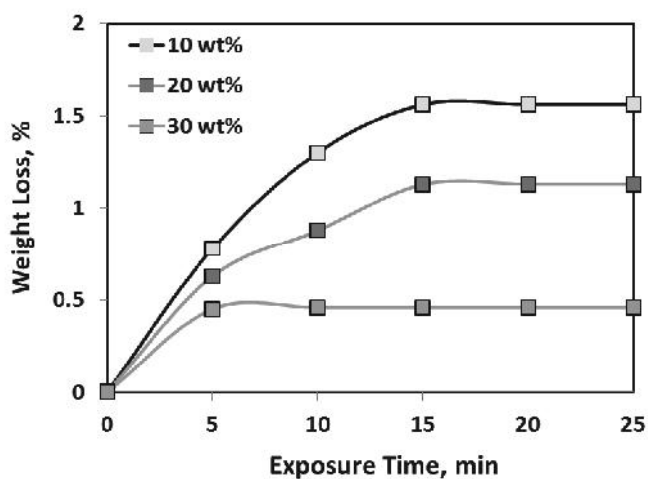


Figure X.4: Adhesion Test Stability for three different washcoat load.

A better adhesion of the washcoat to the cordierite is observed for the sample with 30 wt% for which it was registered a weight loss lower than

0.5%. The higher weight loss was obtained for the sample having the lower washcoat load for which it has been of 1.5%.

Anyway, the results obtained for all the three samples denote a good adhesion and stability of the washcoat on the carrier, by confirming the goodness of the preparation method.

X.3. Catalytic Activity Test

X.3.1 Onset Catalytic Test: Monolith vs Powder

The catalytic performance of the structured catalyst (Figure X.5) was compared with the respective powder sample (Figure X.6) in order to verify the goodness of the preparation and the correct transfer of the catalytic formulation from the powder to the monolith.

In addition, it was studied the *onset* temperature of the catalyst, defined as the temperature at which it verifies an H₂S conversion of about 10%.

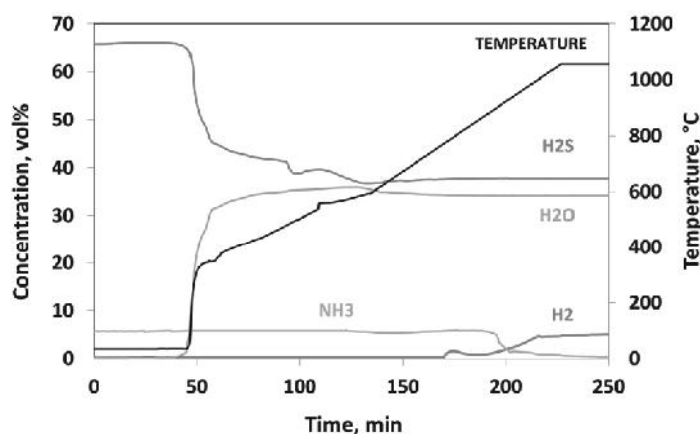
This test is very useful to know the activation temperature of the catalyst, especially if the reaction has to be carried in auto-thermal mode.

For both the catalysts, in order to realize the comparison between the powder and monolith, the onset test was carried out with the same mass of catalyst (Weight Hourly Space Velocity = 9000 h⁻¹) since the contact time is different because the volume occupied by the monolith is not the same of the one occupied by the powder. For the onset test, it was programmed a heating rate of the furnace of 3°C/min.

In Figure X.5 is illustrated the onset test carried out on the monolith.

The feed stream containing H₂S, NH₃ is directly sent to the reactor at room temperature (~34 °C); after ~40 min, the oxygen (that is not analyzed) was added to the stream and subsequently a fast increment of the reactor temperature of ~300°C was observed, accomplished by a strong reduction of the H₂S concentration and the increase of the water.

From the temperature of 300°C, the heating of the reactor up to 1060°C has followed the heating rate of the furnace.



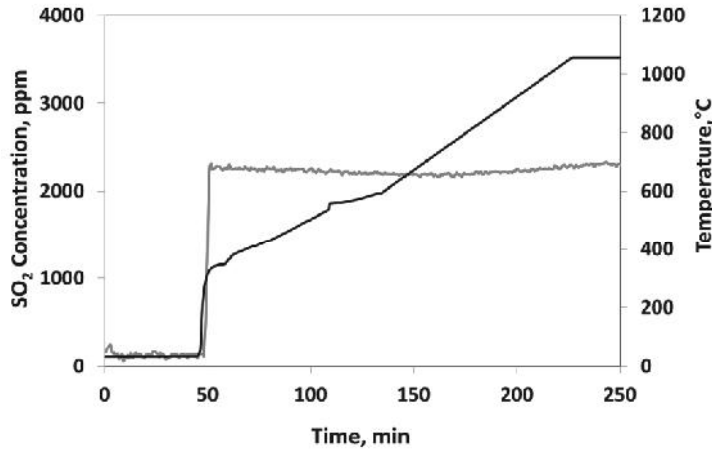


Figure X.5: Onset Catalytic Test on 5Fe-10Mo Monolith ($H_2S^{IN} = 64.8$ vol%, $NH_3^{IN} = 5.5$ vol%, $O_2/H_2S+NH_3 = 0.24$, $\tau = 2.12$ s).

It is interesting to observe that, the concentration values of H_2S and H_2O are almost the same in the overall temperature range, while, the reactions that involve the H_2 formation and the NH_3 consumption, occur only starting from the temperature of $800^\circ C$. At $T = 1060^\circ C$ the NH_3 is completely converted and the concentration of H_2 does not suffer variations. As regards to the SO_2 concentration, the formation is obviously correlated to the addition of the oxygen in the feed; also, in this case, it is important to note that, compared to what expected by the equilibrium, the concentration is even of ~ 2000 ppm, suggesting that this catalyst, already low temperature, promotes the Claus reaction that involves the SO_2 conversion to Sulphur.

The onset test for the powder sample is showed in Figure X.6.

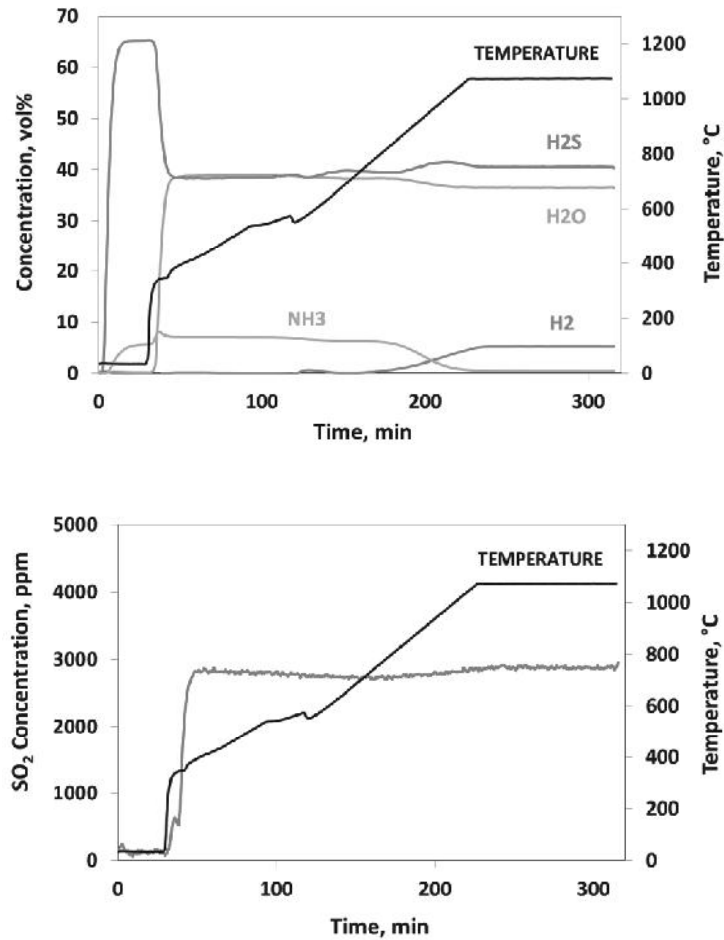


Figure X.6: Onset Catalytic Test on 5Fe 10Mo Powder ($H_2S^{IN} = 64.8$ vol%, $NH_3^{IN} = 5.5$ vol%, $O_2/H_2S+NH_3 = 0.24$, $\tau = 0.5$ s)

The results clearly showed that the onset temperature and the trend of the concentration profiles are the same for both the samples, confirming that the structured catalyst was correctly prepared.

X.3.2 Stability Test

In order to verify the stability of the structured catalyst prepared, a stability test of ~35 h of time on stream at $T = 1060^\circ\text{C}$ was carried out.

The concentration profiles of the reactants and the products are illustrated in Figure X.7.

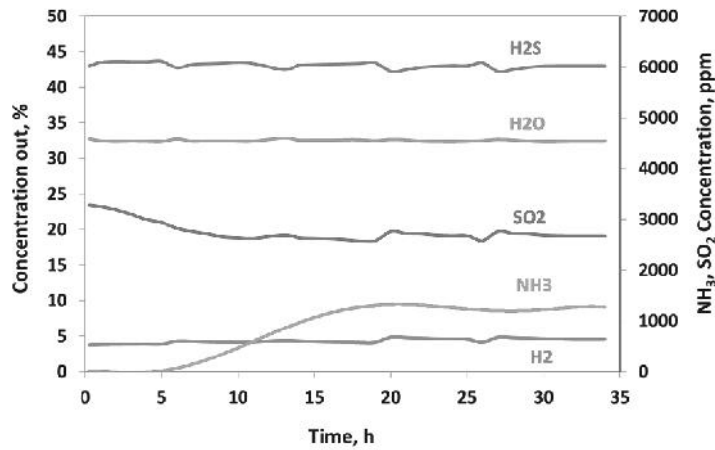


Figure X.7: Stability Test ($T=1060^{\circ}\text{C}$, $O_2/H_2S+NH_3=0.24$, $\tau=1\text{s}$). Profile concentration of H_2S , H_2 , H_2O , NH_3 , SO_2 .

As it is possible to see from the figure, the concentration of H_2S , H_2 , H_2O , SO_2 are very stable during the stability test. An increase of the ammonia concentration starts at about 6h o TOS, and reaches a very low concentration of NH_3 of about 1100 ppm at about ~20 h of time on stream. After that, the value of ammonia concentration is maintained constant until the end of the test. This result is confirmed by the behavior of the NH_3 conversion during the stability test in Figure X.8.

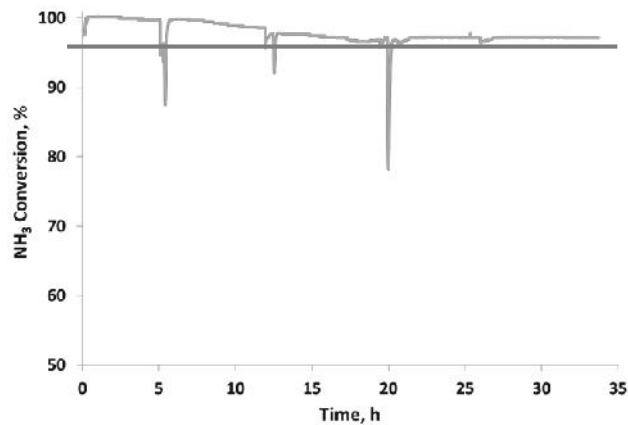


Figure X.8: NH_3 Conversion as function of time on stream ($T=1060^{\circ}\text{C}$, $O_2/H_2S+NH_3=0.24$, $\tau=1\text{s}$).

The trend is slightly decreasing with time on stream, but however, the final ammonia conversion was about 98%.

In conclusion, the duration test has confirmed the stability of the catalyst at so high temperature for 35 h of time on stream without showing any deactivation tendency regarding the H₂S conversion and the H₂ yield. The final values of H₂S conversion, H₂ yield, SO₂ selectivity were respectively equal to 40%, 6%, 1% in good agreement with the ones expected from the equilibrium.

XI SOUR GAS SOAP™ vs Claus Process

The feature of Kinetics Technology SOUR Gas SOAP™ (Selective & Oxidative Auto-thermal Process) is the production of valuable products: hydrogen and liquid Sulphur by catalytic oxidative cracking of sour gas instead of the production of SO₂, as for the conventional process technology (Colozzi *et al.*, 2016).

XI.1 Sulphur Recovery Unit (SRU): Best Available Technique

Nowadays environmental regulations all around the world are imposing very stringent SO₂ emission requirements.

The main targets of the SRU to be installed in a new industrial complex can be summarized as follow:

- SO₂ emissions not higher than 150 mg/Nm³ (50 ppm vol.);
- Complete destruction of impurities contained in Sour Gases feedstock (NH₃, HC, COS, CS₂, RSH, HCN etc.);
- Maximize energy recovery;
- Reduction of the fixed and operating costs;

The block diagram of Sulphur Recovery Unit with KT Proprietary “RAR™ Process” is presented in Figure XI.1.

SOUR GAS SOAP™ vs Claus Process

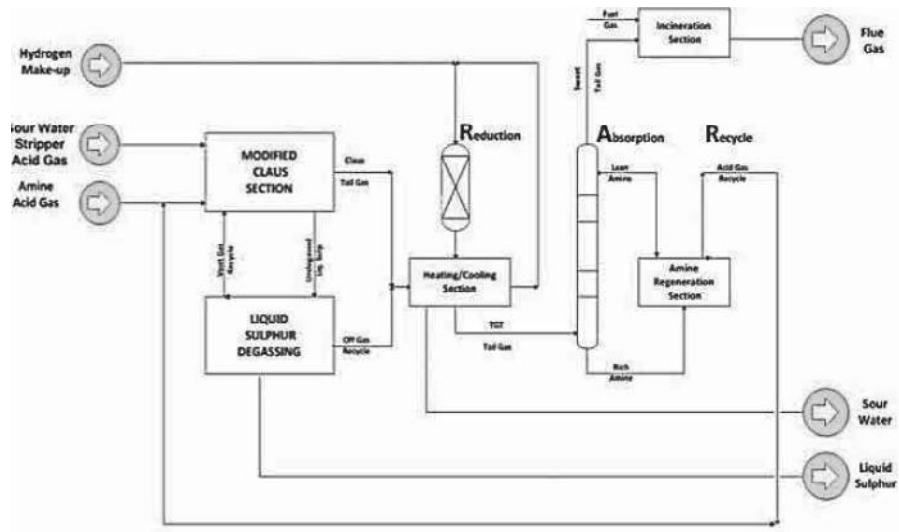


Figure XI.1: Block Diagram of SRU with RAR Process.

The KT proprietary RAR™ Process is a Reductive Amine based Tail Gas Treatment capable of achieving the maximum of the overall Sulphur Recovery Efficiency (SRE > 99.9+%) nowadays requested by the market.

The Modified Claus section of SRU can achieve a SRE of 92-96% when provided with two reactors and 94-98% when provided with three reactors, therefore, the addition of a Tail Gas Treatment section is always required to achieve a SRE higher than 99.9% as requested by the market.

The produced liquid sulphur is treated in the liquid sulphur degassing section where hydrogen polysulfides and H₂S are completely removed. In order to minimize the SO₂ all the gas released during the liquid sulphur degassing are recycled back to Claus and TGT section.

In the proprietary KT Tail Gas Treatment section, the Claus Tail Gas is mixed with Hydrogen Rich Gas from battery limits.

Tail Gas is then sent to the Hydrogenation Reactor, where all components containing Sulphur (COS, CS₂, SO₂) are reduced and/or are hydrolyzed to H₂S.

The H₂S contained in Tail Gas is removed by the use of amine solution. The amine solution is normally regenerated in a dedicated Amine Regeneration Section, included in the Sulphur Recovery Unit.

Sweet Tail Gas with few ppm of H₂S is sent to the Thermal Incinerator to be converted to SO₂ before flue gases are released to the atmosphere.

XI.2 NEW Sulphur Recovery Unit

All the knowledge and data acquired from the UNISA laboratory tests have allowed KT to set-up an optimized process simulations of the Novel Process choosing the best process scheme and the best operating conditions (Colozzi *et al.*, 2016).

The New Concept of SRU designed by KT is a simplification of current SRU plant configuration thanks to the innovative Reaction Furnace filled with KT proprietary catalyst (Catalytic Reaction Furnace, CRF) followed by only one Sulphur Condenser, a Liquid Sulphur Degassing section and TGT section. The reason of such “minimal” configuration is strictly related to the new idea to operate the Claus Section in a different way:

- Use of a totally new and KT Proprietary Catalyst developed by UNISA in the Reaction Furnace to minimize SO_2 production;
- Use of a specific ratio $\text{H}_2\text{S}/\text{O}_2$ in order to maximize the production of hydrogen minimizing the production of SO_2 ;
- Use of oxygen (enriched air) instead of ambient air;

The new SRU concept developed by KT is reported in Figure XI.2.

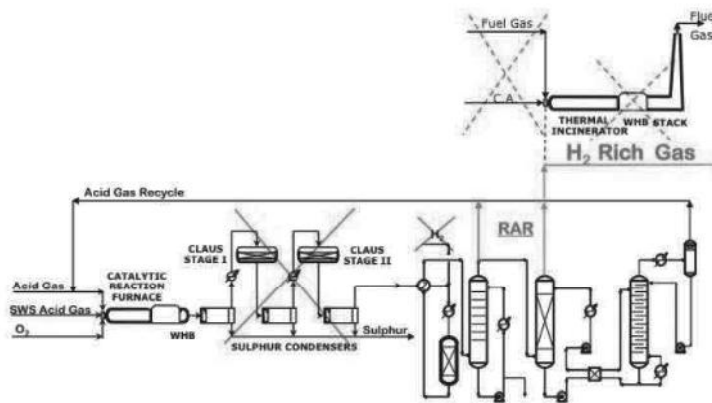


Figure XI.2: Process Flow Scheme “New Concept of SRU”.

The conventional plant configuration consists of a Modified Claus Section equipped with two Claus reactors followed by a Reductive TGT amine based with a dedicated Amine Regeneration system and the relevant Thermal Incineration section. Liquid Sulphur Degassing section is also foreseen.

SOUR GAS SOAP™ vs Claus Process

The Novel Process is equipped only with a Catalytic Reaction Furnace System and a Sulphur Condenser followed by a Reductive TGT amine based with a dedicated Amine Regeneration System and Liquid Sulphur Degassing Section with full recycle of H₂S to Claus and TGT section. Thermal Incinerator is foreseen but designed to be operated only during start-up and shut-down scenarios.

XI.3 Conclusion

The Sour Gas SOAP™ prove to be an environmental friendly solution capable to valorize Sour Gases, which is considered a waste in all industrial complexes, in Hydrogen Rich Gas, a valuable product achieving the goal of “zero emissions”.

Especially, the major value of the new technology Innovation is to have created an alternative to traditional SRU process, able to produce Hydrogen rich gas instead of SO₂ emission.

The main advantages of the New SRU configuration and Novel Process are summarized here below:

- Possibility to achieve SO₂ emissions lower than 50 mg/Nm³ (18 ppm Vol.), this is not possible with the current Reductive Amine Based Best Available Technique;
- Complete destruction of COS, CS₂, hydrocarbons, RSH, ammonia, HCN and other impurities in the Catalytic Reaction Furnace;
- Installation of only one Catalytic Converter System;
- Claus Catalytic Converters system is no more necessary due to low content of SO₂ in the process gas from the Catalytic Reaction Furnace.
- The Novel Process will produce a lower quantity of exhaust catalyst compared to the conventional one;
- The reduced number of equipment makes the Investment Cost of the Novel Process cheaper than the conventional one. In addition also the associated maintenance costs will be reduced;

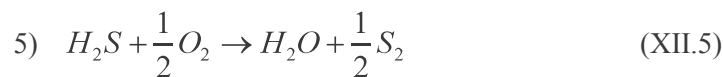
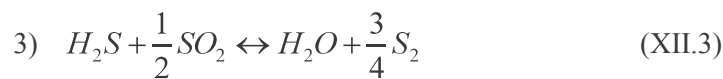
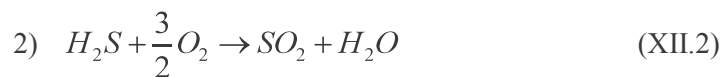
The major advantage of the novel process is the higher overall SRE. Indeed SRE of H₂S Cracking + TGT is 99.9++% much higher than 99.9+% of current BAT. The reason of this difference is due to the fact that in the Novel Process the quantity of Total Sulphur (H₂S + COS + CS₂) in the top of TGT Absorber is much lower than in the conventional one;

XII KINETIC MODEL

XII.1 Homogeneous Phase

Starting from the obtained experimental results, a macroscopic kinetic model of H_2S thermal decomposition in the presence of oxygen was developed through the identification of the main reactions able to describe the complex system.

In particular, the mathematical model was developed assuming that the following five reactions occur in the reaction zone (Eqs. XII.1-5):



The kinetic expressions, provided by the literature (Kaloidas *et al.*, 1989;

Balaev *et al.*, 2001; Monnery *et al.*, 2000) and employed in the model, are the following (Eqs.XII.6-10):

$$r_1 = k_1 \left(P_{H_2} P_{S_2}^{\frac{1}{2}} - \frac{1}{K_{eq1}} P_{H_2S} \right) \quad (\text{XII.6})$$

$$r_2 = k_2 P_{O_2} P_{H_2S} \quad (\text{XII.7})$$

$$r_3 = k_3 \left(P_{H_2S} P_{SO_2}^{\frac{1}{2}} - \frac{1}{K_{eq2}} P_{H_2O} P_{S_2}^{\frac{3}{4}} \right) \quad (\text{XII.8})$$

$$r_4 = k_4 P_{O_2} P_{H_2S} \quad (\text{XII.9})$$

$$r_5 = k_5 P_{O_2} P_{H_2S} \quad (\text{XII.10})$$

where:

r_1 : rate of reaction 1

r_2, r_4, r_5 : rate of reactions 2, 4 and 5

r_3 : rate of reaction 3

K_{eq1} : Equilibrium constant of reaction 1 [$\text{atm}^{-0.5}$]

K_{eq2} : Equilibrium constant of reaction 3 [$\text{atm}^{+0.25}$]

P_i : Partial pressure of component i-th [atm]

k_1, k_3 : Kinetic constant of reaction 1 and 3 [$\text{min}^{-1} \cdot \text{atm}^{-1.5}$]

k_2, k_4, k_5 : Kinetic constant of reaction 2, 4 and 5 [$\text{min}^{-1} \cdot \text{atm}^{-2}$]

The mass balances for each component are reported below, by assuming the reactor as a plug flow reactor (PFR) (Eq.XII.11-16):

$$\text{H}_2\text{S balance: } \dot{Q} \cdot \frac{dy_{H_2S}}{dV} = r_1 - r_2 - r_3 - r_4 - r_5 \quad (\text{XII.11})$$

$$\text{H}_2 \text{ balance: } \dot{Q} \cdot \frac{dy_{H_2}}{dV} = -r_1 + r_4 \quad (\text{XII.12})$$

$$\text{SO}_2 \text{ balance: } \dot{Q} \cdot \frac{dy_{\text{SO}_2}}{dV} = r_2 - 0.5r_3 + r_4 \quad (\text{XII.13})$$

$$\text{S}_2 \text{ balance: } \dot{Q} \cdot \frac{dy_{\text{S}_2}}{dV} = -0.5r_1 + 0.5r_5 + 0.75r_3 \quad (\text{XII.14})$$

$$\text{O}_2 \text{ balance: } \dot{Q} \cdot \frac{dy_{\text{O}_2}}{dV} = -1.5r_2 - r_4 - 0.5r_5 \quad (\text{XII.15})$$

$$\text{H}_2\text{O balance: } \dot{Q} \cdot \frac{dy_{\text{H}_2\text{O}}}{dV} = r_2 + r_3 + r_5 \quad (\text{XII.16})$$

The initial conditions are the following:

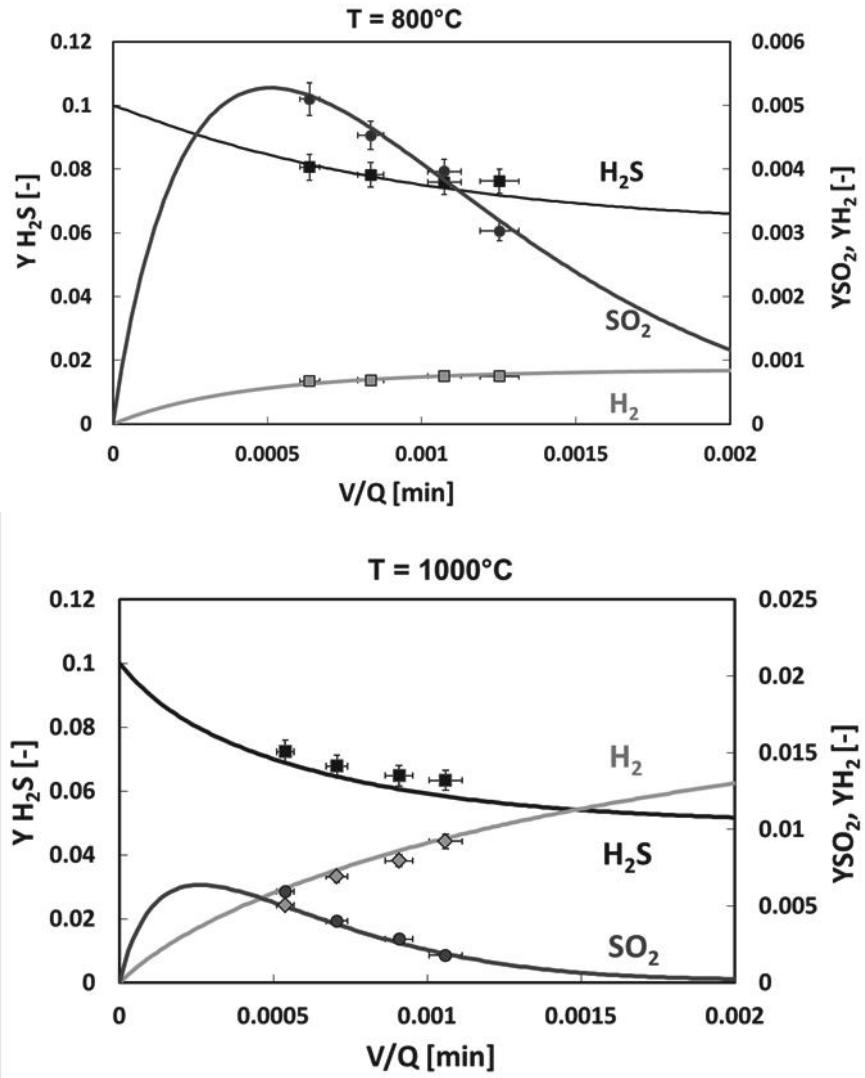
$$\begin{aligned} V=0 & \quad y_{\text{H}_2\text{S}} = 0.1 \\ V=0 & \quad y_{\text{O}_2} = 0.1 \cdot R \text{ (where R is the feeding O}_2\text{/H}_2\text{S molar ratio)} \\ V=0 & \quad y_{\text{H}_2} = y_{\text{SO}_2} = y_{\text{S}_2} = y_{\text{H}_2\text{O}} = 0 \end{aligned}$$

where:

$$\begin{aligned} Q: & \text{ Total flow rate [cm}^3 \text{ (stp) \cdot min}^{-1}\text{]} \\ y_i: & \text{ fraction volume of component i-th[-]} \\ V: & \text{ Reaction volume [cm}^3\text{]} \\ V/Q: & \text{ Residence time [min]} \end{aligned}$$

The differential equations system was solved by using the Euler method.

Primary goal of the simulation by mathematical model is to identify the apparent kinetic constants k_1 , k_2 , k_3 , k_4 and k_5 using nonlinear regression analysis of the experimental data obtained at 700, 900, 1000 and 1100 °C as a function of the residence time at a fixed feeding molar ratio ($\text{O}_2/\text{H}_2\text{S} = 0.2$) as reported in Figure XII.1. The nonlinear regression procedure was performed using the least-squares approach, based on the minimization of the sum of squared residuals between the experimental data and the values given by the mathematical model. The comparison between the experimental results with the model behavior is showed in the same Figure XII.1.



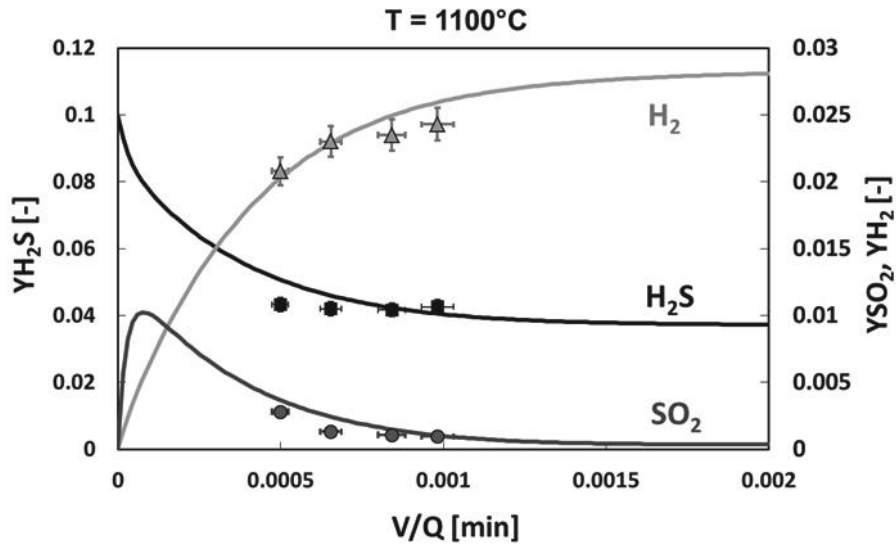


Figure XII.1: Comparison between model calculation and experimental data at 800°C (a), 1000°C (b), 1100°C (c) as function of the residence time. ($y_{H_2S}^{IN} = 0.1$, $O_2/H_2S=0.2$).

The results obtained from the model and the experimental data at different temperatures, have shown that, for low residence time, the oxidation reactions were promoted with SO_2 production, showing a maximum value.

With the increase of residence time, we have obtained a decrease of the molar fraction of SO_2 because of the Claus reaction giving rise to the SO_2 conversion to sulfur.

With regard to the hydrogen production, it is formed through the reactions 1, 4, immediately reaching a constant value for high residence time.

The kinetic constants values were calculated in the overall investigated temperature range, and thereafter it was estimated, for each reaction, the apparent activation energy value through the use of the Arrhenius plot (Figure XII.2).

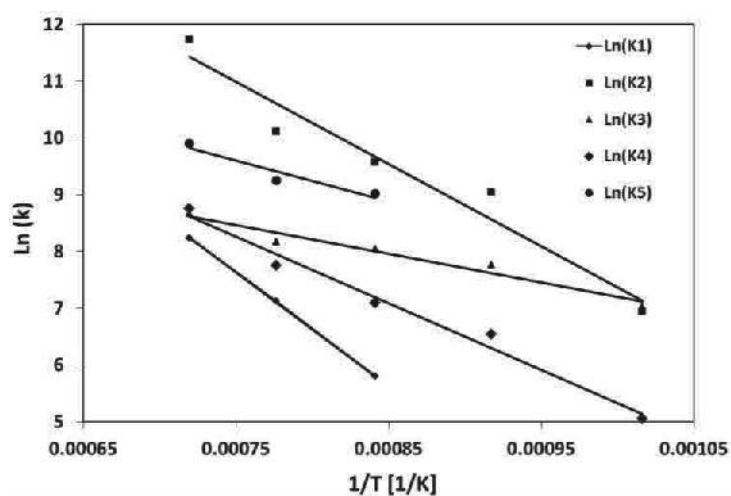


Figure XII.2: Arrhenius plot used for the evaluation of apparent activation energy.

The obtained values of the activation energy are illustrated in Table XII.1.

Table XII.1: Activation Energy obtained from the linear interpolation of the Arrhenius plot [kcal/mol].

E_{a1}	E_{a2}	E_{a3}	E_{a4}	E_{a5}
40	29	10	23	14

The values of E_{a1} , E_{a2} , E_{a3} are in good agreement with the values reported in the literature (Dowling *et al.*, 1999 & Tesner *et al.*, 1991).

The accuracy of the model was also tested at 900°C, in order to demonstrate the predictive capability of the model (Figure XII.3).

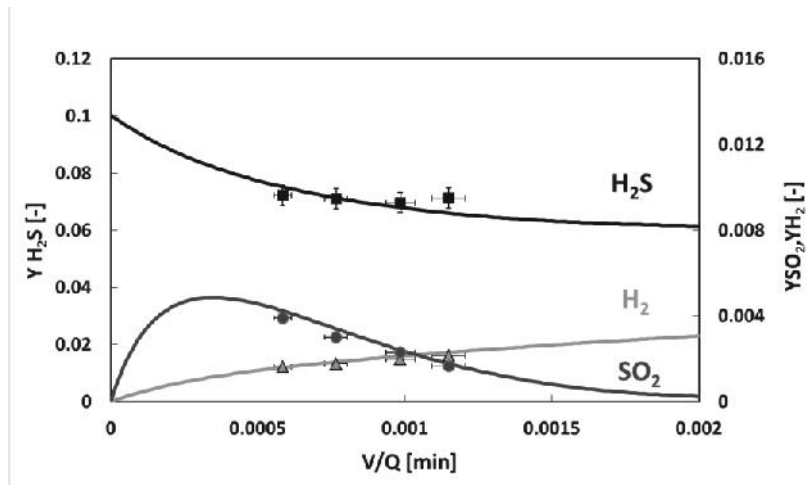


Figure XII.3: Comparison between model calculation and experimental data at 900°C as a function of the residence time. ($y_{H_2S}^{IN} = 0.1$, $O_2/H_2S=0.2$).

The predictive ability of the model was also tested with a different $O_2/H_2S = 0.25$ at 1000°C and 1100°C and, as shown in Figure XII.4 a very good agreement between the mathematical model calculations and the experimental data was achieved.

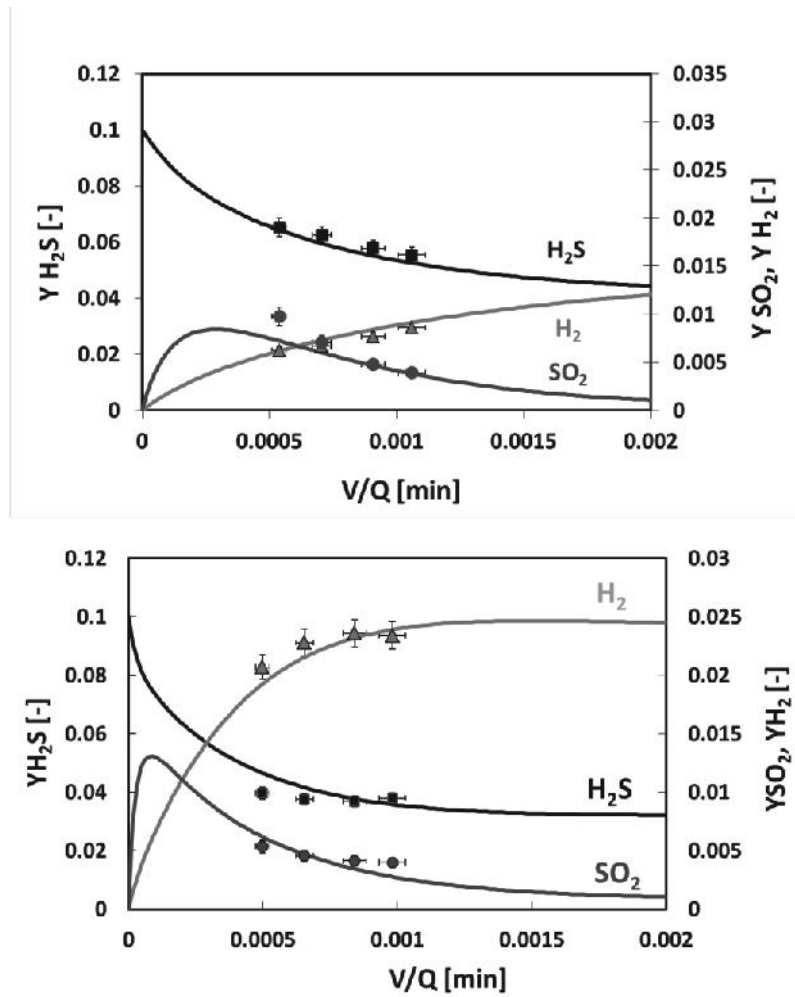


Figure XII.4: Comparison between model calculation and experimental data at 1000°C (a) and 1100°C (b) as function of the residence time. ($y_{H_2S}^{IN} = 0.1$, $O_2/H_2S = 0.25$).

XII.2 Heterogeneous Phase (Catalyst 10 Mo/ γ -Al₂O₃)

The modeling of the heterogeneous system was realized starting from the experimental data obtained without the catalyst in homogeneous phase. The hypothesized reaction system previously remains unchanged.

In this case, in addition to the homogeneous contribution of each reaction, the catalytic contribution was also considered.

The kinetic expressions adopted in this case are following reported (Eqs.XII.17-21).

$$r_{1cat} = k_{1cat} P_{H_2} P_{S_2}^{\frac{1}{2}} - k_{1cat_inversa} P_{H_2S} \quad (XII.17)$$

$$r_{2cat} = k_{2cat} P_{O_2} P_{H_2S} \quad (XII.18)$$

$$r_{3cat} = k_{3cat} P_{H_2S} P_{SO_2}^{\frac{1}{2}} - k_{3cat_inversa} P_{H_2O} P_{S_2}^{\frac{3}{4}} \quad (XII.19)$$

$$r_{4cat} = k_{4cat} P_{O_2} P_{H_2S} \quad (XII.20)$$

$$r_{5cat} = k_{5cat} P_{O_2} P_{H_2S} \quad (XII.21)$$

r_{1cat} : Rate Catalytic of Reaction 1

r_{2cat} , r_{4cat} , r_{5cat} : Rate Catalytic of Reactions 2, 4 e 5

r_{3cat} : Rate Catalytic of Reaction 3

k_{1cat} , k_{3cat} : Kinetic constants of the catalytic reactions 1 and 3 [$\text{min}^{-1} \cdot \text{atm}^{-1.5} \cdot \text{cm}^3/\text{g}_{cat}$]

$k_{1cat_inversa}$: Kinetic constant of the reverse catalytic reaction 1 [$\text{min}^{-1} \cdot \text{atm}^{-1} \cdot \text{cm}^3/\text{g}_{cat}$]

$k_{3cat_inversa}$: Kinetic constant of the reverse catalytic reaction 3 [$\text{min}^{-1} \cdot \text{atm}^{-1.75} \cdot \text{cm}^3/\text{g}_{cat}$]

k_{2cat} , k_{4cat} , k_{5cat} : Kinetic constants of the catalytic reactions 2, 4 e 5 [$\text{min}^{-1} \cdot \text{atm}^{-2} \cdot \text{cm}^3/\text{g}_{cat}$]

The mass balances for each component are reported below, by assuming the reactor as a plug flow reactor (PFR) (Eqs.XII.22-27):

$$\text{H}_2\text{S balance: } \dot{Q} \frac{dy_{\text{H}_2\text{S}}}{dV} = r_1 - r_2 - r_3 - r_4 - r_5 + (r_{1\text{cat}} - r_{2\text{cat}} - r_{3\text{cat}} - r_{4\text{cat}} - r_{5\text{cat}}) \cdot \rho_{\text{cat}}$$

(XII.22)

$$\text{H}_2 \text{ balance: } \dot{Q} \frac{dy_{\text{H}_2}}{dV} = -r_1 + r_4 + (-r_{1\text{cat}} + r_{4\text{cat}}) \cdot \rho_{\text{cat}}$$

(XII.23)

$$\text{SO}_2 \text{ balance: } \dot{Q} \frac{dy_{\text{SO}_2}}{dV} = r_2 - 0.5r_3 + r_4 + (r_{2\text{cat}} - 0.5r_{3\text{cat}} + r_{4\text{cat}}) \cdot \rho_{\text{cat}}$$

(XII.24)

$$\text{S}_2 \text{ balance: } \dot{Q} \frac{dy_{\text{S}_2}}{dV} = -0.5r_1 + 0.5r_3 + 0.75r_3 + (-0.5r_{1\text{cat}} + 0.5r_{3\text{cat}} + 0.75r_{3\text{cat}}) \cdot \rho_{\text{cat}}$$

(XII.25)

$$\text{O}_2 \text{ balance: } \dot{Q} \frac{dy_{\text{O}_2}}{dV} = -1.5r_2 - r_4 - 0.5r_5 + (-1.5r_{2\text{cat}} - r_{4\text{cat}} - 0.5r_{5\text{cat}}) \cdot \rho_{\text{cat}}$$

(XII.26)

$$\text{H}_2\text{O balance: } \dot{Q} \frac{dy_{\text{H}_2\text{O}}}{dV} = r_2 + r_3 + r_5 + (r_{2\text{cat}} + r_{3\text{cat}} + r_{5\text{cat}}) \cdot \rho_{\text{cat}}$$

(XII.27)

The initial conditions are the following:

$$\begin{aligned} V=0 & \quad y_{\text{H}_2\text{S}} = 0.1 \\ V=0 & \quad y_{\text{O}_2} = 0.1 \cdot R \text{ (where R is the feeding O}_2\text{/H}_2\text{S molar ratio)} \\ V=0 & \quad y_{\text{H}_2} = y_{\text{SO}_2} = y_{\text{S}_2} = y_{\text{H}_2\text{O}} = 0 \end{aligned}$$

where:

$$\begin{aligned} Q: & \text{ Total flow rate [cm}^3 \text{ (stp)} \cdot \text{min}^{-1}] \\ y_i: & \text{ fraction volume of component i-th [-]} \\ V: & \text{ Reaction volume [cm}^3] \\ V/Q: & \text{ Contact time [min]} \\ \rho_{\text{cat}}: & \text{ Catalyst Bulk Density} \end{aligned}$$

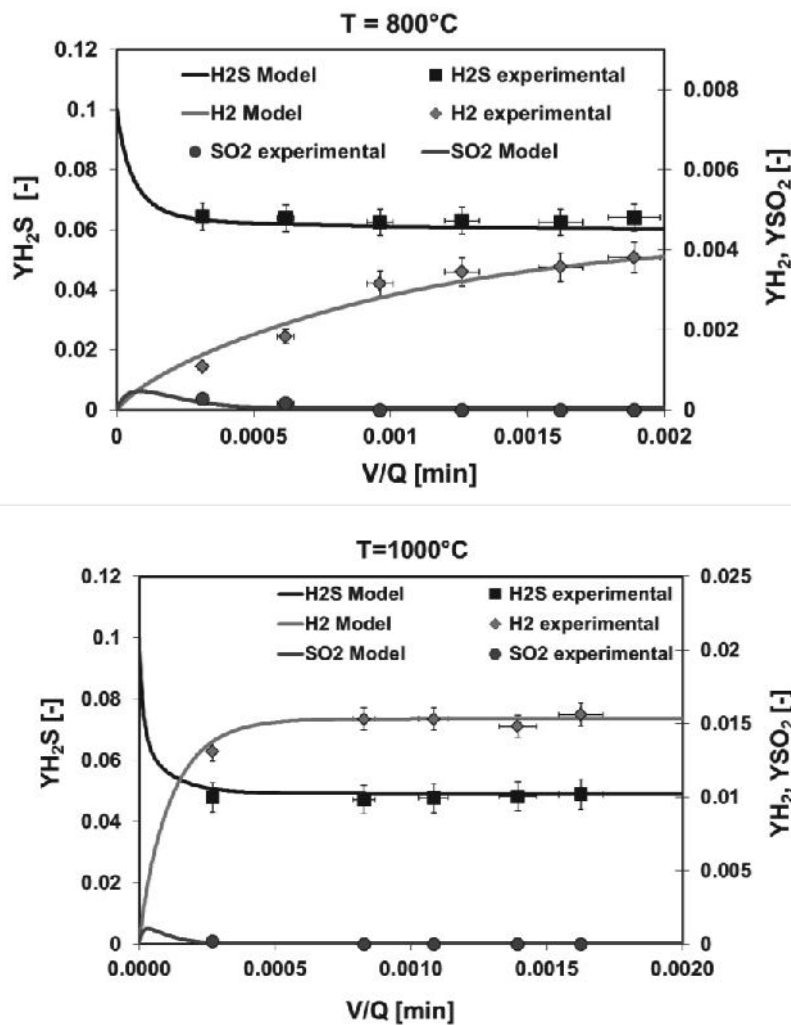
The system of differential equations was numerically integrated by using the Euler method.

Similarly to the homogeneous case, the values of the activation energy of each reaction were obtained by minimizing the sum of the standard deviations between the model data and experimental values with an $O_2/H_2S = 0.2$.

The kinetic constants of the homogeneous reactions, at each temperature, have been set equal to the values previously estimated from mathematical modeling of the homogeneous system.

The results of the regression were been the kinetic constant of the catalytic reactions.

In Figure XII.5 are illustrated the results of the model calculation compared with the experimental data at 800-1000-1100 °C.



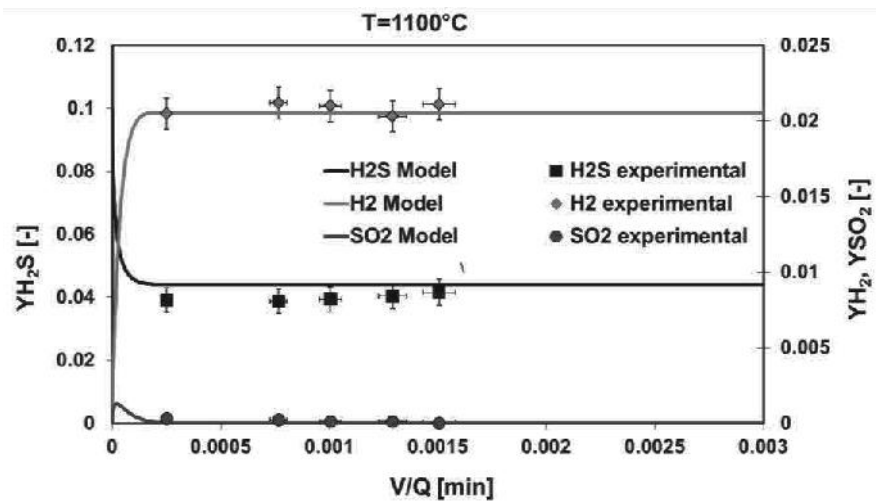


Figure XII.5: Comparison between model calculation and experimental data at 800°C 1000°C 1100°C, and a function of the contact time. ($y_{H_2S}^{IN} = 0.1$, $O_2/H_2S=0.2$).

The results obtained from the model and the experimental data at different temperatures, have shown that, for low contact times, the oxidation reactions were promoted with SO_2 production, showing a maximum value.

With the increase of contact time, a decrease of the molar fraction of SO_2 has been achieved because of the Claus reaction giving rise to the SO_2 conversion to sulfur.

In order to underline the difference between the alumina support and the Mo-based catalyst, the kinetics constants are compared in the Arrhenius plot (Figure XII.6).

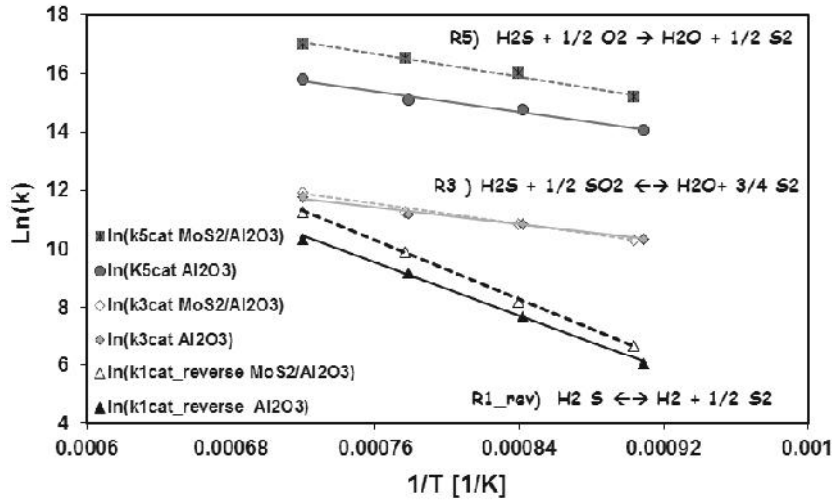


Figure XII.6: Arrhenius plot of the catalytic reactions of H_2S Decomposition (R1), Claus (R3) and Partial Oxidation of H_2S (R5). ($y_{H_2S}^{in} = 0.1$, $O_2/H_2S = 0.2$).

It is possible to observe that the addition of Mo-species on alumina support has promoted the partial oxidation of H_2S to Sulphur and the H_2S decomposition to hydrogen and Sulphur; relatively to the Claus reaction, no significant difference between the Mo-based catalyst and alumina was observed between 800°C and 1000°C, but at temperature higher than 1000°C, this reaction is slightly promoted from the Mo-based catalyst.

In Table XII.2 are shown the experimental values of the activation energy calculated for the catalytic system in presence of Al_2O_3 and 10Mo-based catalysts and the related literature values. From the comparison, it is evident that there is a good agreement between the literature and the values obtained from the model calculation.

Table XII.2: Comparison of Activation Energy between Catalytic Model ($10\text{MoS}_2/\text{Al}_2\text{O}_3$, Al_2O_3) and Literature.

	Ea, [Kcal/mol]		
	10 $\text{MoS}_2/\text{Al}_2\text{O}_3$	Al_2O_3	Literature
H ₂ S Recombination	29	21	23 [Hawboldt,2000 a]
H ₂ S Decomposition	50	45	45 [Hawboldt, 2000 a]
Claus Reaction	17	14	16 [Hawboldt,2000 b]
Partial Oxidation of H ₂ S	19	17	-

The predictive capability of the model was verified in the range of temperature of 800-1000°C with an H₂S inlet concentration equal to 20 vol% in presence of Mo-based catalyst (Figure XII.7).

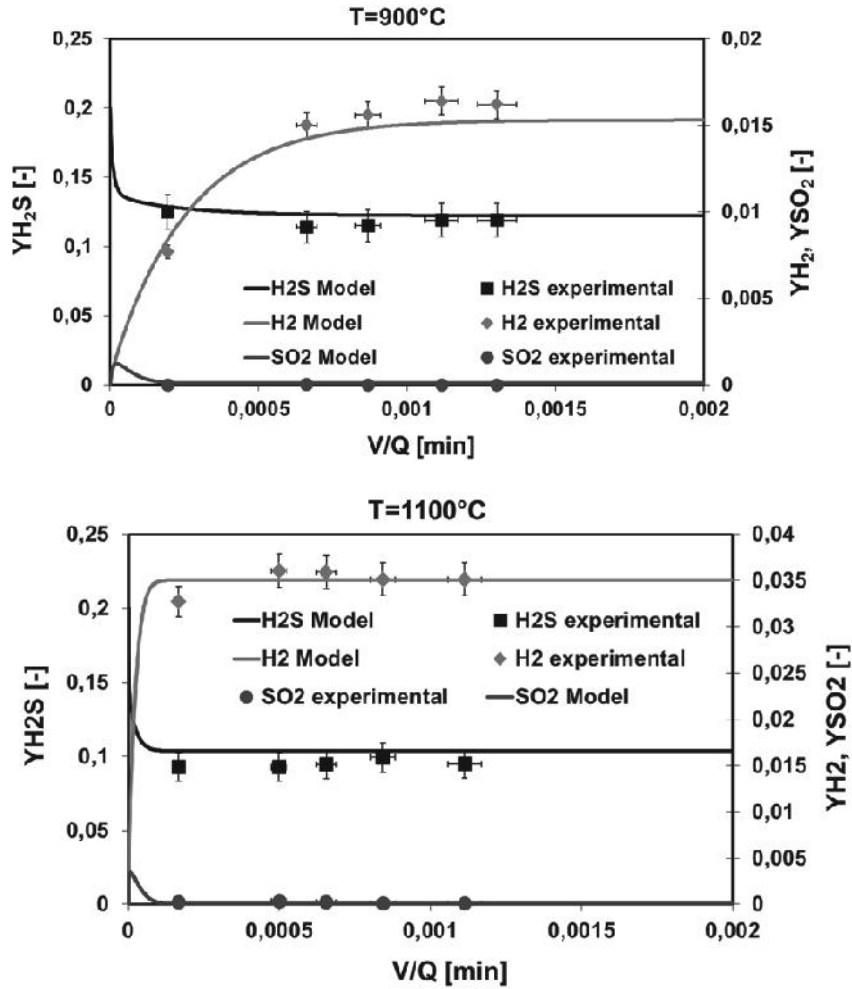


Figure XII.7: Model Prediction at 900°C and 1100°C with $y_{H_2S}^{dN} = 0.2$ ($O_2/H_2S=0.2$).

A good agreement of the experimental data with the model calculation was achieved in the same operating conditions for the Al_2O_3 and the Mo-based catalyst.

XII.3 Microscopic Kinetic Model in Homogeneous Phase

A chemical kinetic model was developed to study the reaction of H_2S thermal oxidative decomposition in homogeneous phase by using the Cantera software (Goodwin, 2001, Barba *et al.*, 2017).

Some different mechanism (Sour gas Mechanism, including Aramco Mech 1.3, Sulphur Mechanism 5.2, GRI-MECH 3.0 Mechanism) were used in order to evaluate the reaction oxidation system at different regimes and then the kinetic global mechanism (Metcalfé *et al.*, 2013, Zhou *et al.*, 2013, Leeds 2005).

The mechanism adopted is retrieved by the literature (Zhou *et al.*, 2013) and it is based on the lean H_2S oxidation.

Different pathway reactions, depending on the O_2 content in excess, are summarized in Figure XII.8.

In particular, when the $\text{O}_2/\text{H}_2\text{S}$ decreases, additional pathways, as shown in the scheme, from dashed and dotted lines, start to become competitive.

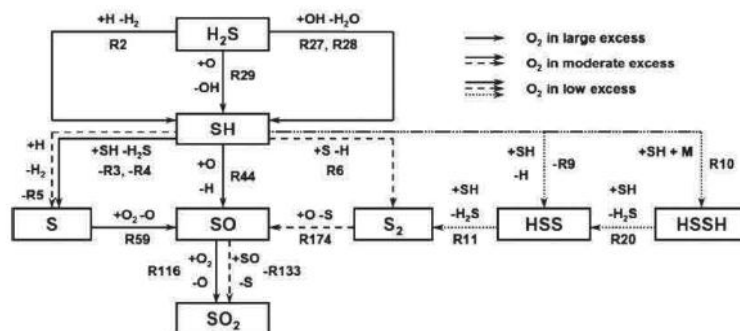


Figure XII.8: Schematic mechanism proposed by Zhou *et al.* for fuel lean H_2S oxidation with main consumption pathways (Zhou *et al.*, 2013).

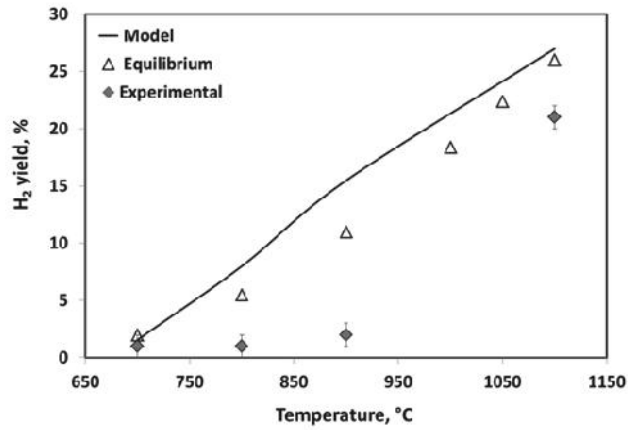
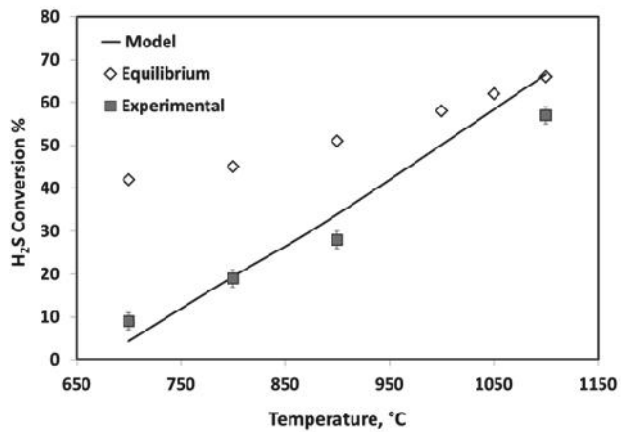
In all the cases, H_2S is largely consumed by H , OH and O , forming the SH radical.

At high $\text{O}_2/\text{H}_2\text{S}$, S is predominantly converted to SO which is further oxidized to SO_2 .

When the $\text{O}_2/\text{H}_2\text{S}$ decreases, the concentration of S increases and S_2 appears as an important intermediate through reaction of S with SH . Its consumption does not occur because the O_2 , in this condition, is less available.

Our previous experimental results obtained by varying the temperature, molar feed ratio and residence time (RT) were compared with the model calculations (Palma *et al.*, 2015).

The values obtained from the model calculation are compared with experimental data and thermodynamic equilibrium by varying the temperature between 700 and 1100 °C in terms of H₂S conversion, H₂ yield, SO₂ selectivity (Figure XII.9) (Barba *et al.*, 2017).



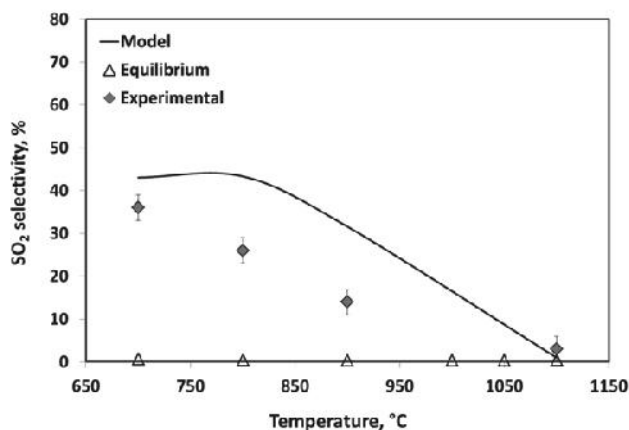


Figure XII.9: Comparison of model data predictions (straight line), with equilibrium (dotted line) and experimental values (markers) in terms of H_2S conversion, H_2 yield and SO_2 selectivity as a function of temperature ($O_2/H_2S = 0.2$, $RT = 150$ ms).

By considering the equilibrium calculations, the increase of the temperature determines the increase of H_2S conversion and H_2 yield with a very low SO_2 selectivity that is lower than 1% in the whole range of temperature considered.

It is important to note that at higher temperature values, particularly over 1000 °C, the model predictions of H_2S conversion, H_2 yield, SO_2 selectivity are in good agreement with the thermodynamic equilibrium ones.

Conversely, for temperatures lower than 1100 °C, the H_2S conversion calculated by the model is lower than that predicted by the thermodynamic equilibrium, whereas the H_2 yield is quite comparable to that expected by the equilibrium.

For what concern the SO_2 selectivity, the model predictions are very far from the thermodynamic calculations, and in particular, the model showed higher values in the range 700 - 1000 °C, with a good agreement at the highest temperature value.

The disagreement between the model and the thermodynamic may be explained by considering that the selected residence time of 150 ms is very short and does not allow to the reaction system to approach the equilibrium composition.

The influence of the feed molar ratio (O_2/H_2S) was also investigated on the H_2S conversion, H_2 yield, and SO_2 selectivity at 1100°C with a residence time of 150 ms.

The behavior of the main reaction parameters obtained by the model simulation in the range of O_2/H_2S from 0.2 to 0.35 is compared with the equilibrium data and the experimental values (Figure XII.10).

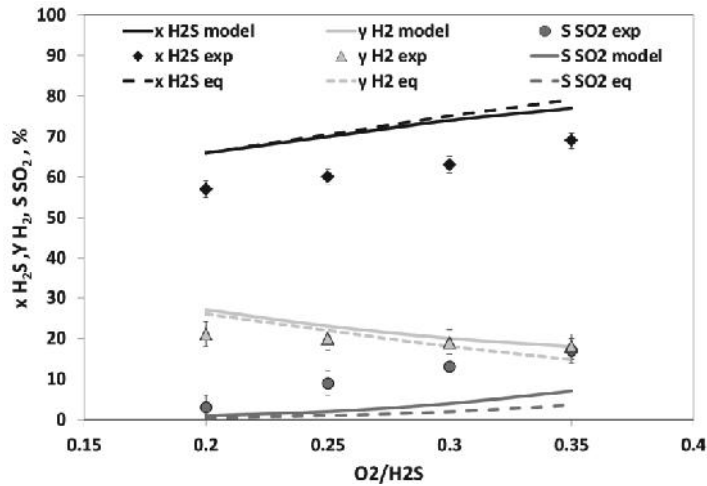


Figure XII.10: Comparison of simulation predictions with equilibrium and experimental values in terms of H_2S conversion, H_2 yield, and SO_2 selectivity as a function of O_2/H_2S ($T = 1100$ °C, $RT = 150$ ms).

It's possible to observe that the data obtained from the simulation are very close to the ones expected from the thermodynamic equilibrium by varying the O_2 concentration, except for the SO_2 selectivity that is slightly higher than the calculated value.

In Figure XII.11, it is reported the behavior of the main reaction parameters at 900°C.

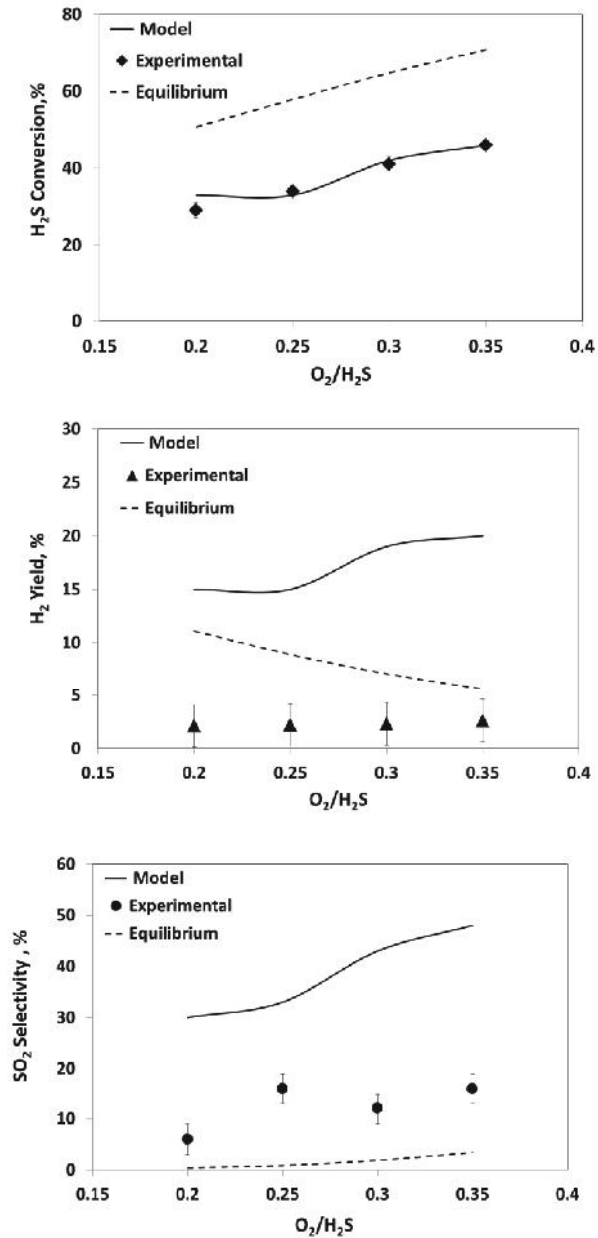


Figure XII.11: Comparison of the model calculation (straight line) with experimental results (markers) and equilibrium values (dotted line) in terms of H_2S conversion, SO_2 selectivity and H_2 yield by changing the O_2/H_2S at 900 C and $RT = 300$ ms.

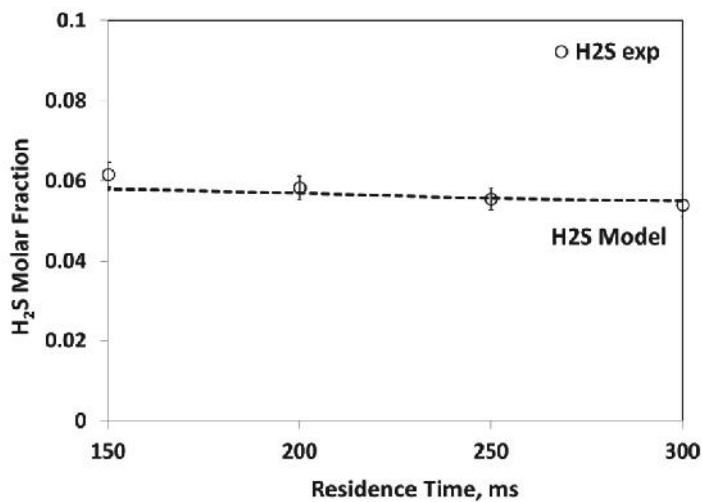
In this case, at the lower reaction temperature ($T=900^{\circ}\text{C}$), the H_2 yield and SO_2 selectivity calculated from the model, are higher than the experimental values, whereas the H_2S conversion values are close to those obtained experimentally.

The differences observed between the calculated H_2 yield and SO_2 selectivity with respect to that obtained from the experimental tests could be ascribed to the adopted kinetic model, which refers to complex mechanisms developed for the oxidation of lean H_2S . The model describes very well the H_2S oxidation reaction with O_2 in large excess, that leads to H_2 and SO_2 formation by secondary reactions (Zhou *et al.*, 2013).

The H_2 formation occurs primarily in the reactions of H with H_2S and, at lower O_2 concentrations, with SH in accordance to the reaction $\text{SH} + \text{H} \rightarrow \text{S} + \text{H}_2$ (Zhou *et al.*, 2013).

Based on these considerations, when the oxygen concentration is very low, as for the experimental tests, the model is unable to evaluate the right contribution of the Claus reaction, which determines the SO_2 consumption, involving a higher H_2 formation by the model prediction due to the overestimated thermal decomposition reaction.

The simulation at the highest O_2 content, corresponding to the ratio $\text{O}_2/\text{H}_2\text{S}$ of 0.35, i.e. in rich oxidation condition, at temperature of 900°C was also performed. The molar compositions obtained through the simulations and experimental tests are compared in Figure XII.12.



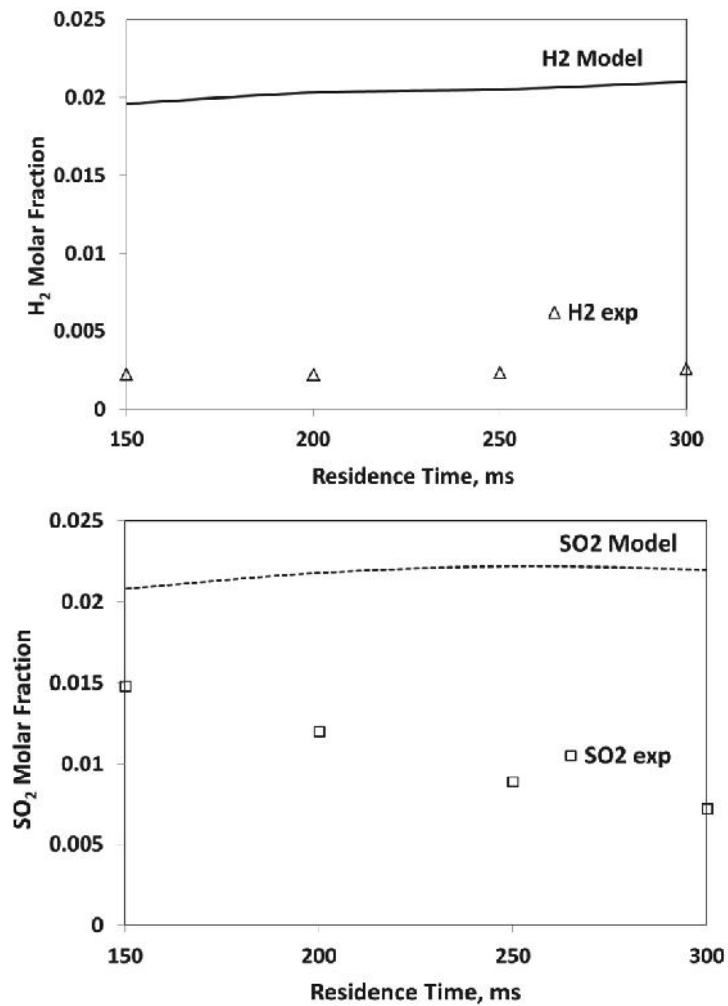


Figure XII.12: Comparison of experimental molar fractions (H_2S , SO_2 , H_2) (markers) with the simulation predictions (straight line) by varying the residence time ($T = 900^\circ C$, $O_2/H_2S = 0.35$).

It is worth noting that both the H_2S and O_2 molar fractions are in good agreement with the values obtained from the experimental tests, whereas the calculated H_2 and SO_2 molar fractions result higher in relation to the experimental data.

The scenario is very different at $1100^\circ C$ and with a residence time of 300 ms. The comparison of the experimental results with the model calculation, reported in Table XII.3, shows that the values of H_2S

conversion, H₂ yield and SO₂ selectivity are very similar, suggesting that at high temperatures, the model is able to describe the reaction system.

Table XII.3: Comparison of molar fraction experimental and calculated at 1100°C and RT = 300 ms (O₂/H₂S = 0.2).

	Experimental	Model
H ₂ S Conversion,%	57	67
H ₂ Yield, %	24	26
SO ₂ Selectivity,%	2	2

XIII CONCLUSIONS

The reaction of oxidative decomposition of H₂S was studied as a possible alternative to the Claus Process for the simultaneous production of H₂ and sulphur.

To this purpose, the thermodynamic analysis was initially carried out by studying the effect of several parameters on the equilibrium calculations, in order to identify the optimal operating conditions to maximize the H₂S conversion, H₂ yield, minimizing the selectivity to SO₂. Moreover, the thermal shade of the reaction system has been evaluated in order to establish the conditions to make the system able to work in auto-thermal conditions.

The thermodynamic calculation has shown that is necessary to achieve temperatures higher than 1000°C to ensure values of industrial interest for H₂S conversion and H₂ production with an O₂/H₂S = 0.2 allowing to achieve the lowest value of SO₂ selectivity, high H₂ selectivity and to carry out the reaction in auto-thermal conditions.

The presence of methane and ammonia have determined a lower H₂S conversion because of the competition reactions for the consumption of oxygen; in order to guarantee good efficiency conversion of CH₄, NH₃, the thermodynamic analysis suggested to work at temperatures of 1000-1100°C, modulating the oxygen concentration in a manner to obtain the total NH₃ conversion.

The starting point for the study of the H₂S oxidative decomposition reaction, was the analysis of the diluted system (10 vol% H₂S) in homogeneous phase by varying the temperature, molar feed ratio (O₂/H₂S) and residence time. The results have shown that, in order to obtain the highest H₂S conversion (60%) and the H₂ yield (20%), together with a low SO₂ selectivity (3%), at a fixed residence time of 150 ms, a reaction temperature of about 1100°C must be reached.

Subsequently, MoS₂-based catalysts supported on alumina with different MoS₂ loading (in the range 5-20 wt%) were prepared, characterized and tested by changing the main operating conditions, such as temperature (700-1100°C), contact time (20-40 ms) and H₂S inlet

concentration (10-40 vol%). The MoS₂/Al₂O₃ catalyst at 10 wt % of the MoS₂ content has shown a good H₂ yield (8%), H₂S conversion (50%), low SO₂ selectivity (1%) at 1000°C by feeding a stream containing 40 vol% of H₂S.

Relatively to this catalyst, a kinetic macroscopic model able to describe the main reactions occurring in the system was developed and compared with the homogeneous phase system. The results obtained from the model calculation, have pointed that, the catalyst promotes also the Claus reaction, besides the H₂S decomposition and the partial oxidation reactions.

Different catalysts (5CoS₂-10MoS₂, 5FeS₂-10MoS₂, and 5FeS₂/Al₂O₃) were investigated in presence of methane and ammonia, because, in presence of CH₄ in the feed stream, MoS₂-based catalyst has favored the formation of undesired by-products (COS, CS₂).

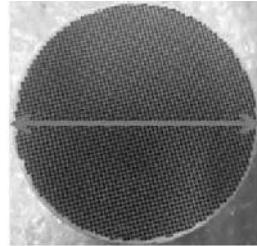
The sample 5FeS₂-10MoS₂/Al₂O₃ has exhibited the better performances at T=1060°C and at low contact times (20-40 ms). In particular, it was observed that MoS₂ is important for the depression of SO₂, while the FeS₂ is selective for the abatement of COS, CS₂.

In presence of ammonia, in order to obtain a complete conversion, was necessary to employ higher contact time (1 sec) and temperatures in the range 1060-1100°C.

Based on these results, the catalytic formulation was transferred from the powder to the cordierite monolith honeycomb, by the washcoating procedure. The adhesion of the washcoat on the cordierite, analyzed with SEM and ultrasonic tests, have confirmed the homogeneity of the washcoat layer and a good mechanical stability.

Finally, on the structured catalyst, a stability test of ~35 h was carried out at T=1060°C, evidencing no deactivation phenomena and the almost total NH₃ conversion (98%), resulting then a good candidate for the reaction of H₂S oxidative decomposition to sulphur and hydrogen at high temperature.

In conclusion, based on the good results obtained, the optimized catalytic formulation was transferred to Johnson Matthews company (leader in the development and manufacture of catalysts), for the preparation of structured catalyst that will be tested in the Pilot Plant under construction in Shanghai (Cina) by Kinetics Technology.



D= 80 mm



L= 110 mm

The demonstration Pilot Plant will validate the new recovery sulphur technology proposed by KT (described in the Chapter XI). Start –up of the demonstration on plant is expected in the next year.

References

- Adewale, R. A., Berrouk, A. S., Dara, S. A. (2016) Simulation of hydrogen production from thermal decomposition of hydrogen sulfide in sulfur recovery units. *Journal of Cleaner Production*, **112**, 4815-4825.
- Adesina, A. A., Meeyoo, V., Foulds, G. (1995) Thermolysis of Hydrogen Sulphide in an Open Tubular Reactor. *Int. J. Hydrogen Energy*, **20**, 777-783.
- Al-Shamma, L. M., Naman, S. A. (1989) Kinetic study for thermal production of hydrogen from H₂S by heterogeneous catalysis of vanadium sulfide in a flow system. *International Journal of Hydrogen Energy*, **14** (3), 173-179.
- Amorim, B. V., Moura, F. J., Brocchi, E., Vieira Maria, J. P., Rupp, M. T. (2012), *Metallurgical and Materials Transactions B* **43** (4), 781-786.
- Argyle, M. D., Ackerman, J. F., Muknahallipatna, S., Hamann, J. C., Legowski, S., Zhang, Ji-Jun, Zhao, G., Alcanzare, R. J., Wang L., Plumb, O. A. (2004) Novel Composite Hydrogen-Permeable Membranes for Non-Thermal Plasma Reactors for the Decomposition of Hydrogen Sulfide; University of Wyoming Department of Chemical and Petroleum Engineering and Department of Electrical and Computer Engineering, Laramie WY.
- Asadullah, M. Ito S.-I., Kunimori, K., Yamada, M., Tomishige, K. (2002) *Environmental Science and Technology*, **36**, 4476–4481.
- Aynsley, E. E., Pearson, T. G., Robinson, P. L. (1935) The Kinetics of the Reaction between Hydrogen and Sulphur. Part I. *J. Chem. Soc.*, 58-68.
- Balaev, A. V., Konshenko, E. V., Spivak, S. I., Ismagilov, F. R., Dzhemilev, UM. (2001) Modeling of partial oxidation of hydrogen sulfide over metal oxide catalysts. *Doklady Chemistry*, **376**, 34-37.
- Ballaguet, J. P., Barrere Tricca, C. (2006) Encyclopedia of hydrocarbons “Sulphur Cycle”, 137-160.
- Barba, D., Cammarota, F., Vaiano, V., Salzano, E., Palma, V. (2017) Experimental and numerical analysis of the oxidative decomposition of H₂S. *Fuel*, **198**, 68-75.

- Beychok, M. (2013) Hydrodesulfurization. <http://www.eoearth.org/view/article/171121>.
- Bellows R. J. (1999) Technical Challenges for Hydrocarbon Fuel Reforming, DOE, Baltimore, MD.
- Benson, S. W. (1976) Thermochemical Kinetics, 2nd Ed., John Wiley, New York.
- Bergwerff, J. A., Jansen, M., Leliveld, B. R. G., Visser, T., De Jong, K. P., Weckhuysen, B. M. (2006) Influence of the preparation method on the hydrotreating activity of MoS₂/Al₂O₃ extrudates: A Raman microspectroscopy study on the genesis of the active phase. *Journal of Catalysis*, **243**, 2, 296–302.
- Binoist, M., Clark, P. D., Archambault, D. (2003) Kinetic study of the pyrolysis of H₂S. *Ind. Eng. Chem. Res.*, **42**, 3943-3951.
- Bishara, A., Salman O. A. (1987) Thermochemical Decomposition of hydrogen sulfide by solar energy. *International Journal of Hydrogen Energy*, **12** (10), 679-685.
- Borgarello, E., Kalyanasundaram, K., Gratzel, M., (1982) *Helv. Chim. Acta*; **65**, (243).
- Borgarello, E., Serpone, N., Gratzel, M., Pelizzetti, E., (1986) *Inorg. Chim. Acta*, **112**, 197.
- Brancaccio, E. (2010) Assisted H₂S catalytic decomposition for H₂ production [PhD thesis].
- Bromberg, L., Cohn, D. R., Rabinovich, A., Alexeev, N. (1999) *International Journal of Hydrogen Energy*, **24**, 1131–1137.
- Goodwin, D. G. (2001) Cantera User's Guide Fortran Version Release 1.2.
- Cao, D., Adesina A. A. (1999) Fluidised bed reactor studies of H₂S decomposition over supported bimetallic Ru catalysts. *Catalysis Today*, **49** (1-3), 23-31.
- Carrieri, D., Kolling, D., Ananyev, G., Dismukes, G. C. (2006) *Industrial Biotechnology*, **2**, 133–137.
- Chandler, B. D., Schabel, A. B., Pignolet, L. H. (2000) *Journal of Catalysis*, **193**, 186–198.
- Chemat, F., Esveld, D. C., Poux, M., and Di-Martino J. L. (1998) *Microwave Power and Electromagnetic Energy*, **33** (2) 88-94.
- Chen, G. Li, Q. Lv, X. Deng, N., Jiao, L. (2004) Proceedings of the ASME Turbo Expo, Production of hydrogen-rich gas through pyrolysis of biomass in a two stage reactor, American Society of Mechanical Engineers, New York, NY, United States/Vienna, Austria, 711–721.

Chin, Hilton S., Karant, K., Mehrotra A. K., and Behie L. A. (2001) The Fate of Methane in a Claus Plant Reaction Furnace. *The Canadian Journal of Chemical Engineering*, **79** (4), 482-490.

Chivers, T., Hyne, J. Lau, C. (1980) The thermal decomposition of hydrogen sulphide over transition metal sulfides. *International Journal of Hydrogen Energy*, **5**, 499-506.

Ciambelli, P., Sannino, D., Palma, V., Vaiano, V. (2008) The Effect of Sulphate Doping on Nanosized TiO₂ and MoOx/TiO₂ Catalysts in Cyclohexane Photooxidative Dehydrogenation. *International Journal of Photoenergy*, **8**, 1-8.

Clark, P. D., Wassink, B. (1990) A review of methods for the conversion of H₂S to sulphur and H₂. Alberta Sulphur research Ltd.

Clark, P. D., Dowling, N. I., and Huang, M. (1998) Understanding Claus Furnace Chemistry: Development of a 'Modified' Claus for Low-Content Acid Cases, Oklahoma Center for Continuing Education, University of Oklahoma, pp. 241-263.

Clark, P. D., Dowling, N. I., Huang, M., Svrcek, W. Y., Monnery, D. W., (2001) Mechanisms of CO and COS Formation in the Claus Furnace The University of Calgary, 2500 University Drive N.W., Calgary, Alberta, Canada.

Clark P. D., et al., How do Claus catalysts really work?, in: *Proceedings of the 52nd Laurance Reid Gas conditioning conference*, 24-27 February 2002, Norman, pp.153-176.

Clark, P. D., Dowling, N. I., Huang, M., (2004 b) Catalytic destruction of NH₃ and SO₂ over alumina supported transition metal oxides. *Applied Catalysis A: General*, **274**, 219–227.

Colozzi, M., Cortese, S., Barbato, L., (2016) Innovative way to achieve Zero Emissions in sulphur recovery facilities. *Industrial Plants*, 44-51.

Cox, B. G., Clarke, P. F., Pruden, B. B., (1998) Economics of thermal dissociation of H₂S to produce hydrogen. *Int. J. Hydrogen Energy*, **23**, 531-544.

Davydov, A. A., Marshneva, V. I., and Shepotko, M. L., (2003) *Appl. Catal. A: Gen.*, **244**, 93.

Darwent, B. de B., Roberts, R., The Photochemical and Thermal Decomposition of Hydrogen Sulphide. *Proc. R. Soc. London, Ser. A* (1953), **216**, 344-361.

Demirbas, A., Arin G. (2004) *Energy Sources*, **26**, 1061–1069.

Demirbas, A. (2005) *Energy Sources*, **27**, 1313–1319.

- Demirbas, A., Demirbas, M. F. (2003) *Energy Sources*, **25**, 317–329.
- Digne, M., Marchand, K., Bourges, P. (2007) Monitoring Hydrotreating Catalysts Synthesis and Deactivation using Raman Spectrometry. *Oil & Gas Science and Technology*, **62**, (1), 91-99.
- Dongfang, Wu and Zhang, Hua (2013) Mechanical stability of monolithic catalysts: scattering of washcoat adhesion and failure mechanism of active material. *Ind. Eng. Chem. Res.*, **52**, 14713–21.
- Dowling, N. I., Hyne, J. B., Brown, D. M. (1990) Kinetics of the Reaction between Hydrogen and Sulfur under High-Temperature Claus Furnace Conditions. *Ind. Eng. Chem. Res.*, **29**, 2327-2332.
- Dowling, N. I. and Clark, P. T. (1999) Kinetic Modeling of the Reaction between Hydrogen and Sulfur and Opposing H₂S Decomposition at High Temperatures. *Ind. Eng. Chem. Res.*, **38**, 1369-1375.
- Farrauto, R., Hwang, S., Shore, L., Ruettinger, W., Lampert, J., Giroux, T., Liu, Y., Ilinich, O. (2003) *Annual Review of Materials Research*, **33**, 1–27.
- Faraji, F., Safarik, I., Strausz, O. P. (1998) The direct conversion of hydrogen sulfide to hydrogen and sulfur. *International Journal of Hydrogen Energy*, **23** (6), 451-456.
- Fukuda, K., Dokiya, M., Kameyama, T., and Kotera Y. (1978) Catalytic Decomposition of Hydrogen Sulfide. *Ind. Eng. Chem. Fundam.*, **17** (4), 243-248.
- Funk, J. E. (2001) *International Journal of Hydrogen Energy*, **26**, 185–190.
- Geissler, K., Newson, E., Vogel, F., Truong, T. B., Hottinger, P., Wokaum, A. (2001) *Physical Chemistry Chemical Physics*, **3**, 289–293.
- Gens, T. A. (1994) Decrease in Carbonyl Sulfide in the Feed to Claus Converters by Shift Catalysts. *Ind. Eng. Chem. Res.*, **33**, 1654-1656.
- Goar, B., (1986) Sulfur Recovery Technology, *Energy and Progress*, **6** (2), 71-75.
- Gratzel, M. (2000) *Progress in Photovoltaics: Research and Applications*, **8**, 171–185.
- Grigoriev, S. A., Porembsky, V. I., Fateev, V. N. (2006) *International Journal of Hydrogen Energy*, **31**, 171–175.
- Guijun, Ma, Hongjian, Yan, Jingying, Shi, Xu, Zong, Zhibing, Lei, Can, Li (2008) Direct splitting of H₂S into H₂ and S on CdS-

based photocatalyst under visible light irradiation. *Journal of Catalysis*, **260**, 134–140

Hawboldt, K. A., Monnery, W. D., Svrcek, W. Y. (2000a) *Chemical Engineering Science*, **55** (5), 957-966.

Hawboldt, K. A., Monnery, W. D., Pollock, A., Svrcek W. Y. (2000b) *Chemical Engineering Science*, **55**, 5141-5148.

Hao, X., Guo, L., Xuebao, H. (2002) *Journal of Chemical Industry and Engineering*, **53**, 221–228.

Hilaire, S., Wang, X., Luo, T., Gorte, R. J., Wagner, J. (2001) *Applied Catalysis A*, **215**, 271-278.

Hirsch, A. R. (1999) Long term effects on the olfactory system of exposure to hydrogen sulfide. *Occupational and Environmental Medicine*, **56** (4), 284.

Hoogers, G. (2003), Fuel Cell Technology Handbook, CRC Press, Boca Raton, pp. 5-1–5-23.

Huang, C., Linkous, C. (2007) UV photochemical option for closed cycle decomposition of hydrogen sulfide, patent US 7220390B1.

Kalina, D. W. and Mass, E. T. Jr. (1985) Indirect hydrogen sulfide conversion-I. An acidic electrochemical process. *Int. J. Hydrogen Energy*, **10** (3), 157-162.

Kaloidas, V., Papayannakos, N. (1989) Kinetics of Thermal, Non-Catalytic Decomposition of Hydrogen Sulphide. *Chem. Eng. Sci.*, **44**, 2493-2500.

Kaloidas, V., Papayannakos, N. (1991) Kinetics studies on the catalytic decomposition of Hydrogen Sulphide in a tubular reactor. *Ind. Eng. Chem. Res.*, **30**, 345-351.

Karan, K., Mehrotra, A. K., and Behie, L. A. (1998) COS-Forming Reaction between CO and Sulfur: A High-Temperature Intrinsic Kinetics Study. *Ind. Eng. Chem. Res.*, **37**, 4609-4616.

Karan, K., Mehrotra, A. K., and Behie, L. A. (1999) A high-temperature experimental and modeling study of homogeneous gas-phase COS reactions applied to Claus plants. *Chemical Engineering Science*, **54**, 2999-3006.

Karan, Kunal and Behie, Leo A. (2004) CS₂ Formation in the Claus Reaction Furnace: A Kinetic Study of Methane-Sulfur and Methane-Hydrogen Sulfide Reactions. Department of Chemical and Petroleum Engineering, The University of Calgary.

Kapdan, I. K., Kargi, F. (2006) *Enzyme and Microbial Technology*, **38**, 569–582.

Kilburn, K. H. and Warshaw, R. H. (1995) Hydrogen sulfide and reduced sulfur gases adversely affect neurophysiological functions. *Toxicological Industrial Health*, **11**, 185.

Knight, L. and Presnell, E. (2005) Death by sewer gas: case report of a double fatality and review of the literature. *The American Journal of Forensic Medicine and Pathology*, **26**, 183.

Kovacs, K. L., Maroti, G., Rakhely, G. (2006) *International Journal of Hydrogen Energy*, **31**, 1460–1468.

Kochubei, D. I., Rogov, V. A., Babenko, V. P., Bogdanov, S. V., and Zaikovskii, V. I. (2003) Structure and Thiophene Hydrodesulfurization Activity of MoS₂/Al₂O₃. *Catalysts, Kinetics and Catalysis*, **44** (1), 135–140.

Krumpelt, M. Krause, T. R., Carter, J. D., Kopasz, J. P., Ahmed, S. (2002) *Catalysis Today*, **77**, 3–16.

Krumpelt, (1999) Fuel Processing Session Summary, Baltimore, MD.

Leeds University Sulphur Mechanism, version 5.2, <http://www.chem.leeds.ac.uk/Combustion/sox.html>; 2005.

Legator, M. S., Singleton, C. R., Morris, D. L., and Phillips, D. (2001) Health effects from Chronic low-level exposure to hydrogen sulfide. *Archives of Environmental Health*, **56**, 123.

Levin, D. B., Pitt, L., Love, M. (2004) *International Journal of Hydrogen Energy*, **29**, 173–185.

Levy, A., Merryman, E. L., (1965) *Combustion and Flame*, **9**, 229-240.

Linkous, C. A., Huang, C., Fowler, J. R. (2004) UV photochemical oxidation of aqueous sodium sulfide to produce hydrogen and Sulphur. *Journal of Photochemistry and Photobiology A: Chemistry*, **168**, 153–160.

Luinstra, E. Hydrogen from H₂S - a review of the leading processes. Paper presented at the 1995 GRI Sulfur Recovery Conference, September 24-27, Austin, Texas.

Mbah, J., Krakow, B., Stefanakos, E., and Wolan, J. (2008) Electrolytic Splitting of H₂S Using CsHSO₄ Membrane. *J. Electrochem. Soc.*, **155**, (11), E166-E170.

McHugh, K. (2005) Hydrogen Production Methods, MPR Associates Inc., p.41.

Metcalfé, W. K., Burke, S. M., Ahmed, S. S., Curran, H. J. (2013) *Int. J. Chemical Kinetics*, **45**, 638-675.

- Mizuta, S., Kondo, W., Fujii, K., Iida, H., Isshiki, S., Noguchi, H., Kikuchi, T., Sue, H., Sakai, K. (1991) Hydrogen production from hydrogen sulfide by the Fe-Cl hybrid process. *Ind. Eng. Chem. Res.*, **30**, 1601-1608.
- Monnery, W. D., Hawboldt, K. A., Pollock, A., Svrcek, W. Y., (2000) *Chemical Engineering Science*, **55**, 5141-5148.
- Moraesa, R., Thomasa, K., Thomasa, S. (2012) *Journal of Catalysis*, **286**, 62–77.
- Muller, C. H., Schofield, K., Steinberg, M., & Brodia, H. P. (1979) Sulphur chemistry in flames, 17th Symposium (Int.) on Combustion. The Combustion Institute, Pittsburgh, PA, 867-875.
- Muradov, N. (2003) *Journal of Power Sources*, **118**, 320–324.
- Nath, K. and Das, D. (2004) *Journal of Scientific and Industrial Research*, **63**, 729–738.
- Norbeck, J. M., Heffel, J. W., Durbin, T. D., Tabbara, B., Bowden, J. M., Montani, M. C. (1996) *Hydrogen Fuel for Surface Transportation*. Society of Automotive Engineers Inc., Warrendale, PA, p. 548.
- Norman, J. H. U.S. Patent Number: 4,481,181, (1984), Assigned to GA Technologies Inc., San Diego, CA.
- Palma, V., Barba, D., Vaiano, V. (2015) *International Journal of Hydrogen Energy*, **40**, 106-113.
- Paskall, H. G. (1979) Capability of the modified-Claus process. Calgary (Alberta), *Western Research & Development*, 19-45.
- Patt, J., Moon, D. J., Phillips, C., Thompson, L. (2000) *Catalysis Letters*, **65**, 193–195.
- Paulmier, T., Fulcheri, L. (2005) *Chemical Engineering Journal*, **106**, 59–71.
- Pietrogrande, P., Bezzeccheri, M. (1993) Fuel Processing, in: L.J.M.J. Blomen, Mugerwa M.N. Eds, *Fuel Cell Systems*, Plenum Press, New York, 121–156.
- Pino, L., Recupero, V., Beninati, S., Shukla, A. K., Hegde, M. S., Bera, P. (2002) *Applied Catalysis A: General*, **225**, 63–75.
- Rameshni, M. (2008) Processing High-Ammonia Acid Gas in a SRU.
- Raymont, M.E.D. (1974) Hydrogen Sulfide Thermal Decomposition Ph.D. Thesis, University of Calgary, Calgary, AB, Canada.
- Reed, R. L. (1986) Modified Claus furnace, US Patent 4575453.

Reshetenko, T. V., Khairulin, S. R., Ismagilov, Z. R., Kuznetsov, V. V. (2002) Study of the reaction of high temperature H₂S decomposition on metal oxides (γ -Al₂O₃, α -Fe₂O₃, V₂O₅). *International Journal of Hydrogen Energy*, **27**, 387-394.

Reverberi, A. P., Klemes, J. J., Varbanov, P. S., Fabiano, B. (2016) A review on hydrogen production from hydrogen sulphide by chemical and photochemical methods. *J. Clean. Production*, **136** part B, 72-80.

Ross, J. R. H. in: M.W. Roberts, J.M. Thomas (Eds.), (1974), *Surface and Defect Properties of Solids*, Chemical Society, London p.34.

Rostrup-Nielsen, J. (2003) in: I.T. Horvath (Ed.), *Encyclopedia of Catalysis*, Wiley Interscience, p.4.

Seyfried, L., Garin, F., Gaire, M., Thiebaut, J. M., and Roussy G. (1994) *J. Catal.*, **148**, 281.

El-Shobaky, H. G., Mokhtar, M., Ahmed, A. S. (1999) Effect of MgO-doping on solid-solid interactions in MoO₃/Al₂O₃ system. *Thermochimica Acta*, **327**, 1-2, 39-46.

Skrtic, L. (2006) Hydrogen Sulfide, Oil and Gas, and People's Health; Energy and Resources Group University of California, Berkeley.

Slimane, R. B., Lau, F. S., DiHu, Remon, J., and Khinkis, M. Proceedings of the 2002 U.S. DOE Hydrogen Program Review NREL/CP-610-32405.

Slimane, R. B., Lau, F. S. Khinkis, M., Bingue, J. P., Saveliev, A. V., Kennedy, L. A. (2004) *International Journal of Hydrogen Energy*, **29**, 1471-1477.

Smith, G. P., Golden, D. M., Frenklach, M., Moriarty, N. W., Eiteneer, B., Goldenberg, M., Bowman, C. T., Hanson, R. K., Song, S., Gardiner, W. C., Lissianski, V., Zhiwei, Q. GRI-Mech 3.0, The Gas Research Institute, http://www.me.berkeley.edu/gri_mech/

Song, C. S. (2002) *Catalysis Today*, **77**, 17-49.

Song, M. G., Lee, J. (2006) Stabilization of gamma alumina slurry for chemical-mechanical polishing of copper. *Journal of Colloid and Interface Science*, **300**, 2, 603-611.

Song, H., Zhang, L. Ozkan, U. S. (2007) *Green Chemistry*, **9**, 686-694.

Sørensen, B. (2005) *Hydrogen and Fuel Cells Emerging Technologies and Applications*, Elsevier Academic Press, New York, p. 450.

Steinberg, M. (2004) *Fuel Cell Science*, Engineering and Technology, A Highly Efficient Combined Cycle Fossil and Biomass Fuel Power Generation and Hydrogen Production Plant with Zero CO₂ Emission, American Society of Mechanical Engineers, New York, United States/Rochester, NY, United States, 401–408.

Steinfeld, A. (2005) *Solar Energy*, **78**, 603–615.

Tesner, P. A., Nemivovskii, M. S., and Motyl, D. N., (1991) Kinetics of the thermal decomposition of hydrogen sulfide at 600-1200° C. *Kinetics and Catalysis*, **31**, 1081-1083.

Timm, D. L., Onsan, Z. I. (2001) *Catalysis Review*, **43**, 31–84.

Turner, J., Sverdrup, G., Mann, M. K., Maness, P. C., Kroposki, B., Ghirardi, M., Evans, R. J., Blake, D. (2008) *International Journal of Hydrogen Energy*, **32**, 379–407.

Wang, Y., Chin, Y., Rozmiarek, R. T., Watson, J., Tonkovich, A. L. Y. (2004) *Catalysis Today*, **98**, 575–581.

Wang, H. W., Skeldon P., Thompson G. E. (1998) Thermogravimetric-differential thermal analysis of the solid-state decomposition of ammonium tetrathiomolybdate during heating in argon. *Journal of Materials Science*, **33** (12), 3079-3083.

Wang, H. W., Skeldon, P. (1997) Synthesis and characterization of molybdenum disulphide formed from ammonium tetrathiomolybdate. *Journal of Materials Science*, **32**, 497-502.

Wang, X., Pan, D., Weng, D. Low, Chen-Y. Rice, L. Han, J., and Lu, Y. (2010) A General Synthesis of Cu-In-S Based Multicomponent Solid-Solution Nanocrystals with Tunable Band Gap, Size, and Structure. *J. Phys. Chem. C*, **114** (41), 17293–17297.

Wei, J., Iglesia, E. (2004) *Journal of Physical Chemistry B*, **188**, 4094.

Wills, J. (2006) *Fuel Cell Review*, **2**, 23–26.

Yamada, O. (2006) *Thin Solid Films*, **509**, 207–211.

Yan, Z., Chen, L., Wang, H., Huagong, X. (2006) *Journal of Chemical Industry and Engineering*, **57**, 1432–1437.

Yang, B. L., and Kung H. H. (1994) Hydrogen recovery from hydrogen sulphide by oxidation and by decomposition. *Ind. Eng. Chem. Res.*, **33**, 1090-1097.

Zachariah, M. R., Smith, O. I. (1987) *Combustion and flames*, **69**, 125-139.

Zagoruiko, A. N., Shinkarev, V. V., Vanag, S. V., Bukhtiyarova, G. A., *Catalysis in Industry*, **2**, 343-352.

- Zaman, J., Chakma, A., (1995) *Fuel Processing Technology*, **41**, 159-198.
- Zazhigalov, V. A., Gerei, S. V., Rubanik, M. Ya. (1975) Relationship in the Catalytic Reaction between Hydrogen and Sulfur in the presence of Metal Sulphide. *I. Kinet. Katal.*, **16** (4), 967-974.
- Zhao, S., Gorte, R. J. (2004) *Catalysis Letters*, **92**, 75.
- Zhao, Gui-Bing, (2007) Production of Hydrogen and Sulfur From Hydrogen Sulfide in a Nonthermal-Plasma Pulsed Corona Discharge Reactor. *Chemical Engineering Science*, **72**, 2216-2227.
- Zhang, X., Hayward, D. O., Mingos, M. P. (1999) Apparent equilibrium shifts and hot-spot formation for catalytic reactions induced by microwave dielectric heating. *Chem. Commun.*, 975-976.
- Zhang, X., Hayward, D. O. (2006) Applications of microwave dielectric heating in environment-related heterogeneous gas-phase catalytic system. *Inorganica Chimica Acta*, **359**, 3421-3433.
- Zhou, C. R., Sendt, K., Haynes, B. S. (2013) Experimental and kinetic modelling study of H₂S oxidation. *Proc. Comb. Inst.*, **34**, 625-632.

